Poly(amino ether) based Polymeric and Nanoparticle Systems for Nucleic Acid Delivery and Bioimaging

by

James Ramos

A Dissertation Presented in Partial Fulfillment
of the Requirements for the Degree
Doctor of Philosophy

Approved June 2014 by the
Graduate Supervisory Committee:

Kaushal Rege, Chair
Vikram Kodibagkar
Michael Caplan
Brent Vernon
Antonio Garcia

ARIZONA STATE UNIVERSITY

August 2014

ABSTRACT

Gold nanoparticles have emerged as promising nanomaterials for biosensing, imaging, photothermal treatment and therapeutic delivery for several diseases, including cancer. We have generated poly(amino ether)-functionalized gold nanorods (PAE-GNRs) using a layer-by-layer deposition approach. Sub-toxic concentrations of PAE-GNRs were employed to deliver plasmid DNA to prostate cancer cells in vitro. PAE-GNRs generated using 1,4C-1,4Bis, a cationic polymer from our laboratory demonstrated significantly higher transgene expression and exhibited lower cytotoxicities when compared to similar assemblies generated using 25 kDa poly(ethylene imine) (PEI25k-GNRs), a current standard for polymer-mediated gene delivery. Additionally, sub-toxic concentrations of 1,4C-1,4Bis-GNR nanoassemblies were employed to deliver expression vectors that express shRNA ('shRNA plasmid') against firefly luciferase gene in order to knock down expression of the protein constitutively expressed in prostate cancer cells. The roles of poly(amino ether) chemistry and zeta-potential in determining transgene expression efficacies of PAE-GNR assemblies were investigated. The theranostic potential of 1,4C-1,4Bis-GNR nanoassemblies was demonstrated using live cell two-photon induced luminescence bioimaging. The PAE class of polymers was also investigated for the one pot synthesis of both gold and silver nanoparticles using a small library poly(amino ethers) derived from linear-like polyamines. Efficient nanoparticle synthesis dependent on concentration of polymers as well as polymer chemical composition is demonstrated. Additionally, the application of poly(amino ether)-gold nanoparticles for transgene delivery is demonstrated in 22Rv1 and MB49 cancer cell lines. Base polymer, 1,4C-1,4Bis and 1,4C-1,4Bis templated and modified gold nanoparticles were compared for

transgene delivery efficacies. Differences in morphology and physiochemical properties were investigated as they relate to differences in transgene delivery efficacy. There were found to be minimal differences suggestion that 1,4C-1,4Bis efficacy is not lost following use for nanoparticle modification. These results indicate that poly(amino ether)-gold nanoassemblies are a promising theranostic platform for delivery of therapeutic payloads capable of simultaneous gene silencing and bioimaging.

ACKNOWLEDGMENTS

I would like to begin by expressing my gratitude to my advisor Dr. Kaushal Rege for the guidance and support he has provided during my time at Arizona State University. His help and direction have directly influenced the success I have experienced.

A very special thank you must be extended to Dr. Michael Caplan, Dr. Antonio Garcia, Dr. Vikram Kodibagkar, and Dr. Brent Vernon for their willingness to be members on my committee and the feedback and advice they have provided. I would also like to acknowledge the individuals who aided and trained me in the use of various equipment and procedures. These individuals include I would like to thank Dr. Page Baluch from the W.M. Keck Bioimaging Laboratory and Dr. Su Lin the Director of the Ultrafast Laser Facility and Dr. Lenore Dai the Program Chair for Chemical Engineering. I would also like to extend a thank you to Dr. Huang-Chiao Huang and Dr. Sutapa Barua for their aid in getting me started in productive research in the lab. I would like to thank Jeffery Vu and Kristina Gray for their aid with experimentation and data analysis. I would also like to thank the rest of my colleagues, past and present, including Dr. David Taylor, Dr. Thrimoorthy Potta , Dr. Jacob Elmer, Dr. Bhavani Miryala, Matthew Christensen, Lucas Vu, Beatrice Tamakloe, Karthik Subramaniam, James Faust, Sai Pavan, Candace Walker, Jennifer Lehrman, Amy Mallik and all of our undergraduate and high school researchers. Additionally, research is not possible without funding and I would like to thank the National Science Foundation, The Science Foundation of Arizona, The Arizona State University Dean's Fellowship, the Phoenix Chapter of the ARCS Foundation, and the Ira A. Fulton School of Engineering Ford Graduate Engineering Fellowship.

I would also like to thank all my friends and family for all love and support throughout the years. Foremost I must thank my mother and father for their never ending love, support, understanding, and for pushing me to always strive to do my best.

TABLE OF CONTENTS

Page

LIST OF TABLES

Table Page

LIST OF FIGURES

Figure Page

Figure Page

CHAPTER 1

INTRODUCTION

In several diseases, including cancer diseases, there is an urgent need for formulating platforms that are capable of addressing 1) diagnostics, 2) treatment, and 3) determination of therapeutic effect (therapeutic response)(Young, Figueroa, & Drezek, 2012). Diagnostics involves the specific labeling of malignant tissues so that its localization can be differentiated from that of healthy tissue. Following labeling and localization of the malignant tissue, treatment encompasses a wide range of possible options. One such option is the targeted delivery of a therapeutic payload, including chemotherapeutic drugs or biologicals, for treatment of the disease. In addition to targeted delivery, in many cases, control of the payload release via an external stimulus, as opposed to passive release, may be desirable. This doubly ensures that the payload reaches the desired targeted tissue and will only be released in its specific location. Following treatment, determination of the therapeutic effect is also desirable and may be accomplished in a similar way as the initial labeling. The challenge to encompass these needs in a single treatment modality has resulted in a push towards the formulation of theranostic treatment options, wherein a single platform can address multiple or all of these needs. Recent investigations in nanotechnology have made it possible to develop single-platform theranostics options. More specifically, photoresponsive nanoparticles have demonstrated potential as viable theranostic platforms. Light absorption and surface modification properties of these nanoparticles can be exploited for targeting and labeling diseased tissues via multiple imaging modalities. In addition, their ability to absorb specific wavelengths of light has been exploited for photothermal ablation of malignant

tissue, controlled release of treatment payloads, and combination treatments resulting in synergistic therapeutic options.

Gold Nanoparticles

Plasmonic gold nanoparticles exhibit unique optical and photothermal properties. Surface plasmon resonance of gold nanoparticles allows them to strongly absorb and scatter incident light significantly higher when compared to molecular dyes(Link & El-Sayed, 1999). Thus, they have emerged as promising contrast agents for biological imaging. Some classes of gold nanoparticle are also able to convert resonant energy to heat. Following exposure of near infrared (NIR) electron-phonon and phonon-phonon interactions can convert incident light into heat (Jain, Haung, El-Sayed, & El Sayed, 2007; Oldenburg, Jackson, Westcott, & Halas, 1999). Several classes of gold nanoparticles with the ability to absorb NIR light have been synthesized using chemical(J. Y. Chen et al., 2006; Jana, Gearheart, & Murphy, 2001a, 2001b; Jana, Gearheart, Obare, & Murphy, 2002; Nikoobakht & El-Sayed, 2003; Oldenburg, Averitt, Westcott, & Halas, 1998; Oldenburg, Jackson, et al., 1999; Oldenburg, Westcott, Averitt, & Halas, 1999; Skrabalak, Au, Li, & Xia, 2007; Y. G. Sun, Mayers, & Xia, 2002), and electrochemical(Burdick, Alonas, Huang, Rege, & Wang, 2009; Chang, Shih, Chen, Lai, & Wang, 1999; Martin, 1994; Y. Y. Yu, Chang, Lee, & Wang, 1997) methods. These nanoparticles have been widely investigated for uses in bioimaging, nucleic acid and drug delivery, and photothermal ablation.

Bioimaging and disease detection/diagnostics. Non- and minimally invasive bioimaging techniques are invaluable tools for clinical diagnostics of diseased tissue. Currently, bioimaging techniques, from the molecular to the tissue scale are employed for detection of early-stage cancer, guiding drug and biological therapies, and surgery. Gold nanoparticles are attractive as contrast agents since they can be engineered to overcome limitations of chemical and photostability, detection limits, and compatibility across various imaging modalities, typically associated with conventional contrast agents(Hahn, Singh, Sharma, Brown, & Moudgil, 2011). The use of imaging modalities based on NIR lasers has been increasingly investigated since NIR light can penetrate tissue at greater depths compared to visible light, in addition to minimal tissue scattering, and reduced phototoxicity. Thus, gold nanoparticles, tuned to absorb NIR light, have been widely explored for use in multiple imaging modalities(Durr et al., 2007; J.-L. Li & Gu, 2010; H. F. Wang et al., 2005).

Optical coherence tomography (OCT) is an NIR-based interferometer imaging modality that uses optical scattering media to provide cross-sectional subsurface images. Using NIR irradiation for maximal light penetration into tissue, images are formed based on differences between the absorption to scattering profiles of the medium, with resolution in the micrometer range at penetration depths of 2-3 mm (Fercher, Drexler, Hitzenberger, & Lasser, 2003). Using mouse xenograft colon tumor models, Gobin et al. (Gobin et al., 2007) injected poly(ethylene glycol) (PEG)-conjugated gold nanoshells (PEGylated gold nanoshells) via tail vein. Following 20 h after the injection, OCT images were acquired and accumulation of the gold nanoshells in the tumor resulted in enhanced brightness. Similarly in mouse xenograft epidermoid tumor models, Kah et al. (Kah et al.,

2009) demonstrated that antibody-functionalized PEGylated gold nanoshells increased that fractional concentration of injected gold nanoshells in tumor regions compared to untargeted nanoshells. A reduction in time from 6 to 2 hours was also observed for delivery of nanoshells to the tumor site. Although OCT has deeper tissue penetration compared to that observed with confocal microscopy, there are still limitations for the application of gold nanoparticle OCT in deep tissue imaging(H.-C. Huang, S. Barua, G. Sharma, S. K. Dey, & K. Rege, 2011).

Two-photon luminescence (TPL) imaging uses femto- to pico- second pulsed, high intensity NIR Ti:S lasers in order to deliver a high photon flux to specimens of interest(Perry, Burke, & Brown, 2012). Due to their surface plasmon resonance property, noble metal nanoparticles have emerged as viable contrast agents for TPL. TPL is a serial process in which photons are sequentially absorbed and electrons from the d-band are excited to unoccupied states of the sp-conduction band. Luminescent emission results from the relaxation of the electron-hole pair. Gold nanorods (GNRs) have emerged as particularly appealing for TPL due to facile synthesis, tunable longitudinal plasmon absorbance in the NIR region, and reduced plasmon dampening(Durr, et al., 2007). In a study performed by Wang et al.(H. F. Wang, et al., 2005) picomolar concentrations of sulfide-treated gold nanorods were injected into mice tail vein and visualized flowing through the mouse earlobe vessels in real-time using TPL imaging.

Photoacoustic tomography (PAT) utilizes short-pulsed laser beams that elicit thermoexpansion of an absorber. This results in pressure or photoacoustic (PA) waves that are detected by a wideband ultrasonic detector which allows for 3-dimensional reconstruction of the optical absorption properties of the internal tissue structure. Gold

nanoparticles have proven to be useful contrast agents for PAT due to their unique optical absorption properties(Mallidi et al., 2009; X. Yang, Stein, Ashkenazi, & Wang, 2009). In a study performed by the Wang group(Y. W. Wang et al., 2004) PEGylated gold nanoshells were utilized as PAT contrast agents for imaging rat brain vasculature and demonstrated up to 63% enhancement in optical absorption of brain vasculature following three sequential nanoshell treatments. Additionally, 80% enhancement in cerebral cortex absorption was found following systemic injection of PEGylated gold nanocages (X. M. Yang, Skrabalak, Li, Xia, & Wang, 2007). In a rat model study performed by the Xia group, PAT was used to quantitatively evaluate gold nanocage transport in the lymphatic system and uptake in the lymph nodes. This also enabled mapping of sentinel lymph nodes up to 3.3 cm below skin surface. Gold nanocages were transported to the second and third axillary lymph nodes, which can have potential implications for use in metastatic lymph node mapping. Bioconjugated gold nanocages were employed for active targeting to subcutaneous inoculated melanomas in mouse models, resulting in 300% higher signal enhancement compared to PEG-gold nanocages which demonstrate passive targeting due to the EPR effect(C. Kim et al., 2010).

Drug and Nucleic Acid delivery. The emergence of novel nanomaterials, including gold nanoparticles, has led to new options for delivery of therapeutic agents(Chinnaiyan et al., 2006; Cho, Wang, Nie, Chen, & Shin, 2008; Ghosh, Han, De, Kyu Kim, & Rotello, 2008; Heath & Davis, 2008; H. C. Huang, S. Barua, G. Sharma, S. K. Dey, & K. Rege, 2011; Jabr-Milane et al., 2008; Smith, Duan, Mohs, & Nie, 2008). Due to various controlled delivery mechanisms such as pulsed laser induced gold-thiol bond cleavage (Lu et al., 2010; You, Zhang, & Li, 2010), acidic environment induced release (W. T. Wu, Zhou, Berliner, Banerjee, & Zhou, 2010), diffusion release (Cheng et al., 2010), photothermal modulation and surface coating shrinkage (Sershen, Westcott, Halas, & West, 2000), gold nanoparticles have been extensively investigated as drug and gene delivery vehicles.

Cetuximab (C225) is an FDA approved anti-EGFR antibody for treatment of EGFR-positive colorectal cancer and is currently in different phases of clinical trials for other malignancies(Herbst, Kim, & Harari, 2001; Hynes & Lane, 2005). Gold nanoparticles using Cetuximab as a targeting agent for delivery of low doses of gemcitabine showed significant tumor growth inhibition in an orthotopic model of pancreatic cancer(Patra et al., 2008). AuriTax is a multivalent nanosystem composed of tumor necrosis factor (TNF), paclitaxel, and PEG assembled on 25 nm gold nanoparticles (GNPs). Similarly, Aurimune-T is assembled on a 25 nm GNP with only TNF and PEG. Aurimune-T demonstrated a ten-fold increase in reducing tumor burden compared to TNF alone in animal studies (Paciotti et al., 2004; Patra, Bhattacharya, D., & Mukherjee, 2008).

Gold nanoparticles are promising vectors for non-viral transgene delivery primarily due to the availability of facile surface-modification methods(X. Huang, Neretina, & El-

Sayed, 2009). Surface functionalization of gold nanoparticles allows for tuning of hydrophobicity and charge, which can enhance transgene expression and decrease cytotoxicity(Ghosh, et al., 2008). Additionally, their high surface area-to-volume ratios facilitate high payload carrying capabilities. Gold nanoparticles have been extensively investigated for *in vitro* transgene(A. C. Bonoiu et al., 2009; Ow Sullivan, Green, & Przybycien, 2003; Sandhu, McIntosh, Simard, Smith, & Rotello, 2002; M. Thomas & A. M. Klibanov, 2003) delivery and expression and siRNA(A. C. Bonoiu, et al., 2009; Mahajan et al., 2012; W. Zhang et al., 2011) / shRNA(Ryou et al., 2010) delivery for gene silencing.

Folate receptor-targeted hollow gold nanospheres where used for NIR-induced delivery of siRNA against NF-κB p65 subunits both *in vitro* and *in vivo*(Lu, et al., 2010). NIR irradiation induced a shape transformation in the gold nanoparticles resulting in siRNA release into the cytosol. This *photothermal transfection* resulted in down regulation of NF-κB only in tumors irradiated with NIR light. This down regulation of NF-κB was exploited to sensitize tumors to the chemotherapeutic drug, irinotecan, resulting in growth inhibition. In a study done by Bonoiu et al.(A. Bonoiu et al., 2011) gold nanorods with electrostatically bound siRNA were used to silence approximately 70% of the housekeeping gene, glyceraldehyde 3-phosphate dehydrogenase (GAPDH) in the CA1 hippocampal region of the rat brain at >10 days post-injection. The Prasad group(Masood et al., 2012) demonstrated that down-regulation of the anti-apoptotic sphingosine kinase (Sphk1) gene in head and neck squamous cell carcinoma in subcutaneous tumors grown in mice resulted in radiosensitization and over 50% tumor regression compared to control treatments. In these cases, the down-regulation was

achieved using gold nanorod-siRNA ‘nanoplexes’. Additionally, tumor regression was possible with radiation doses much lower than those commonly used in clinical settings. Ryou et al.(Ryou et al., 2011) reported studies in which mice with subcutaneous xenograft human colon carcinoma tumor models were subcutaneously injected with shRNA-conjugated gold nanoparticles for silencing the Mcl-1L gene. A decrease in tumor size of approximately 36% was observed when compared to control treatments following direct administration into the tumor every 3 days for 30 days, indicating that shRNA treatment reduced tumor growth.

Thermo-chemotherapy. Thermal or hyperthermic therapy is an attractive alternate or co-approach for the ablation of diseased (e.g. cancer) tissue. Due to their unique optical properties several classes of gold nanoparticles have been engineered for use in NIR and radio-frequency (RF)-based hyperthermic therapy(Chatterjee, Diagaradjane, & Krishnan, 2011; El-Sayed, Huang, & El-Sayed, 2005, 2006; Glazer & Curley, 2010; Huang-Chiao Huang, Barua, Kay, & Rege, 2009; H.C. Huang, K. Rege, & J.J. Heys, 2010; Kennedy et al., 2011; Ma et al., 2009). Externally tunable control of NIR irradiation can be employed to achieve hyperthermic temperatures (>43^{o}) at localized sites, which possesses significant advantages over whole-body hyperthermia. As a result, gold nanoparticles (GNPs) have received increased attention for localized administration of hyperthermia for ablation of cancer cells (Cao, 2004) and bacteria(Cortie, 2004).

Pancreatic carcinoma growth in nude balb/c mice xenografts was inhibited for up to 7 weeks following treatment with intraperitoneal-injected gold nanospheres in concert with radio-frequency field exposure(Glazer et al., 2010). Gold nanoshells consisting of a dielectric core surrounded by an ultra-thin gold shell demonstrate photothermal responses

that are tunable in the NIR region(Averitt, Westcott, & Halas, 1999). Nanoshells are often coated with PEG and in cancer therapy investigations can preferentially localize to tumor sites due to the enhanced permeability and retention (EPR) effect(Maeda, Wu, Sawa, Matsumura, & Hori, 2000). In female non-obese diabetic mice, Hirsch et al. (Hirsch et al., 2003) interstitially injected PEGylated gold nanoshells and following NIR laser irradiation demonstrated irreversible thermal destruction of xenograft canine transmissible venereal tumors. O'Neal et al.(O'Neal, Hirsch, Halas, Payne, & West, 2004) injected PEGylated gold nanoshells intravenously into female albino mice bearing murine colon carcinoma tumors. The mice were tumor free for at least a month following NIR laser irradiation. In a related study, PC3-tumor bearing mice were intravenously injected with PEGylated gold nanoshells and demonstrated 93% tumor regression 3 weeks after NIR laser irradiation. Currently, the most advanced application using gold nanoshells for photothermal therapy is currently in early clinical trials for ablation of recurrent head and neck cancer("Pilot Study of AuroLase(tm) Therapy in Refractory and/or Recurrent Tumors of the Head and Neck,").

Cylindrical gold nanorods possess a transverse absorption at 520nm as well as a longitudinal absorption that is tunable in the NIR region. PEGylated gold nanorods injected intratumorally in nude (nu/nu) mice with subcutaneous squamous cell carcinoma xenographs demonstrated over 96% decrease in average tumor growth following NIR laser irradiation; more than 74% decrease in average tumor growth was observed following intravenous injection(Dickerson et al., 2008). In murine colon cancer models, intravenous injection of PEGylated gold nanorods and NIR irradiation resulted in

survival of approximately 44% of the initial mice population 60 days after treatment (Goodrich et al.).

Hyperthermic treatment is limited by cellular thermotolerance, whereby cells are able to maintain viability due to an array of cell survival responses(Cherukuri, Glazer, & Curley, 2010; Hildebrandt et al., 2002). Combinatorial / synergistic treatments for cancer therapy can be developed by engineering nanoparticles that simultaneously deliver chemotherapeutic drugs in concert with hyperthermic treatment for enhanced ablation of cancer cells. In addition, hyperthermia has been shown to increase tumor tissue perfusion, which allows for easier and deeper absorption of chemotherapeutic drugs in tumor tissue, resulting in greater efficacies between the two treatments. Hyperthermia also lowers tumor resistance to various chemotherapeutic drugs including doxorubicin, cisplatin, bleomycin, nitrosoureas, and cyclophosphamide(Dayanc, Beachy, Ostberg, & Repasky, 2008; Kampinga, 2006; Martirosyan, 2012). As such, potential for higher efficacies of cancer cell ablation can be realized by combining the drug delivery and photothermal therapy properties on gold nanoparticles via a photo-chemotherapy approach. Multiple studies have employed different gold nanoparticle platforms for dual delivery of cancer cell-targeted chemotherapeutics and NIR light-based induction of hyperthermia. For example, the antineoplastic drug doxorubicin, has been loaded into hollow gold nanospheres (J. You, R. Zhang, C. Xong, et al., 2012; J. You, R. Zhang, G. Zhang, et al., 2012), hollow gold nanoshells(C. Wu, Yu, & Chu, 2011), and poly(ethylene glycol)–poly(lactic-co-glycolic acid)–Au half-shell nanoparticles(S.-M. Lee et al., 2011; Park et al., 2009) for simultaneous delivery of the drug and NIR photothermal therapy. Additionally, gold nanoshells on silica nanorattles(H. Liu et al., 2011) have been

investigated for delivery of docetaxel along with simultaneous NIR photothermal therapy. Elastin-like polypeptide (ELP)-gold nanorod nanocomposites have also been investigated for dual delivery of the anti-cancer drug, 17-AAG simultaneously with NIR photothermal therapy(H-C. Huang, Yang, Nanda, Koria, & Rege, 2011).

Doxorubicin (DOX)-loaded thermally sensitive micelles/liposomes were found to accumulate greater in xenograft MDA-MB-49 human tumors in mice following GNR-mediated hyperthermia. Additionally, DOX molecule release was triggered via the hyperthermia, and it was found that the combination of the two treatments resulted in higher tumor growth suppression compared to hyperthermia alone and hyperthermia plus free DOX controls(J. H. Park et al., 2010). In murine fibrosarcoma-bearing mice, tail vein injection was used to administer PEG-grafted gold nanospheres covalently linked with tumor necrosis factor alpha (TNF-α). After hyperthermic treatment (by exposure or tumor and surrounding tissue to water bath), it was found that tumor recession was increased when compared to each treatment alone. More recently, PEG-grafted gold nanospheres have been used for delivery of recombinant Tumor Necrosis Factor-alpha (rhTNF a.k.a CYT-6091) in phase I clinical trials; phase II clinical trials are currently in progress(Libutti et al., 2010).

Although promising, one major limitation of administering hyperthermic treatment is the depth of penetration of NIR light. Currently, penetration depths in soft tissue are limited to approximately 2 cm in the most advanced NIR laser systems(Gu, Chen, Xia, Jeong, & Liu, 2005). This results in applications limited to topical or near-surface conditions. However, alternative techniques have been investigated in order increase potential treatment depths. This includes the use of minimally invasive interventional

techniques, where fibers inserted directly into tumors / tissues are used for administration of laser-based hyperthermic treatment. This approach has been applied to hyperthermic treatment for primary and metastatic liver cancer(Gough-Palmer & Gedroyc, 2008; Vogl, Straub, Eichler, Sollner, & Mack, 2004; Vogl, Straub, Zangos, Mack, & Eichler, 2004) as well as in lung metastases(Rosenberg et al., 2009).

Silver Nanoparticles

Though not as widely studied as gold nanoparticles, applications of silver nanoparticles (AgNPs) in biomedicine have also been explored(Arvizo et al., 2012). AgNPs have been found to be plasmonically superior to gold, however their uses have been limited due to their potential toxicity(S. Singh et al., 2010; Sotiriou & Pratsinis, 2011). However, recent investigations have involved the encapsulation of AgNPs within nanothin silica coatings in order to increase their biocompatibility for increased use(Sotiriou et al., 2011; Sotiriou et al., 2010).

The antibacterial activity of nanoscale silver has resulted in investigations in hospital treatment against microbial infections, burns, diabetic skin ulcers, and medical devices. The antimicrobial spectrum of AgNPs is broader than that of most common antibiotics(C. You et al., 2012). This activity is most widely attributed to release of positively charged silver ions that then bind with negatively charged proteins, RNA, and/or DNA which can limit cell replication(Silver, Phung, & Silver, 2006). Encapsulating silver(1) carbene complexes in nanofibers has shown promising results for sustained and effective silver ion delivery over a long periods of time. This provides bactericidal activity and have primarily been applied for wound-or burn-

dressings(Butorac, Al-Deyab, & Cowley, 2011). Nano-Ag sepiolite, which is a soda-lime glass powder containing monodispersed AgNPs with a low melting point possesses high antibacterial activity as well as antifungal activity(Esteban-Tejada, Malpartida, Esteban-Cubillo, Pecharroman, & Moya, 2009). Additionally, AgNPs have been found to be effective virucidal agents against cell-free and cell-associated viruses. For example, AgNPs have been found to exert anti-HIV activity at early stages of the viral replication. Additionally, they inhibit the post-entry stages of the HIV-1 life cycle(Panacek et al., 2009).

Further studies into the cytotoxicity, antibacterial mechanisms, bio-distribution, organ accumulation, degradation and adverse effects due to AgNP treatment are still needed. It was been widely accepted that AgNPs in high concentrations can cause apoptosis in mammalian cells(L. Wei et al., 2010). This toxicity is attributed to AgNPs facilitating generation of intracellular reactive oxygen species (ROS) that result in oxidative damage to proteins and DNA(Boonstra & Post, 2004; Hsin et al., 2008; Vanwinkle et al., 2009). Despite this, AgNPs have great promise for future applications in biomedicine. They show great antimicrobial properties with no report of resistance effect when used in the clinic to date(C. You, et al., 2012). As characterization and continued investigation into the application of AgNPs progress, it is anticipated that they will find significant application in the biomedicine.

CHAPTER 2

TRANSGENE DELIVERY USING POLY(AMINO ETHER)-GOLD NANOROD ASSEMBLIES

Several novel nanomaterials, including gold nanoparticles, are currently being investigated as carriers for delivery of therapeutic agents (Chinnaiyan, et al., 2006; Cho, et al., 2008; Ghosh, et al., 2008; Heath & Davis, 2008; H. C. Huang, et al., 2011; Jabr-Milane, et al., 2008; Smith, et al., 2008). The plasmonic properties of gold nanorods make them attractive for application in biosensing (Castellana, Gamez, & Russell, 2011; L. Guo, Zhou, & Kim, 2011), imaging (Ding et al., 2007; Ha, Carson, Agarwai, Kotov, & Kim, 2011; Pan et al., 2010), photothermal therapy (Choi et al., 2011; X. H. Huang, El-Sayed, Qian, & El-Sayed, 2006; von Maltzahn et al., 2009), and gene and drug delivery(Braun et al.; C. Chen et al., 2006; Salem, Searson, & Leong, 2003). Effective delivery of exogenous genes using appropriate vehicles is a promising approach towards correction of diseases that are genetic in origin. Despite their high efficacies as delivery vectors, viruses suffer from several limitations including immunogenicity, insertional mutagenesis, and high production costs. Non-viral strategies, particularly those that can simultaneously enable delivery and imaging (‘theranostics’), are attractive alternatives to viral vectors in gene therapy applications (Garnett, 1999; Glover, Lipps, & Jans, 2005; Yi, Hahm, & Lee, 2005).

Gold nanoparticles are promising vectors for non-viral transgene delivery due to their unique optical properties and the ability to modify their surfaces using facile methods (X. Huang, et al., 2009). In addition, gold nanoparticles possess high surface area-to-volume ratios which can facilitate high payload (transgene) carrying capabilities.

Surface functionalization of gold nanoparticles allows for tuning of hydrophobicity and charge, which can enhance transgene expression and decrease cytotoxicity (Ghosh, et al., 2008). Polymers have been investigated for functionalization of gold nanoparticles in several applications, including transgene delivery (A. C. Bonoiu, et al., 2009; Ow Sullivan, et al., 2003; Sandhu, et al., 2002; M. Thomas & A. M. Klibanov, 2003). Polymer-functionalized gold nanoparticles demonstrate increased stability, controllable surface properties, and the capacity for additional surface functionalization which further increases their potential for use in therapeutic applications (Q. Wei, Ji, & Shen, 2008).

We previously employed a cationic polymer synthesized in our laboratory (S. Barua et al., 2009b; Kasman, Barua, Lu, Rege, & Voelkel-Johnson, 2009a) primarily for enhancing the colloidal stability of gold nanorods in biological media (H. C. Huang, K. Rege, & J. J. Heys, 2010). In this study, we describe an investigation into polymer type, plasmid DNA loading, and physicochemical properties of poly(amino ether)-functionalized gold nanorods in determining the efficacy of transgene delivery and expression using these vehicles. Poly(amino ether) or PAE-functionalized GNR (PAE-GNR) assemblies were generated by depositing polyelectrolyte multilayers on cetyltrimethyl ammonium bromide based gold nanorods (CTAB-GNRs); candidates from a cationic poly(amino ether) library recently synthesized in our laboratory were employed in the current study (S. Barua, et al., 2009b). PAE-GNRs are stable in cell culture media, and are also able to bind plasmid DNA by means of electrostatic interactions. PAE-GNRs were employed to successfully deliver plasmid DNA expressing the luciferase reporter protein to human prostate cancer cells; PAE-GNRs based on 1,4C-1,4Bis, a cationic polymer generated in our laboratory demonstrated higher transgene (luciferase)

expression efficacies, and lower or comparable cytotoxicities compared to assemblies generated using 25 kDa poly(ethylene imine) (PEI25k), a current standard for polymer mediated gene delivery.

MATERIALS AND METHODS

Gold Nanorod (GNR) Synthesis. The seed-mediated method (Nikoobakht & El-Sayed, 2003) was used for the synthesis of the gold nanorods (CTAB-GNRs). Briefly, a seed solution was prepared by adding 5 ml of 0.2 M cetyltrimethyl ammonium bromide (CTAB) to 5 ml of 0.0005 M auric acid ($HAuCl_4.3H_20$). The addition of 0.6 ml of iced water-cooled 0.01 M sodium borohydride was used to reduce the solution. The growth solution was prepared by adding 5 ml of 0.001 M auric acid to 5 ml of 0.2 M CTAB containing 250 µl of 0.004 M silver nitrate. The growth solution was reduced by the addition of 70 µl of 0.0788 M L-ascorbic acid. Seed solution (12 µl) was added to the growth solution and continuously stirred for four hours to allow for the generation of the gold nanorods. CTAB-GNRs, with absorbance maxima at different wavelengths between 750-900 nm, were generated by modulating the silver nitrate concentration in the growth solution.

Polymer Synthesis. Polymer synthesis was carried out as described previously (S. Barua, et al., 2009b). Briefly 1,4-cyclohexanedimethanol diglycidyl ether (1,4C) and 1,4-bis(3-aminopropyl) piperazine (1,4Bis), neopentylglycol diglycidyl ether (NPDGE) and diethylenetriamine (DT), and 1 4 butanediol diglycidyl ether (1,4BDGE) and 1,4Bis were reacted in equimolar amounts at room temperature in order to generate 1,4C-1,4Bis, NPGDE-DT, and 1,4BDGE-1,4Bis cationic polymers, respectively. The polymerization reaction was carried out in 20 ml glass scintillation vials for 16 hours. Following the

reaction, polymers were dissolved at a concentration of 10 mg/mL in phosphate-buffered saline (0.01 X PBS) and the solution pH was adjusted to 7.4 using 30% hydrochloric acid in deionized (DI) water in order to compensate for the basicity of the cationic polymer. The extent of polymerization was determined by comparing reactive amine concentrations at initial mixing of monomer reagents (time – 0h) and after 16 hours polymerization using the ninhydrin assay as described previously (S. Barua, et al., 2009b; Kasman, et al., 2009a).

Polymer Molecular Weight Determination. Molecular weights (MWs) of polymers were measured by gel permeation chromatography (GPC) system (Waters 1515) with a refractive index detector (Waters 2414) with ultrahydrogel column (Waters linear) at a flow rate of 1 ml/min at 35°C. Water containing 0.1% trifluoroacetic acid and 40% acetonitrile was used as a mobile phase. Poly (2-vinylpyridine) standards (MW: 3000; 7,000; 12,000; 35,000; 70,000) were used to calibrate the GPC instrument for molecular weight determination.

Generation of Poly(amino ether)-functionalized Gold Nanorod (PAE-GNR) Assemblies. Dispersions of GNRs with an optical density of 0.5 in 1.5 mL microcentrifuge tubes were centrifuged at 6000 rcf for 10 minutes using a Microfuge 18 centrifuge (Beckman Coulter) in order to remove excess CTAB surfactant. The supernatant was removed and the GNRs were redispersed in 100 µL of a poly(styrene sulfonate) (PSS) solution (10 mg/mL in 0.01XPBS; ~1.5 mM salt concentration). This dispersion was immediately sonicated for 30 minutes to allow for the formation of PSS-coated GNRs (PSS-CTAB-GNRs). Excess PSS was removed by centrifugation at 6000 rcf for 10 minutes. PSS-CTAB-GNRs were then redispersed in 300 µL of nanopure water

and 200 µL of different poly (amino ethers) (10 mg/mL in 0.01XPBS) were added to these dispersions which were immediately sonicated for 30 min to allow for the formation of the PAE-coated-PSS-CTAB-GNRs or PAE-GNRs. The PAE-GNRs were finally resuspended in serum-free media in order to monitor their stability and for use in *in vitro* experiments.

Determination of PAE-GNR Stability in Media. PAE-GNRs were prepared as described above and dispersed in serum-free media (SFM). Absorption spectra from 400-999 nm were determined at different times using a temperature-controlled plate reader (BioTek Synergy 2) for up to 48 hours.

Generation and Characterization of Plasmid DNA-loaded PAE-GNR Assemblies. ***Plasmid DNA.*** The pGL3 control vector (Promega Corp., Madison, WI), which encodes for the modified firefly luciferase protein under the control of an SV40 promoter, was used for transgene expression studies. E.coli (XL1 Blue) cells containing the pGL3 plasmid DNA were cultured overnight (16 h, 37 °C, 150 rpm) in 15 mL tubes (Fisher) in 5 mL of Terrific Broth (MP Biomedicals, LLC). The cultures were then centrifuged at 5400*g* and 4°C for 10 min. Plasmid DNA was purified according to the QIAprep Miniprep Kit (Qiagen) protocol and DNA concentration and purity were determined based on absorbance at 260 and 280 nm, determined using a NanoDrop spectrophotometer (ND-1000; NanoDrop Technologies). Plasmid DNA concentrations of 200-300 ng/µL were typically obtained and volumes were adjusted in order to load between 10-200 ng of plasmid DNA on PAE-GNRs prior to transfections.

Plasmid DNA Loading on PAE-GNRs. PAE-GNRs (optical density 0.25 a.u.) were incubated with different amounts (10-200 ng) of pGL3 plasmid DNA in the presence of serum-free media for 30 min leading to the formation of PAE-GNR-pGL3 assemblies. These were centrifuged at 6000 rcf for 10 min, redispersed in serum-free media, and monitored for colloidal stability using the GNR near infrared (longitudinal) absorption peak for up to 6 h (duration of transfection experiments described below) as previously described. The amount of plasmid DNA remaining in the supernatant after centrifugation was determined using ethidium bromide, a DNA intercalating dye. Ethidium Bromide (1 µg of 0.5 mg/ml; Sigma-Aldrich**)** was added to each sample. Solutions were transferred to a black 96 well plate and fluorescence was measured with excitation at 320 nm and emission at 600 nm using a plate reader (BioTek Synergy 2), similar to methods previously described (Boger, Fink, Brunette, Tse, & Hedtick, 2001; K Rege, Shanghui Hu, James A. Moore, Jonathan S. Dordick, & Steven M. Cramer, 2004; Rege et al., 2005a). Known plasmid DNA amounts in solution were used as standards for calibration of the assay.

Determination of Zeta Potential of PAE-GNR Assemblies. Stable PAE-GNR dispersions in SFM were prepared as described above and set to an optical density of 0.25 and co-incubated with 0, 50, or 100 ng of pGL3 plasmid DNA. Dispersions were transferred into folded capillary zeta cells (Malvern). Zeta potential values were determined using a dynamic light scattering machine (Malvern).

PAE-GNR Mediated Transgene Expression in Human Cancer Cell Lines.

Cell Culture. The PC3 human prostate cancer cell line was obtained from the American Type Culture Collection (ATCC, VA). PC3-PSMA human prostate cancer cells (Gong et

al., 1999), were a generous gift from Dr. Michel Sadelain of the Memorial Sloan Cancer Center, New York, NY and were used as received. RPMI 1640 with L-glutamine and HEPES (RPMI-1640 medium), Pen-Strep solution: 10000 units/mL penicillin and 10000 µg/mL streptomycin in 0.85% NaCl, and fetal bovine serum (FBS) were purchased from Hyclone. Serum-Free medium (SFM) consists of RPMI-1640 medium plus 1% Pen-Strep (1000 units/mL penicillin and 1000 µg/mL). Serum containing medium (SCM) consists of SFM plus 10% FBS. Cells were cultured in a 5% CO_2 incubator at 37ºC using RPMI-1640 medium containing 10% heat-inactivated FBS and 1% antibiotics (Pen-Strep).

PAE-GNR Cytotoxicity. Stable PAE-GNR dispersions in SFM were prepared as described above and set to an optical density of 0.25. PC3 or PC3-PSMA human prostate cancer cells were seeded in 24 well plates at a density of 50,000 cells/well and allowed to attach overnight in a 37ºC, 5% CO_2 incubator. Volumes ranging from 5 µL to 100 µL of the PAE-GNRs were added to each well and the final well volume was brought up to 500 µL with serum-free media, such that the final GNR O.D. in each well ranged from 0.0025 to 0.125 A.U, in order to carry out a dose-response study. The cells were then incubated for 6 hours after which the SFM was replaced with SCM. After incubation, cell viability was determined using the 3-(4,5-dimethylthiazol-2-yl)-2,5-diphenyltetrazolium bromide (MTT) cell proliferation assay kit (ATCC CA# 30-1010k). This assay involves the enzymatic conversion of the MTT substrate to purple-colored formazan in metabolically active cells. This activity is widely employed as an indicator of cell viability and proliferation (Hayon, Dvilansky, Shpilberg, & Nathan, 2003); loss of metabolic activity was used as an indirect indicator of loss of cell viability upon PAE-GNR treatment. Following addition of the MTT reagent (2 h at 37 °C), cells were treated with a lysis

buffer from the kit and kept at room temperature in the dark for 2 h in order to lyse cells and solubilize the MTT product. The absorbance of each well was measured using a plate reader (BioTek Synergy 2) at 570 nm to assay for the blue MTT product. For data analysis, absorbance readouts were normalized to the live (untreated) and dead (5 µL of 30% hydrogen peroxide treated) controls.

Transfections. PC3 and PC3-PSMA human prostate cancer cells were cultured as described above. Cells were seeded in 24-well plates (Costar) at a density of 50,000 cells/well and allowed to attach overnight. Sub-toxic amounts of PAE-GNR-pGL3 plasmid assemblies were added to each well in the presence of serum-free media for 6 h. The media was then replaced with serum-containing media for 48 h following which, cells were permeabilized with 150 µL of cell lysis buffer (Promega, Madison, WI). The luciferase activity in cell lysates was measured using a luciferase assay kit (Promega, Madison, WI) in a plate reader (BioTek Synergy 2). The relative light unit (RLU) readouts determined from the assay were normalized with respect to protein concentration in the respective cell lysates, measured using the Pierce BCA Protein Assay Kit (Pierce Biotechnology, Rockford, IL). Transgene expression efficacy was based on luciferase activity in cell lysates, which was expressed as relative light units (RLU) per milligram (mg) (RLU / mg) of protein. Transfection experiments were performed at least in triplicate.

RESULTS AND DISCUSSION

We have previously developed a library of cationic polymers and evaluated them for plasmid DNA delivery and transgene expression in cancer cell lines (S. Barua, et al., 2009b; S. Barua & K. Rege, 2010). Interfacing these poly(amino ethers) with gold

nanorods can eventually lead to multifunctional nanoassemblies that can be employed in transgene delivery, optical / X-Ray CT imaging, and photothermal treatment to cancer cells. In the current work, we describe the generation of poly(amino ether)-gold nanorod (PAE-GNR) assemblies using a layer-by-layer deposition approach (H. C. Huang, et al., 2010). Three recently developed cationic polymers, 1,4C-1,4Bis (M_w=5,076 g/mol), 1,4BDGE-1,4Bis (M_w=16,381 g/mol), and NPGDE-DT (M_w=12,146 g/mol) were employed to generate the assemblies in this study. We chose the 1,4C-1,4Bis polymer since it demonstrated significantly higher transgene expression efficacies compared to 25 kDa poly(ethylene imine) when delivered as polymer: plasmid DNA complexes (polyplexes) (S. Barua, et al., 2009b; S. Barua & K. Rege, 2010). A previously untested but related polymer, 1,4BDGE-1,4Bis, was synthesized and investigated, since the amine monomer (1,4 Bis) in this polymer is the same as that in the 1,4C-1,4Bis polymer and the cross-linking diglycidyl ethers are different between the two. A third polymer, NPGDE-DT, was also included for generating PAE-GNR assemblies; the polymer was used as an unrelated control, since the two constituent monomers are not related to the 1,4C-1,4Bis polymer. We investigated the stability, plasmid DNA loading capacity, and zeta potential of these assemblies followed by an evaluation of their cytotoxicity and transgene expression efficacies in prostate cancer cell lines. PEI-25k-GNR assemblies were investigated as controls in this current study, since this polymer is widely used as a standard for polymeric gene delivery. In the following studies, the maximum longitudinal (NIR) optical density (O.D.) for the PAE-modified gold nanorod assemblies is used as an indication of concentration. Using inductively coupled plasma optical emission spectrometry (ICP-OES) we found a linear relationship between O.D. and gold

concentration (**Figure 2.1**) for gold nanorods with a maximum longitudinal absorption peak at both 750 and 800 nm, indicating that the peak NIR O.D. was an excellent surrogate for gold / GNR concentration.

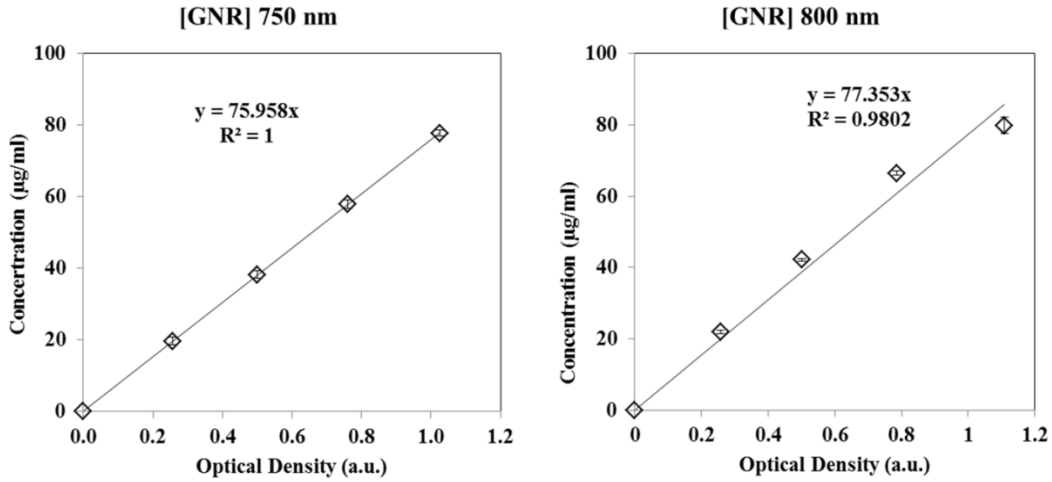

Figure 2.1. *Linear relationship between GNR optical density and concentration determined by ICP-OES*

Stability of PAE-GNRs. Previous results indicated that GNR-based assemblies were less stable in phosphate-buffered saline (PBS) and serum-free medium (SFM) compared to DI water and serum-containing media (H. C. Huang, et al., 2010). The optical stability of different PAE-GNRs dispersed in serum-free media (SFM, RPMI-1640) was therefore investigated. As seen in **Figure 2.2**, minimal loss of the longitudinal peak in the NIR region was observed for all PAE-GNR dispersions following the six-hour incubation period in media, which is particularly promising since cells are transfected over this period of time. Less than 20% loss was observed in the longitudinal peak after incubating PAE-GNRs for 48h, indicating that PAE-GNRs were generally stable in dispersion over this duration; it is possible that a small fraction of PAE-GNR assemblies aggregates and precipitates over the 48 h duration.

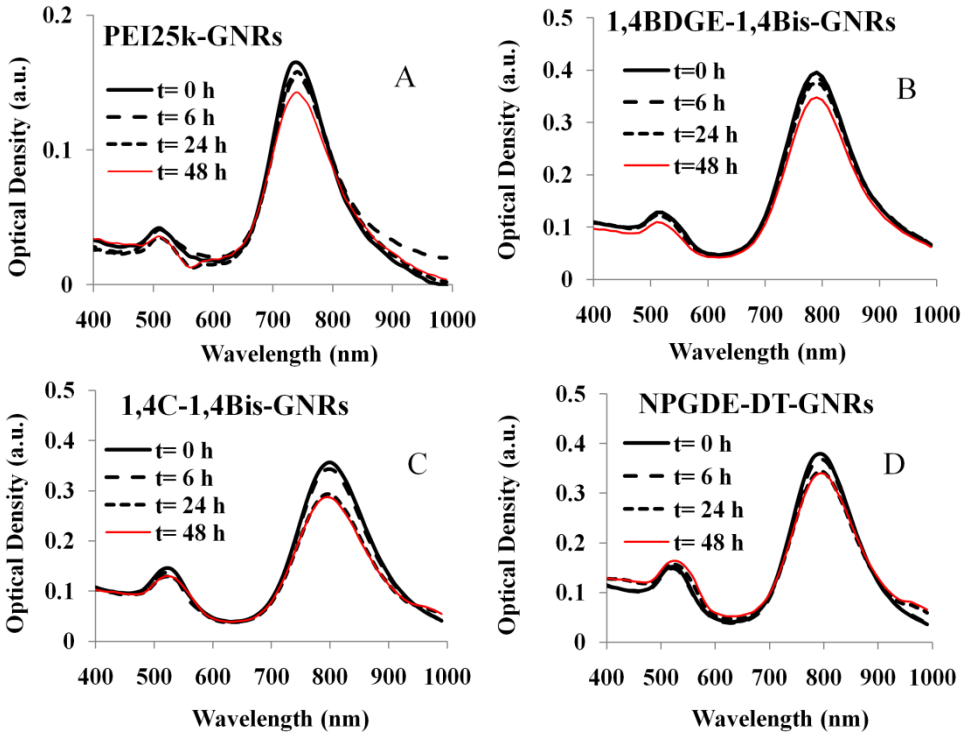

Figure 2.2. *Optical stability of (A) PEI25k-GNRs, (B) 1,4BDGE-1,4Bis-GNRs, (C) 1,4C-1,4BisGNRs (D) NPGDE-DT-GNRs dispersed in serum-free media. Absorbance spectra were monitored from 400 to 999 nm for up to 48 h.*

PAE-GNR Assemblies Exhibit Similar or Reduced Cytotoxicities Compared to PEI25k-GNR Assemblies. The cytotoxicities of the different PAE-GNRs were investigated with PC3 and PC3-PSMA human prostate cancer cells; PEI25k-GNR assemblies were used as controls. It was found that 1,4C-1,4Bis-GNRs and 1,4BDGE-1,4Bis-GNRs resulted in lower loss of PC3 cell viability compared to those generated with PEI25k (**Figure 2.3a**). NPGDE-DT-GNRs exhibited a greater loss of cell viability compared to PEI25k-GNRs. A similar observation was seen with the PAE-GNRs in PC3-PSMA cells at lower PAE-GNR concentrations. At lower concentrations, 1,4C-1,4Bis-GNRs and 1,4BDGE-1,4Bis-GNRs had similar or less loss of cell viability as compared

to PEI25k-GNRs (**Figure 2.3b**), indicating some variability based on the cell line under investigation. As was seen in PC3 cells, NPGDE-DT-GNRs exhibited the highest loss of cell viability of the PAE-GNR assemblies that were tested. It is important that some polymers chosen from our library possess similar if not lesser cytotoxicities than PEI25k (Vicennati, Giuliano, Ortaggi, & Masotti, 2008), since it may be possible to deliver higher amounts of plasmid DNA with higher doses of these PAE-GNRs. For purpose of use in further experiments in this study, a loss of cell viability of 30% was deemed as the upper limit of cytotoxicity that could be tolerated.

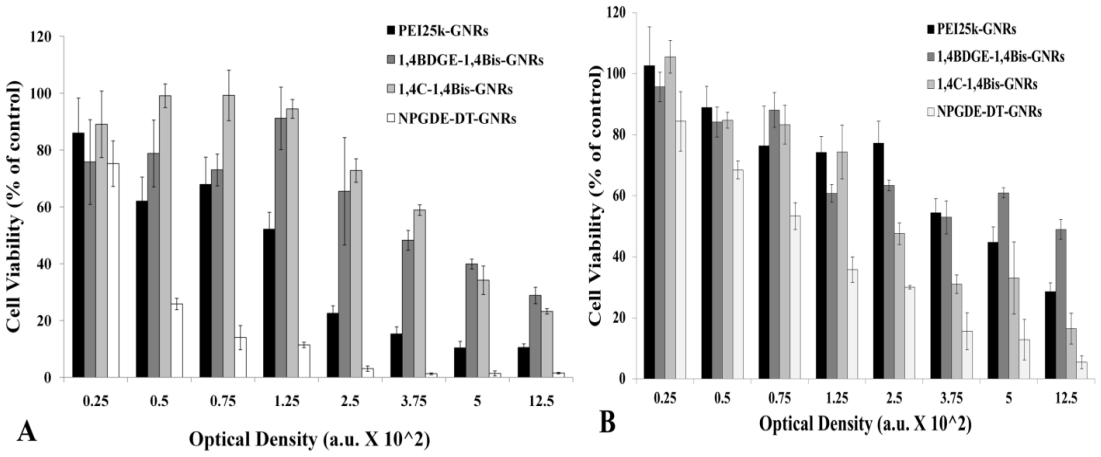

Figure 2.3 *– Cytotoxicity of PEI25k-GNRs and PAE-GNRs towards (A) PC3 and (B) PC3-PSMA cells as determined using the MTT assay. Cell viability is reported as percentage of untreated cells (control).*

Plasmid DNA Loading onto PAE-GNRs. Cationic polymers have been increasingly used as non-viral vehicles for delivering nucleic acids into a variety of mammalian cells (Kulkarni, Mishra, Fraser, & Davis, 2005; Lou, Peng, Chen, Wang, & W., 2009). Given their ability to deliver plasmid DNA into cells (S. Barua, et al., 2009b; S. Barua & K. Rege, 2010), we hypothesized that poly(amino ethers) generated in our laboratory would exhibit similar efficacies following functionalization on GNRs. The

pGL3 plasmid DNA was incubated with PAE-GNRs for 6 h in order to determine plasmid DNA binding efficacies of the assemblies. Following centrifugation, the supernatant was tested for plasmid DNA content using an ethidium bromide-based fluorescence assay. Ethidium bromide is a DNA intercalating dye which is commonly used as a stain for nucleic acids and to determine DNA content (Geall & Blagbrough, 2000). As seen in **Table 2.1**, all PAE-GNRs were found to bind and retain greater than or equal to 97% of the initially loaded plasmid DNA for plasmid DNA loadings up to 100 ng. These results indicate that poly(amino ether)-based PAE-GNRs strongly bind plasmid DNA and minimal, if any, losses of loaded plasmid DNA are anticipated for the duration of the transgene delivery experiments with PAE-GNR assemblies. As a result of these high loadings (>97%) in all cases, the amount of pGL3 plasmid DNA loaded on PAE-GNRs was approximated to be the same as that used initially in the loading experiments (i.e. 100% loading was assumed).

Table 2.1 *– Percentage of pGL3 plasmid DNA loading on PEI25k-GNRs and PAE-GNRs for initial DNA amounts of 50 ng and 100 ng. Data are presented as mean values ± one standard deviation.*

Polymer-Modified GNRs	**pGL3 Plasmid DNA Loaded (% of initial)**	
	50 ng	**100 ng**
PEI25k-GNRs	97.0 ± 1.3	98.4 ± 0.3
1,4BDGE-1,4Bis-GNRs	98.1 ± 1.1	99.2 ± 0.9
1,4C-1,4Bis-GNRs	99.0 ± 0.8	96.9 ± 1.2
NPGDE-DT-GNRs	100 ± 0.7	98.3 ±1.8

1,4C-1,4Bis-GNRs and 1,4BDGE-1,4Bis-GNRsPAE-GNRs, loaded with different amounts of plasmid DNA, were dispersed in SFM and the absorption spectra of the assemblies were monitored for 6 h in order to determine their colloidal stability over the period that they are incubated with cells for transgene delivery. Minimal changes were observed in the longitudinal peak of PAE-GNRs. In the cases of 1,4C-1,4Bis-GNRs and 1,4BDGE-1,4Bis-GNRs after loading of 50 ng (**Figure 2.4c and b respectively**) and 100 ng plasmid DNA (**Figure 2.4g and f respectively**), the longitudinal peak was slightly higher by approximately 0.01 A.U. at 6 h compared to 0 h. This increase in the longitudinal peak is likely within limits of experimental error and may be explained by some evaporation of the media during experimental conditions. In contrast, the maximal longitudinal absorption peak decreased and the spectrum broadened in case of PEI25k-GNRs and NPGDE-DT-GNRs upon incubation for six hours after loading 50 ng (Figure 3a and d respectively) and 100 ng of plasmid DNA. This is most likely due to aggregation of these assemblies following plasmid DNA loading, which leads to a reduction in the stabilizing cationic charge due to the surface PAE layer. Despite these modest changes in the absorption spectrum following addition of plasmid DNA, the stability is sufficient for these assemblies to be useful for transgene delivery.

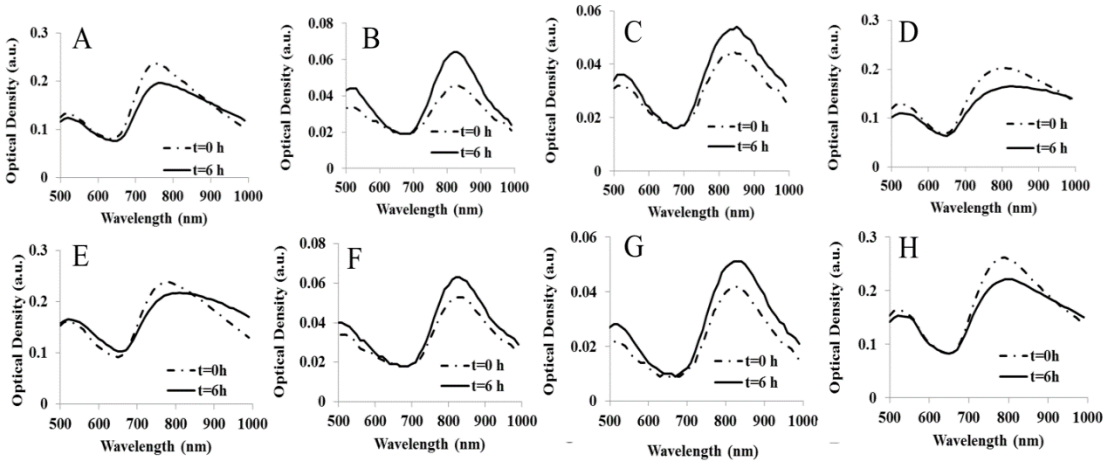

Figure 2.4. *Optical stability of PEI25k-GNRs with (a) 50 ng pGL3 DNA, 1,4BDGE-1,4Bis-GNRs with (b) 50 ng pGL3 DNA, 1,4C-1,4Bis-GNRs with (c) 50 ng pGL3 DNA, NPGDE-DT-GNRs with (d) 50 ng pGL3 DNA, PEI25k-GNRs with (e) 100 ng pGL3 DNA, 1,4BDGE-1,4Bis-GNRs with (f) 100 ng pGL3 DNA, 1,4C-1,4Bis-GNRs with (g) 100 ng pGL3 DNA, and NPGDE-DT-GNRs with (h) 100 ng pGL3 DNA.*

Zeta potentials of PEI25k-GNRs and PAE-GNR assemblies with and without plasmid DNA were determined (**Figure 2.5**) in order to further investigate their stability. In the absence of plasmid DNA, all PAE-GNRs possessed a positive zeta potential greater than 10 mV, with 1,4C-1,4Bis-GNR assemblies demonstrating the highest value of approximately 17 mV. The positive zeta potential value indicates that the cationic polymer coating is in fact on the outermost layer of the PAE-GNRs. Addition of 50 ng plasmid DNA resulted in a reduction of zeta potential of all assemblies except those based on PEI25k-GNRs. This decrease can be explained by the shielding of the initial positively charged coating polymer by negatively charged DNA. Further addition of plasmid DNA (100 ng) caused a charge reversal in all PAE-GNRs, except for those based on the 1,4C-1,4Bis-polymer which decreased but remained positive. This observation suggests that increased coverage of the PAE-GNR surface with plasmid DNA leads to a

charge reversal of these assemblies. As shown previously, 1,4C-1,4Bis-GNR assemblies bind and retain over 98% of plasmid DNA. Although we did not test this further, the lack of charge reversal most likely indicates that higher amounts of plasmid DNA can be loaded onto this PAE-GNR. However, it is desirable to have the PAE-GNRs retain a net positive charge after addition of plasmid DNA, since excess positive charge can facilitate interactions with negatively charged cell surfaces, leading to efficacious cellular uptake of the PAE-GNR-pGL3 assemblies and expression of the delivered transgene.

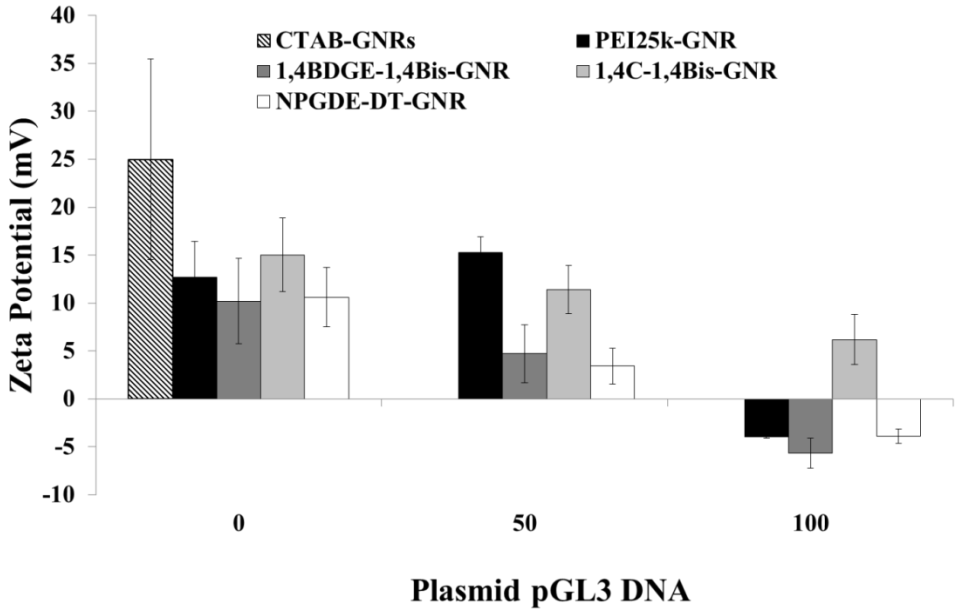

Figure 2.5. *Zeta potential measurements of PAE-GNRs and PEI25k-GNRs at an optical density of 0.0025 a.u. with and without pGL3 plasmid DNA. As the loaded plasmid DNA amount increases zeta potential decreases due to the anionic nature of DNA.*

PAE-GNR Mediated Delivery of Plasmid DNA to Prostate Cancer Cells *in vitro.* PC3 and PC3-PSMA human prostate cancer cells were treated with sub-toxic concentrations of PAE-GNRs and PEI25k-GNRs loaded with 10-200 ng of pGL3 plasmid DNA, in order to determine the efficacy of different PAE-GNRs for transgene expression. The final GNR O.D. was maintained at 0.0025 in each well since PAE-GNRs

were not toxic to cells under these conditions. This was carried out to ensure that only plasmid DNA amounts changed, while maintaining the same amount of GNRs across these experiments.

A dose-dependent trend was observed for luciferase expression (absolute RLU/mg values) in both PC3 (**Figure 2.6a**) and PC3-PSMA cells (**Figure 2.6b**). Luciferase expression was found to be maximal typically between 40 ng and 60 ng of loaded pGL3 DNA, after which, it declined slightly and leveled off to a lower value. This observed trend is likely due to an optimized condition in which both, the amount of plasmid DNA, as well as net positive surface charge of the PAE-GNRs allow for sufficient cellular interaction and uptake for transgene expression. This is supported by the previously described observation; at a loading of 50 ng pGL3 plasmid, all PAE-GNRs still exhibited a positive zeta potential. The decline in luciferase expression with pGL3 plasmid DNA loadings greater than 60 ng correlates with zeta potential data, which indicated reduced but positive zeta potential for 1,4C-1,4Bis-GNRs and negative zeta potential values for PEI25k-GNRs, 1,4BDGE-1,4Bis-GNRs and NPGDE-DT-GNRs (e.g. at 100 ng plasmid DNA in **Figure 2.5**). This can result in repulsion of PAE-GNR-pGL3 assemblies from negatively charged cell surfaces leading to reduced uptake and lower levels of transgene expression. It is likely that further increase in the amount of plasmid DNA on PAE-GNRs may completely shield the positive charges present on the outermost layer of the PAE-GNRs resulting in further decline of transgene expression. Although PAE-GNRs are able to bind significant amounts of plasmid DNA, increasing loading results in decrease in the zeta potential of these nanoassemblies, which reduces their efficacies for transgene expression.

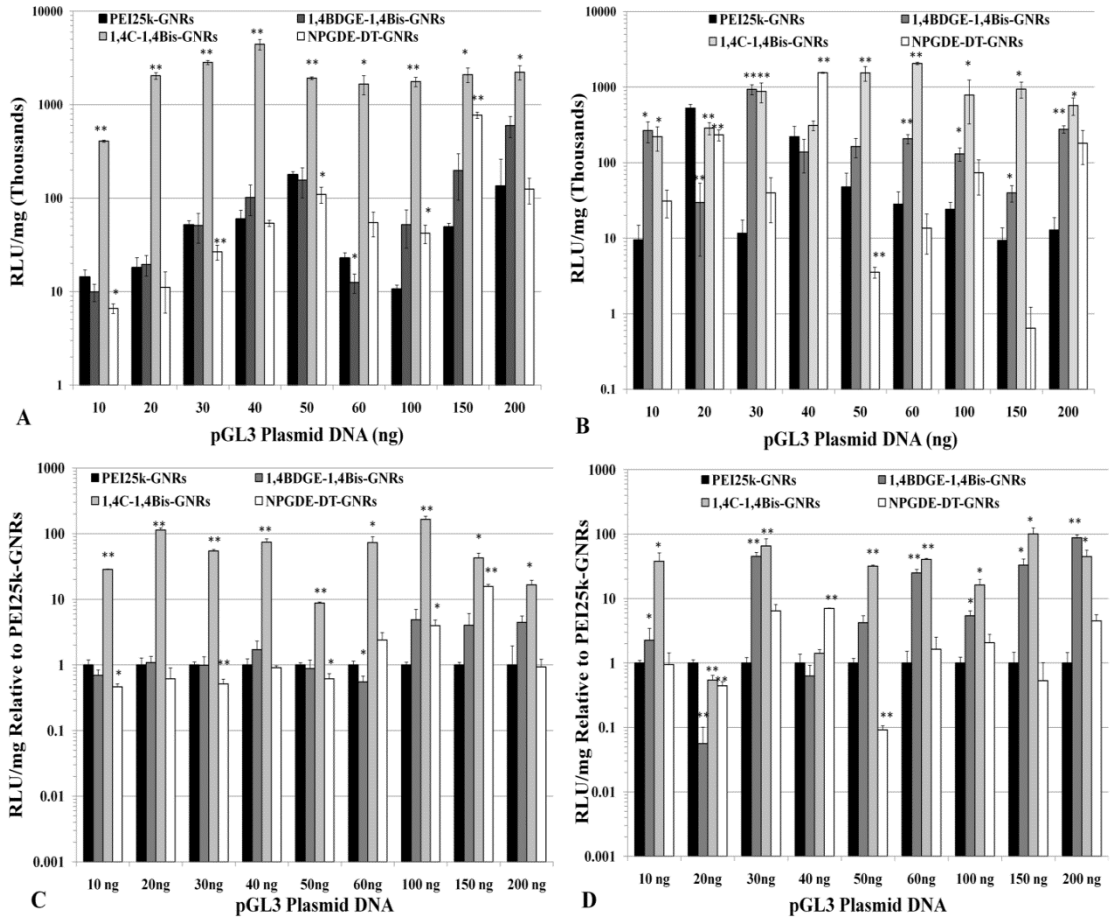

Figure 2.6 – *Absolute values of transgene (luciferase) expression in (A) PC3 and (B) PC3-PSMA cells with PEI25k-GNRs and PAE-GNRs at an optical density of 0.0025 a.u. loaded with different amounts of pGL3 plasmid DNA (ng). Transgene (luciferase) expression in (C) PC3 and (D) PC3-PSMA reported relative to PEI25k-GNRs (* $p<0.05$; ** $p<0.01$; Student t-test). Luciferase expression, in relative luminescence units (RLU) was analyzed 48 h post transfection and normalized to total protein content (mg) resulting in RLU /mg values.*

It was observed that 1,4C-1,4Bis-GNR-pGL3 assemblies exhibited up to 165-fold enhanced luciferase expression in PC3 cells (**Figure 2.6c**) and up to 100-fold enhanced luciferase expression in PC3-PSMA cells (**Figure 2.6d**) compared to those based on PEI25k-GNRs. The highest enhancements compared to 25kDa pEI were observed for plasmid DNA loadings of 100 ng and 150 ng for PC3 and PC3-PSMA cells, respectively.

These statistically significant levels of enhancement in luciferase expression can be partially attributed to the zeta potentials of the respective PAE-GNRs. For example, in case of PC3 cells, 1,4C-1,4Bis-GNR-plasmid DNA assemblies retain a net positive charge compared to those for PEI25k, which exhibit a charge reversal (**Figure 2.5**). Furthermore, these findings are consistent with previous observations that transgene expression with 1,4C-1,4Bis-pGL3 polyplexes (polymer-plasmid DNA complexes) was higher than that observed with PEI25k (S. Barua, et al., 2009b; S. Barua & K. Rege, 2010). These results are significant since polymers which demonstrate high efficacies for transgene expression as polyplexes can be interfaced with gold nanorods without compromise of efficacy. Other PAE-GNRs exhibited similar or statistically significant higher levels of luciferase expression compared to PEI25k-GNRs in both, PC3 and PC3-PSMA cell lines, indicating that polymer candidates from our library result in significantly higher or at least comparable efficacies to that seen with PEI25k.

Higher doses of plasmid DNA-loaded 1,4C-1,4Bis-GNR and PEI25k-GNR assemblies were employed in order to investigate if higher levels of luciferase expression could be achieved by increasing the dose of plasmid DNA-loaded PAE-GNRs delivered. Doses of up to 0.01 a.u. PAE-GNR optical densities and those that exhibited less than 30% loss of cell viability in both, PC3 and PC3-PSMA cells, were employed. As previously mentioned, the linear relationship between maximum longitudinal O.D. and gold concentration facilitates the use of O.D. as a surrogate for GNR concentration under these conditions. A ratio of plasmid DNA to PAE-GNR of 50 ng to 0.0025 a.u. (GNR optical density in absorbance units) was chosen based on the optimal pGL3 plasmid range between 40ng to 60 ng described previously. The 1,4C-1,4Bis-GNR and PEI25k-

GNR concentration and plasmid DNA loaded used were both doubled to 0.005 a.u. and 100 ng, respectively and quadrupled to 0.01 a.u. and 200 ng plasmid DNA, respectively in order to maintain the same optimal PAE-GNR to DNA ratio, while simultaneously increasing the amounts of plasmid DNA as well as PAE-GNRs. It was observed that increased PAE-GNR concentrations and pGL3 plasmid amount did not result in increased luciferase expression for cells treated with 1,4C-1,4Bis-GNRs. However, in case of PEI25k-GNR-pGL3 assemblies, luciferase expression rose up by approximately 12- and 18-fold in PC3 (**Figure 2.7a**) and PC3-PSMA (**Figure 2.7c**) cells, respectively compared to PEI25k-GNR-pGL3 assemblies with 50 ng plasmid DNA and O.D. of 0.0025 a.u. As a result, the expression of 1,4C-1,4Bis-GNRs relative to PEI25k-GNRs showed lower values (**Figure 2.7b and 2.7**). It is likely that transgene expression with PAE-GNRs based on the 1,4C-1,4Bis polymer is already at a maximum at the previously used lower concentrations, and therefore, higher plasmid DNA amounts do not enhance this efficacy. Although higher concentrations of PEI25k-GNRs, resulted in increased transgene expression, lower amounts of plasmid DNA were required in case of 1,4C-1,4Bis-GNR assemblies compared to PEI25k-GNR assemblies in order to obtain similar levels of transgene expression.

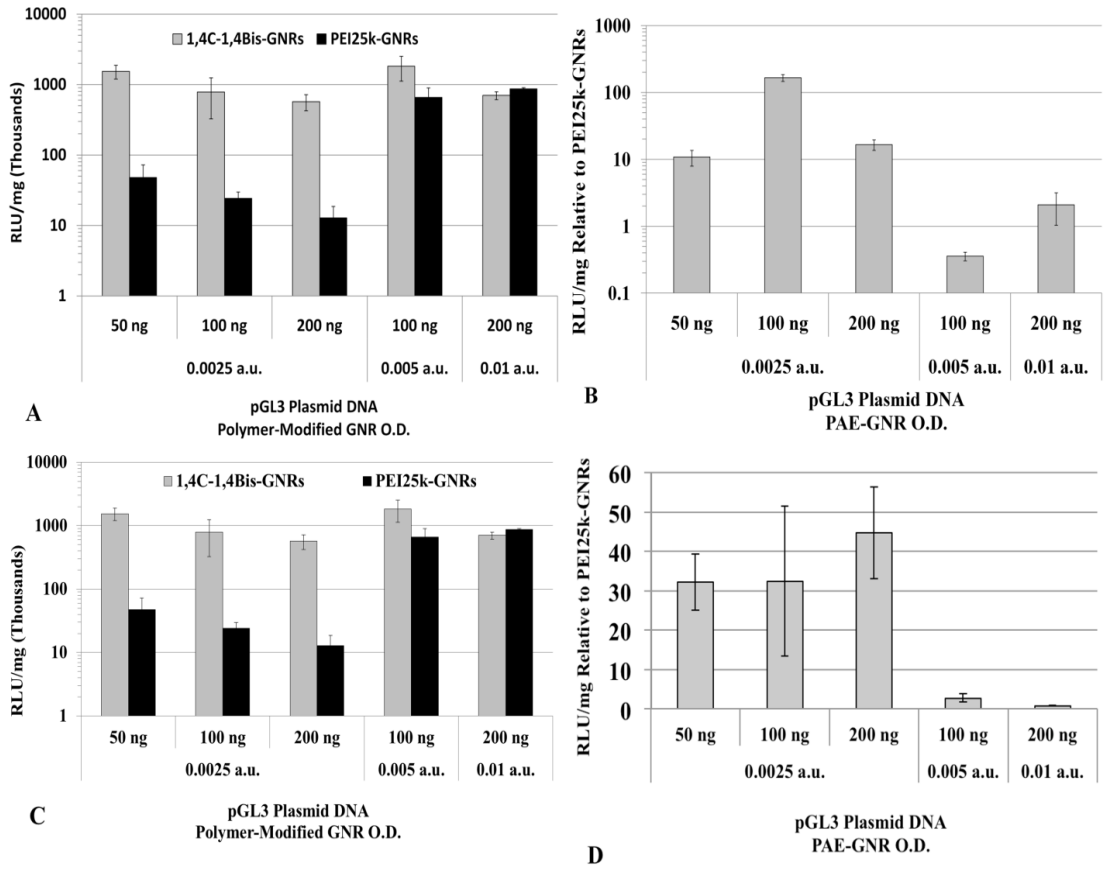

Figure 2.7 *– Transgene expression with higher concentrations of PAE-GNRs used for transfection. Luciferase expression values for 1,4C-1,4Bis-GNRs are reported as absolute values for (A) PC3 and (C) PC3-PSMA human prostate cancer cells and relative to PEI25k-GNRs for (B) PC3 and (D) PC3-PSMA cells. Luciferase expression, in relative luminescence units (RLU) was analyzed 48 h post transfection and normalized to protein content (RLU /mg).*

Plasmid DNA (50 ng pGL3)-loaded 1,4C-1,4Bis-GNRs were evaluated for efficacy of transgene expression in serum-containing media. It was found that the absolute RLU/mg expression values in SCM decreased by approximately 10-fold of that observed in PC3 cells (**Figure 2.8a**) and by approximately 3-fold in PC3-PSMA cells (**Figure 2.8b**) in the absence of serum. A drop in transgene expression can be expected since interactions of these assemblies with serum proteins can result in lower efficacies

(H.-C. Huang, et al., 2009). However, the observed levels transgene expression in presence of serum indicate that PAE-GNRs may be viable candidates for further investigations for combined imaging and transgene delivery in vivo.

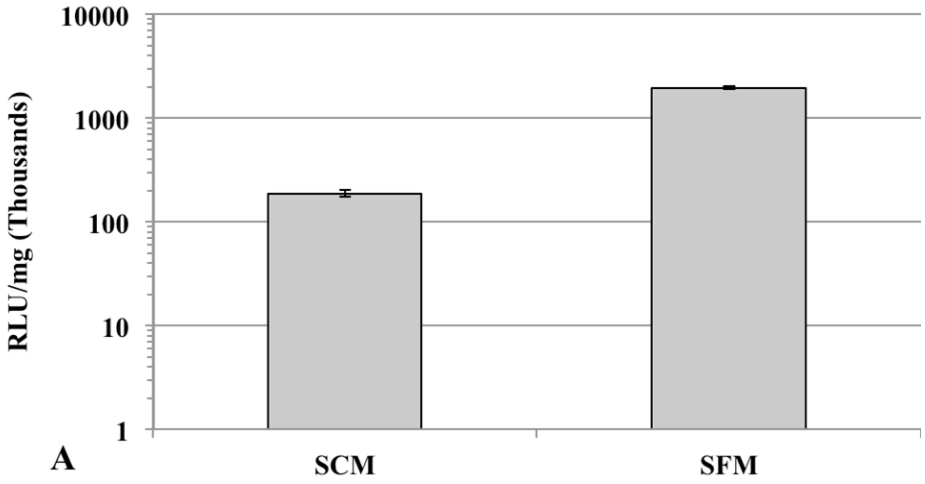

Figure 2.8 *– Comparison of 1,4C-1,4Bis-GNR mediated luciferase expression in (A) PC3 and (B) PC3-PSMA cells in serum-containing media (SCM) and serum-free media (SFM). The optical density of gold was set at 0.0025 and PAE-GNRs loaded with 50 ng pGL3 DNA were employed in all experiments. Values are reported in relative luminescence units (RLU) 48 h post transfection and normalized to protein content (RLU /mg).*

CONCLUSIONS

We have synthesized PAE-GNRs using select candidates from a cationic polymer library recently synthesized in our laboratory. These PAE-GNRs are stable in media and demonstrate the capacity to bind to plasmid DNA. Subtoxic concentrations of PAE-GNRs demonstrated the ability to mediate transgene delivery and expression in two prostate cancer cell lines. PAE-GNRs based on one of our cationic polymers, the 1,4C-1,4Bis polymer, demonstrated higher transgene expression efficacy and lower cytotoxicity when compared to PEI25k-GNR assemblies. Our results indicate that

engineering PAE-GNRs leads to a gold-based nanoassembly that combines high stabilities, low cytotoxicities, and the ability to deliver transgenes to cancer cells. These PAE-GNRs also have the potential to be used for photothermal ablation, photothermally enhanced delivery, optical imaging, further surface functionalization, and for carrying other anionic (bio)molecules for delivery to cells, making them a powerful theranostic platform.

CHAPTER 3

POLY(AMINOETHER)-GOLD NANOROD ASSEMBLIES FOR SHRNA PLASMID-INDUCED GENE SILENCING

Gene silencing using RNA interference (RNAi) is a promising therapeutic approach against several diseases (D. Kim & Rossi, 2009; Y. P. Liu et al., 2009; Pecot, Calin, Coleman, Lopez-Berestein, & Sood, 2011), and is a useful tool in biotechnology. RNAi involves formation of an intracellular RNA-induced silencing complex (RISC), which can execute targeted post-transcriptional gene silencing via sequence-specific degradation of mRNAs. Post transcriptional RNAi is characterized by high sequence specificity and potency in silencing gene expression, mediated by 21-25 nucleotide double stranded small interfering RNA (siRNA). Alternatively, expression cassettes (plasmid DNA) can be designed for the intracellular expression of short hairpin RNA (shRNA) molecules, which, after cellular processing, result in the formation of an antisense strand that is specific to the sequence of the target gene(Grimm et al., 2006; M Scherr, Battmer, Ganser, & Eder, 2003). Following delivery of the expression cassette to the nucleus, a primary shRNA transcript containing a RNA "hairpin" loop is transcribed by RNA polymerase II or III. After nuclear processing, shRNA molecules are exported to the cytoplasm where they interact with the dicer protein. Dicer cleaves the hairpin loop, resulting in the formation of double stranded RNA molecules. These molecules act in a similar fashion to siRNA molecules, which are small (~21 base pair) double-stranded RNA molecules. The processed shRNA then interacts with a group of proteins, resulting in the formation of the RNA-induced silencing complex (RISC). In cases of both, shRNA

transcript formation and cytoplasmic siRNA delivery, RISC formation enzymatically cleaves the target mRNA transcript, thus silencing protein expression by preventing translation(Rao, Vorhies, Senzer, & Nemunaitis, 2009). Studies have shown the potential of RNAi for use in targeting tumor cell growth(Uchida et al., 2004), metastasis(Duxbury, Ito, Zinner, Ashley, & Whang, 2004), angiogenesis(Takei, Kadomatsu, Yuzawa, Matsuo, & Muramatsu, 2004), and chemoresistance(A. Singh et al., 2008) which are all critical components of tumor growth; pre-clinical studies have also showed promise of RNAi for silencing cancer-related targets(M. Scherr et al., 2003; G. Yang, Cai, Thompson-Lanza, Bast Jr, & Liu, 2004).

Naked / uncomplexed nucleic acids demonstrate poor efficacies of passive entry into cells and are easily degraded by endogenous nucleases, which necessitates their delivery via viral or non-viral methods (Bartlett, Su, Hildebrandt, Weber, & Davis, 2007). Several delivery methods, including viruses, have been investigated as vehicles for silencing genes in mammalian cells. However, safety concerns related to viral vectors have prompted discovery and evaluation of non-viral vectors, including those based on polymers and nanoparticles, for delivering nucleic acids for gene silencing(A. C. Bonoiu, et al., 2009; G. et al., 2009; Kesharwani, Gajbhiye, & Jain, 2012; Yezhelyev, Qi, O'Regan, Nie, & Gao, 2008).

The emergence of novel nanomaterials has led to new options for delivery of therapeutic and imaging agents(Ghosh, et al., 2008; H. C. Huang, et al., 2011; T. Wang, Mancuso, Kazmi, et al., 2012). Nanoscale vehicles that possess simultaneous delivery and imaging capabilities are attractive theranostic vectors for administration of exogenous nucleic acids(Garnett, 1999; Glover, et al., 2005; Yi, et al., 2005). Gold

nanoparticles have been investigated for delivery of nucleic acids(Conde et al., 2012; Chu Hu, Peng, Chen, Zhong, & Zhuo, 2010; S. T. Kim et al., 2012b; Ramos & Rege, 2012b; Lucas Vu, James Ramos, Thrimoorthy Potta, & Kaushal Rege, 2012) as well as chemotherapeutic drugs(Ramos, Taylor, & Rege, 2012), for different applications in biotechnology and medicine. In addition, their optical properties, high surface-area-to-volume ratios, biocompatibility, and ease of surface functionalization(X. Huang, et al., 2009) make gold nanoparticles attractive in simultaneous delivery and imaging (i.e. theranostics) applications. Functionalization of gold nanoparticles allows for tunable control of hydrophobicity, size, and charge, which can enhance payload delivery and decrease cytotoxicity(Ghosh, et al., 2008). In particular, polymers are attractive candidates for functionalizing surfaces of gold nanoparticles, and have been investigated in several applications, including nucleic acid delivery(A. C. Bonoiu, et al., 2009; Song, Du, Sun, Zhang, & Wang, 2010; M. Thomas & A. M. Klibanov, 2003). Gold nanorods (GNRs), have been widely investigated in (bio)sensing(Castellana, et al., 2011; L. Guo, et al., 2011; H. C. Huang et al., 2008), imaging(Ding, et al., 2007; Ha, et al., 2011; Pan, et al., 2010), photothermal therapy(Choi, et al., 2011; X. H. Huang, et al., 2006; von Maltzahn, et al., 2009), and gene and drug delivery(Braun, et al.; C. Chen, et al., 2006; Salem, et al., 2003). Two-photon induced luminescence in GNRs has been shown to be highly efficient, both in vitro and in vivo(Durr, et al., 2007). In addition, due to their ability to absorb near infrared (NIR) light, excitation wavelengths in this region can be used in vivo due to minimal tissue scattering and phototoxicity(J.-L. Li & Gu, 2010; H. F. Wang, et al., 2005).

We have recently described the use of combinatorial methods for generating libraries of linear polyamine-derived poly(aminoether) (PAE) cationic polymers(S. Barua, et al., 2009b; S. Barua et al., 2011b; Lucas Vu, et al., 2012) for transgene expression following delivery of plasmid DNA, as well as for enhancing adenoviral delivery to cells resistant to viral transduction(Kasman, et al., 2009a). In these studies, the PAE synthesized from 1,4-cyclohexanedimethanol diglycidyl ether (1,4C) and 1,4-bis(3-aminopropyl) piperazine (1,4Bis) or 1,4C-1,4Bis emerged as a lead candidate for non-viral transgene expression following plasmid DNA delivery. 1,4C-1,4Bis had comparable molecular weight values (M_n=3.9 kDa, M_w=23.5 kDa, and polydispersity (PD)=5.96) when compared to branched pEI25k (M_n=10 kDa, M_w=25 kDa, and PD=2.5). This polymer demonstrated lower cytotoxicity and higher transgene expression efficacy than pEI25k at higher polymer to plasmid DNA ratios(S. Barua, et al., 2009b) in PC3-PSMA prostate cancer cells when compared to branched pEI25k. In a previous study, gold nanorods were coated with polymers from this library using a layer-by-layer deposition approach (**Figure 3.1**), resulting in PAE-GNR nanoassemblies(H.-C. Huang, et al., 2009; Lucas Vu, et al., 2012) capable of transgene delivery, hyperthermia, and two-photon induced luminescence imaging. We previously reported that plasmid DNA-loaded PAE-GNR nanoassemblies, based on the 1,4C-1,4Bis polymer (i.e. 1,4C-1,4Bis-GNR nanoassemblies), demonstrated higher luciferase expression efficacy and lower cytotoxicity in PC3 prostate cancer cells *in vitro* when compared to PEI25k-GNR nanoassemblies(Ramos & Rege, 2012b). Based on these findings, 1,4C-1,4Bis-GNR assemblies (‘nanoassemblies’) were investigated for delivery of plasmids that express shRNA molecules (‘shRNA plasmids’) for silencing genes in prostate cancer cells in the

current study. While several strategies, including those based on gold nanoparticles have been explored for siRNA delivery(A. Bonoiu, et al., 2011; A. C. Bonoiu, et al., 2009; Mahajan, et al., 2012; Masood, et al., 2012; W. Zhang, et al., 2011), non-viral strategies for shRNA plasmid delivery are largely under-explored despite several potential advantages of this approach. In this study, we demonstrate the efficacy of PAE-GNR nanoassemblies for the delivery of shRNA plasmids for gene silencing, and additionally examine their theranostic potential for live-cell imaging using two-photon induced luminescence facilitated by gold nanorods.

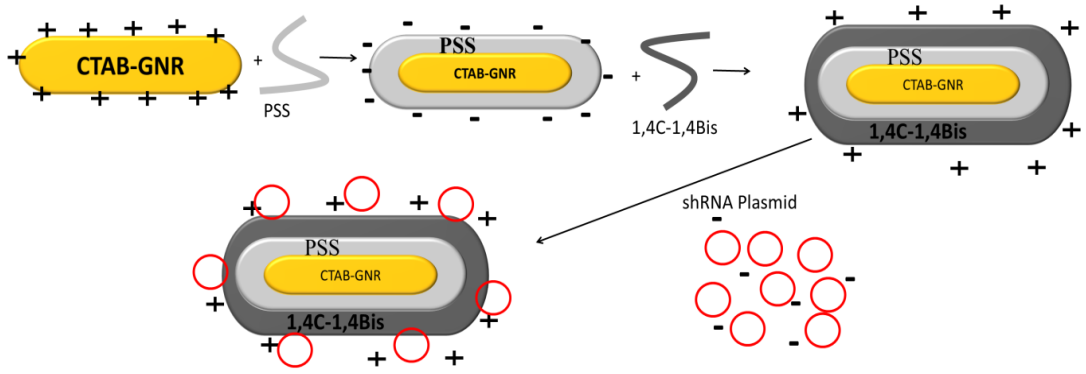

Figure 3.1. *Simplified schematic of nanoassembly generation and shRNA plasmid loading. Positively charged CTAB-templated GNRs are first modified with an anionic polymer, poly(styrene sulfonate) or PSS coat via electrostatic interactions, resulting in PSS-GNR nanoassemblies with a net negative charge. PSS-GNRs are then coated with a cationic 1,4C-1,4Bis poly(amino ether) resulting in positively charged nanoassemblies. This then allows for loading of anionic shRNA plasmids on the nanoassemblies for gene silencing.*

MATERIALS AND METHODS

Generation of Gold Nanorods (GNRs) . The seed-mediated method(Johnson, Dujardin, Davis, Murphy, & Mann, 2002; Nikoobakht & El-Sayed, 2003) was used for the synthesis of cetyltrimethyl ammonium bromide (CTAB)-templated gold nanorods (CTAB-GNRs). Briefly, a seed solution was prepared by adding 5 ml of 0.2 M CTAB to

5 ml of 0. 5 mM auric acid ($HAuCl_4.3H_20$). Iced water-cooled 10 mM sodium borohydride (0.6 ml) was added to reduce the solution. The growth solution was prepared by adding 5 ml of 1 mM auric acid to 5 ml of 0.2 M CTAB containing 250 µl of 4 mM silver nitrate. The growth solution was reduced by the addition of 70 µl of 0.0788 M L-ascorbic acid. Seed solution (12 µl) was added to the growth solution and continuously stirred for four hours to allow for the generation of the gold nanorods. The concentration of silver nitrate in the growth solution was modulated in order to generate CTAB-GNRs, with absorbance maxima at different wavelengths (750-900 nm) in the near infrared (NIR) region of the absorption spectrum.

Synthesis of the 1,4C-1,4Bis poly(aminoether). Synthesis of the 1,4C-1,4Bis polymer was carried out as described previously(S. Barua, et al., 2009b). Briefly 1,4-cyclohexanedimethanol diglycidyl ether (1,4C) and 1,4-bis(3-aminopropyl) piperazine (1,4Bis) were reacted in equimolar amounts at room temperature in 20 mL glass scintillation vials for 16 h leading to the generation of the 1,4C-1,4Bis polymer. Following the reaction, polymers were dissolved at a concentration of 10 mg/mL in phosphate-buffered saline (0.01 X PBS), and the solution pH was adjusted to 7.4 using 30% hydrochloric acid in deionized (DI) water in order to compensate for the basicity of the cationic polymer. The extent of polymerization was determined by comparing reactive amine concentrations at initial mixing of monomer reagents (time – 0h) and after 16 hours polymerization using the ninhydrin assay as described previously(S. Barua, et al., 2009b; Kasman, et al., 2009a). A decrease in amine concentration by ~60% was used as an indicator of polymer formation.

Generation of 1,4C-1,4Bis-GNR Assemblies ('Nanoassemblies'). Dispersions of GNRs with an optical density of 0.5 at the maximal absorbance wavelength were centrifuged at 6000 rpm for 10 minutes in 1.5 mL microcentrifuge tubes using a Microfuge 18 centrifuge (Beckman Coulter, Brea, CA), in order to remove excess CTAB surfactant. The supernatant was removed, and the GNRs were redispersed in 100 µL poly(styrene sulfonate) (PSS) solution (10 mg/mL in 0.01X PBS; ~1.5 mM salt concentration). This dispersion was immediately sonicated for 30 minutes to allow for the formation of PSS-coated GNRs (PSS-CTAB-GNRs). Excess PSS was removed by centrifugation at 6000 rpm for 10 minutes and the supernatant was discarded. PSS-CTAB-GNRs were then re-dispersed in 300 µL nanopure water, and 200 µL 1,4C-1,4Bis polymer (10 mg/mL in 0.01X PBS) were added to the dispersions. These were immediately sonicated for 30 min to allow for the formation of the 1,4C-1,4Bis-PSS-CTAB-GNR nanoassemblies. Excess 1,4C-1,4Bis polymer was removed by centrifugation at 6000 rpm for 10 minutes and the supernatant was discarded. The nanoassemblies were finally resuspended in serum-free media (SFM) for use in cell-based experiments.

Generation and Characterization of Expression Vector-loaded Nanoassemblies

Expression Vectors. Luc25 and Luc29 shRNA plasmid expression vectors(Grimm, et al., 2006) were generous gifts from Professor Mark A. Kay, Stanford School of Medicine, Palo Alto, CA. In these vectors, sdsAAV vector plasmid was engineered such that it contained the U6 promoter followed by unique Bbs I restriction enzyme sites, allowing insertion of shRNAs as annealed oligonucleotides with appropriate overhangs. Hairpins were designed such that the sense came before the

antisense strand separated by a 7 to 9 nucleotide loop. Luc25 contained a 25 nucleotide stem length with the sense strand (5'-3'): GGTGGCTCCCGCTGAATTGGAATCC and antisense strand (3'-5'): **GGATTCCAATTCAGCGGGAGCCACC**, separated by a loop sequence of (5'-3') TCAAGAG. Luc29 contained a 29 nucleotide stem length with the sense strand (5'-3'): ATCGGGCGGCTCTCGCTGAGTTGGAATCC and antisense strand (3'-5'): **GGATTCCAATTCAGCGGGAGCCACC**TGAT separated by a loop sequence of (5'-3;) GAAGCTTG, with underlined nucleotides denoting mismatches between the strands. Residues in bold-face font are common to both, Luc25 and Luc 29, and participate in RISC formation leading to gene silencing. Luc 29 has additional four bases (TGAT) in the antisense strand compared to Luc 29. The dc-H1121GFPshRNA-SR expression vector was a generous gift from Dr. Matthias Eder(M Scherr, et al., 2003) of Hannover Medical School, Hannover, Germany and is denoted as shEGFP for this study. The pEGFP plasmid consisting of a 4.7 kbp reporter vector pEGFP-C1 encoding enhanced green fluorescent protein (EGFP) under the control of the cytomegalovirus (CMV) promoter was purchased from Clontech (Palo Alto, CA). Competent DH5α E. coli cells were transformed with the expression vectors and cultured overnight in presence of the ampicillin for Luc25, Luc29, and shEGFP and kanamycin for pEGFP plasmids (16h, 37°C, 150 rpm) in 5 mL Terrific Broth (MP Biomedicals, LLC, Solon, OH) in 15 mL tubes (Fisher, Waltham, MA) in a shaker-incubator. The cultures were then centrifuged at 6000 rpm and 4°C for 10 min. Plasmid DNA was purified according to the QIAprep Miniprep Kit (Qiagen, Valencia, CA) protocol and DNA concentration and purity were determined based on absorbance readings at 260 nm and 280 nm, determined using a NanoDrop spectrophotometer (ND-1000; NanoDrop Technologies,

Wilmington, DE). Plasmid DNA concentrations were set between 150-300 ng/µL, and volumes were adjusted in order to load between 10-100 ng of shRNA plasmid on nanoassemblies prior to transfections.

shRNA plasmid Expression Vector Loading on Nanoassemblies.

Nanoassemblies (optical density 0.1 a.u. at 800 nm) were incubated with different amounts (10-100 ng) of Luc25, Luc29, pEGFP, or shEGFP expression vectors for 30 min in serum-free media, leading to the formation of vector-loaded nanoassemblies. The amount of shRNA plasmid expression vector remaining in the supernatant after centrifugation was determined using ethidium bromide, a DNA intercalating dye. Ethidium Bromide (1 µg of 0.5 mg/ml; Sigma-Aldrich, St. Louis, MO) was added to each sample. Solutions were transferred to a black 96 well plate, and fluorescence was measured using excitation at 320 nm and emission at 600 nm with a plate reader (Synergy 2 Multi-Mode Microplate Reader, BioTek, Winooski, VT), similar to methods previously described(K. Rege, S. Hu, J. A. Moore, J. S. Dordick, & S. M. Cramer, 2004; Rege, et al., 2005a). Known plasmid DNA amounts in solution were used as standards for calibration of the assay. The amount of shRNA plasmid loaded on the nanoassemblies was determined using mass balance by subtracting the amount of shRNA plasmid in the supernatant from the initial amount used for loading.

Determination of Hydrodynamic Diameter of Nanoassemblies. Unloaded and shRNA plasmid-loaded nanoassemblies were generated in serum-free media as described above. The hydrodynamic diameter of nanoassemblies was determined via dynamic light scattering (DLS) using a particle sizer (Corrvus Advanced Optical Instruments). The hydrodynamic diameter was reported in nanometers (nm).

Determination of Zeta Potential of Nanoassemblies. Nanoassemblies were prepared as described above, set to an optical density of 0.1, and co-incubated with 0, 10, 15, 20, 25, 50 or 100 ng of Luc25, Luc29, pEGFP or shEGFP expression vectors. Dispersions (in serum-free media) were transferred to the manufacturer's reusable zeta cell (Beckman Coulter, Brea, CA) and zeta potential values were determined using a Delsa™ Nano Submicron Particle Size and Zeta Potential Particle Analyzer (Beckman Coulter, Brea, CA). Zeta Potential values were reported in millivolts (mV).

Nanoassembly-mediated shRNA plasmid Delivery to Human Prostate Cancer Cells

Cell Culture. The 22Rv1-Luc human bone-metastatic prostate cancer cell line(Sramkoski et al., 1999) constitutively expresses the firefly luciferase gene, and was a generous gift from Professor Christina Voelkel-Johnson, Medical University of South Carolina, Charleston, SC as part of an ongoing collaboration. RPMI 1640 with L-glutamine and HEPES (RPMI-1640 medium), Pen-Strep solution: 10000 units/mL penicillin and 10mg/mL streptomycin in 0.85% NaCl, and fetal bovine serum (FBS), were purchased from Hyclone. Serum-free medium (SFM) consisted of RPMI-1640 medium plus 1% Pen-Strep (1000 units/mL penicillin and 1mg/mL streptomycin), and serum-containing medium (SCM) consists of SFM plus 10% FBS. Cells, as received, were cultured in a 5% CO_2 incubator at 37^{o}C using RPMI-1640 medium containing 10% heat-inactivated FBS and 1% antibiotics (Pen-Strep).

Nanoassembly Cytotoxicity. Stable nanoassemblies in SFM were prepared as described above and set to an optical density of 0.1 at 800 nm. 22Rv1-Luc human prostate cancer cells were seeded in 96 well plates at a density of 8,400 cells/well and allowed to attach overnight in a 37^{o}C, 5% CO_2 incubator. Volumes ranging from 3.75 µL

to 37.5 µL of shRNA plasmid expression vector loaded nanoassemblies were added to each well, and the final well volume was brought up to 150 µL with serum-free media. The final GNR O.D. ranged from 0.0025 to 0.025 a.u. in each well, resulting in a dose-response study. The cells were then incubated for 6 hours after which, serum-free media was replaced with serum-containing media. After 72 hours incubation, cell viability was determined using the 3-(4,5-dimethylthiazol-2-yl)-2,5-diphenyltetrazolium bromide (MTT) cell proliferation assay kit (ATCC CA# 30-1010k, Manassas, VA). This assay involves the enzymatic conversion of the MTT substrate to purple-colored formazan in metabolically active cells, and is widely employed as an indicator of cell viability and proliferation(Hayon, et al., 2003). Loss of metabolic activity, determined from the MTT assay, was employed as an indirect indicator of loss of cell viability upon nanoassembly treatment. Following addition of the MTT reagent (2 h at 37°C), cells were treated with a lysis buffer from the kit and kept at room temperature in the dark for 2 h in order to lyse cells and solubilize the MTT product. The absorbance of each well was measured using a plate reader (Synergy 2 Multi-Mode Microplate Reader, BioTek, Winooski, VT) at 570 nm to assay for the blue-colored MTT product. Absorbance readouts were normalized to the live (untreated) and dead (5 µL of 30% hydrogen peroxide treated) controls in order to obtain toxicity data for different nanoassemblies.

Luciferase Silencing using shRNA plasmid-loaded Nanoassemblies and* Mirus *Trans*IT®-LT1-*shRNA plasmid complexes. 22Rv1-Luc human prostate cancer cells were cultured as described above and seeded in 96-well plates (Costar, Washington DC) at a density of 8,400 cells/well. Cells were allowed to attach to the plates overnight in a 37ºC, 5% CO_2 incubator. Experiments with Mirus- TransIT®LT1 were carried out in

order to compare the efficacy of our nanoassemblies with a commercially available transfection agent; the Mirus TransIT®-LT1 reagent was a generous gift from Dr. Joshua LaBaer, Biodesign Institute, Arizona State University, Tempe, AZ. The shRNA plasmid was complexed at a ratio of 100 ng plasmid to 0.3 µL of Mirus *Trans*IT®-LT1stock solution, based on the manufacturer's recommendation. Different sub-toxic amounts of shRNA plasmid-loaded nanoassemblies and Mirus *Trans*IT®-LT1-shRNA plasmid complexes were added to each well in presence of serum-free media for 6 h, resulting in a dose response study. The media was then replaced with serum-containing media for 72 h following which, cells were permeabilized with 50 µL 1X cell lysis buffer (Promega, Madison, WI). Luciferase activity in cell lysates was measured using a luciferase assay kit (Promega, Madison, WI) using a plate reader (Synergy 2 Multi-Mode Microplate Reader, BioTek, Winooski, VT). Relative luminescence units (RLU) readouts from the assay were normalized with respect to protein concentration in the corresponding cell lysates; protein amounts were measured using the Pierce BCA Protein Assay Kit (Pierce Biotechnology, Rockford, IL). Gene silencing efficacy was based on luciferase activity in cell lysates, which was expressed as relative light units (RLU) per milligram (mg) (RLU / mg) of protein. EGFP fluorescence expression in 22Rv1-Luc cells treated with pEGFP plasmid DNA was visualized using an Inverted Epifluorescent Microscope (AxioObserver D1, Zeiss, Oberkochen, Germany) following 72 hours of treatment. All transfection experiments were performed at least in triplicate.

Two-Photon Induced Luminescence Imaging of Nanoassemblies. 22Rv1-Luc cells were seeded at a density of 50,000 cells/well in 500 µL serum-containing media on glass cover slips placed at the bottom of a 24 well plate, and allowed to attach overnight

in a 37ºC, 5% CO_2 incubator. Nanoassemblies, with or without loaded shRNA plasmids, were dispersed in serum-free media at a final optical density of 0.0025 a.u. Cells were treated with nanoassemblies for 6 hours in serum-free medium, which was then replaced with serum-containing medium. Glass coverslips were then removed from the 24 well plate and submerged in 4 mL of 1X PBS in a 6 well plate and a femtosecond Ti:Sapphire laser (Spectra Physics, Mai Tai) set to a wavelength of 800 nm and 18 mW was used to visualize the two photon luminescence of GNRs. Luminescence signals were acquired using an Ultima IV In Vivo Laser Scanning Microscope (Prairie Technologies, Middleton, WI) with a 63X water immersion objective. Following image acquisition, the same linear adjustments to brightness and contrast were applied to the entirety of each image using Axiovision processing software to highlight the two-photon signal of the nanoassemblies. All data represented in the original image were presented in the modified image.

Statistical Analysis. All experiments were carried out at least in triplicate. Statistical significance between the control and each experimental test condition was determined using the two-tailed Student's t-test; p values < 0.05 were considered statistically significant. Data are represented as mean ± standard error.

RESULTS AND DISCUSSION

Two distinct shRNA plasmid expression vectors, Luc25 or Luc29 (described in the experimental section), targeted against the sequence for luciferase mRNA, were employed in the current study. Both vectors contain the same core 25 nucleotide antisense (targeting) sequence, with the primary difference being the addition of four nucleotides in the Luc29 expression vector(Grimm, et al., 2006). This results in a stem

length of 25 and 29 nucleotides for the Luc25 and Luc29 expression vectors, respectively. It has been observed that shRNA constructs with poor efficacies can be improved by increasing construct stem length(J. Yu, Taylor, DeRuiter, Vojtek, & Turner, 2003), and that longer hairpins are more active due to improved processing by the Dicer protein(D. Kim et al., 2005; Paddison, Caudy, Bernstein, Hannon, & Conklin, 2002; Rose et al., 2005; Siolas et al., 2005). In addition to the difference in stem length, the Luc29 construct also contains mismatched bases in the sense strand. In some cases, mutations have been observed to arise following introduction of the expression constructs into *E. coli*(Miyagishi, Sumimoto, Miyoshi, Kawakami, & Taira, 2004). It has been reported that designing constructs with mutations already incorporated in the sense strand can both allow for easier sequencing as well as decreasing instances of bacterially-derived mutations(McIntyre & Fanning, 2006; Miyagishi, et al., 2004). However, introduction of increased amounts of mutations has been observed to affect the shRNA transcript's suppression activity. It has been observed that introduction of more than 3-7 C to T, 3 A to G, 5 G to A, and/or 4 A to C swaps in the sense strand can decrease the shRNA suppression activity(McIntyre & Fanning, 2006; Miyagishi, et al., 2004). Conversely, introduction of minimal mismatches has also been observed to increase suppression activity of the shRNA constructs(H. Wu et al., 2011). Similar observations were observed with siRNA; decrease in suppression activity was not observed until the introduction of up to 3-5 mismatched in the sense strand(Hamada et al., 2002). However, siRNA suppression activity was also found to increase depending on the position and number of mismatches(H. Wu, et al., 2011). As the focus of the current study is to investigate the potential of the nanoassemblies to delivery plasmid shRNA, we employed

two distinct and previously investigated shRNA expression vectors, Luc25 and Luc29. Of relevance to the current studies, higher silencing levels were observed with viral Luc29 constructs in mice, while silencing with viral luc25 constructs was comparably lower in a previous study which developed these transcripts(Grimm, et al., 2006). A pEGFP expression vector plasmid (plasmid DNA), which expresses the enhanced green fluorescent protein (EGFP), was employed as one control in the current study, due to its lack of silencing capabilities. In addition, an expression vector encoding shRNA targeted to GFP was used since it possesses no silencing capabilities against the luciferase gene, but to a different target, namely GFP. Silencing studies were carried out in 22Rv1-Luc cells, a human bone-metastatic prostate cancer cell line engineered to constitutively express luciferase.

The maximum longitudinal near infrared (NIR) GNR optical density (O.D.), measured in absorbance units (a.u.), is used as a surrogate for concentrations in case of nanoassemblies. Previous results in our laboratory, using inductively coupled plasma optical emission spectrometry (ICP-OES), demonstrated a linear relationship between O.D. and gold concentration for gold nanorods with a maximum longitudinal absorption peaks at 750 or 800 nm(Ramos & Rege, 2012b), indicating that the peak NIR O.D. was an excellent surrogate for GNR concentration.

Characterization of Expression Vector Loading on Nanoassemblies. Previous results in our laboratory indicated that nanoassemblies demonstrated high binding efficacies for plasmid DNA(Ramos & Rege, 2012b). We therefore reasoned that these nanoassemblies might be able to bind Luc25, Luc29, pEGFP, and shEGFP expression plasmid vectors with appreciable efficacies. Ratios of 10 ng shRNA plasmid to 0.0025

a.u. nanoassemblies, 25 ng shRNA plasmid to 0.0025 a.u. nanoassemblies, or 100 ng shRNA plasmid to 0.0025 a.u nanoassemblies were first employed in the loading experiments. As seen in **Table 3.1**, nanoassemblies were able to bind almost 100% of the initially loaded expression vectors in all cases. Following these observations, we considered that 100% of the expression vectors initially employed for loading was bound to the nanoassemblies under the conditions studied.

Table 3.1. *Percentage of initial amount of expression vector loaded on nanoassemblies at different loading ratios. Data are presented as mean values ± standard error (n=3).*

Expression Vector Loaded onto 1,4C-1,4Bis-GNRs	**Expression Vector (ng): 1,4C-1,4Bis-GNRs (a.u.)**		
	10ng to 0.0025a.u.	**25ng to 0.0025a.u.**	**100ng to 0.0025a.u.**
Luc25	100 ± 0 (%)	100 ± 0 (%)	99.9 ± 0.01 (%)
Luc29	100 ± 0 (%)	100 ± 0 (%)	99.9 ± 0.02 (%)
pEGFP	100 ± 0 (%)	100 ± 0 (%)	100 ± 0.04 (%)
shEGFP	100 ± 0 (%)	99.8 ± 0.2 (%)	99.8 ± 0.3 (%)

Hydrodynamic diameters of shRNA plasmid-loaded nanoassemblies were then measured in order to determine if their size would be suitable for cellular uptake / gene silencing. It is acknowledged that DLS reports for spherical morphologies, and therefore, the sizes for gold nanorod-based assemblies were primarily used as indicators. Bare/unloaded nanoassemblies were 12 ± 0.5 nm (**Figure 3.2**) in diameter, while the hydrodynamic diameters were in the range of 62 ± 3 to 84 ± 6 nm following loading of 10 ng shRNA plasmid on 0.0025 a.u. nanoassemblies. This increase in the nanoassembly hydrodynamic diameter can be attributed to the loading of the expression vectors. The

hydrodynamic diameter of all nanoassemblies increased to a range of 79-92 nm at a loading ratio of 15 ng shRNA plasmid to 0.0025 a.u. nanoassemblies, 125-141 nm at a loading ratio of 20 ng shRNA plasmid to 0.0025 a.u. nanoassemblies, 128-175 nm at a loading ratio of 25 ng shRNA plasmid to 0.0025 a.u. nanoassemblies, and 185-360 nm at a loading ratio of 50 ng shRNA plasmid to 0.0025 a.u. nanoassemblies, all of which indicate loading of increasing amounts of the expression vectors. Hydrodynamic diameters of ~209 ± 9 nm and ~258 ± 13 nm were observed when 0.0025a.u nanoassemblies were loaded with 100ng Luc 25 and Luc29 shRNA plasmid, respectively, indicative of the higher loading of the expression vectors. However, at this loading ratio, the pEGFP- and shEGFP-loaded nanoassemblies had hydrodynamic diameters of ~1041 ± 65 nm and ~458 ± 114 nm, respectively. This significant increase in size is indicative of aggregation of the nanoassemblies following expression vector loading, likely due to bridging between nanoassemblies in the dispersion, although the exact reasons for these increases are not clear. Since transfection agents are generally effective at particle sizes of 200 nm or less(Lai, Bae, Yoshida, Kataoka, & Kwon, 2010; Y. H. Wang et al., 2011), we hypothesized that delivery efficacy would likely be reduced when 100 ng shRNA plasmid were loaded on 0.0025 a.u nanoassemblies, and continue to be diminished if additional amounts of expression vectors were added. As a result, 0-100ng expression vectors were loaded on 0.0025 a.u. nanoassemblies for subsequent studies.

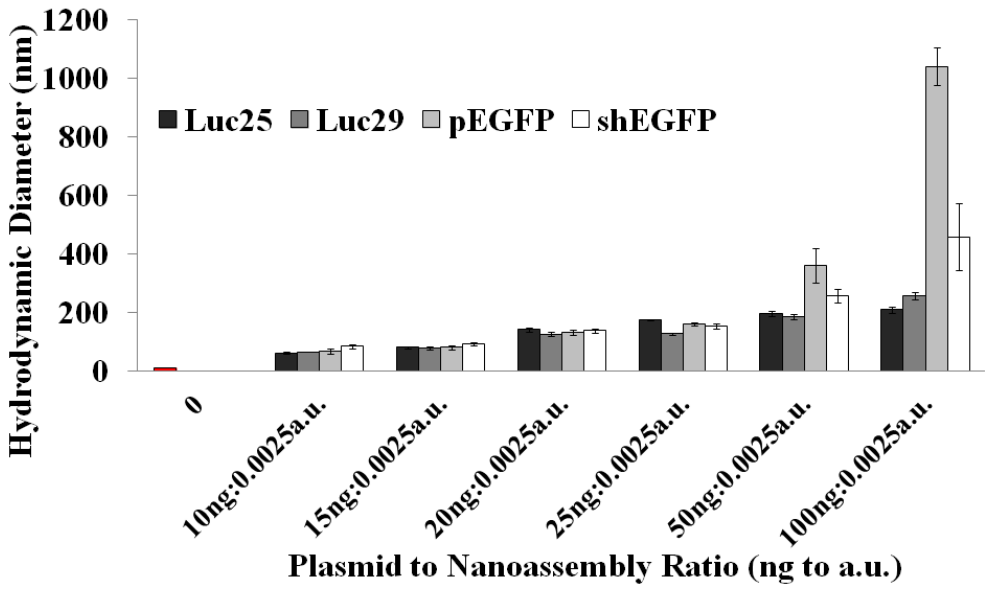

Figure 3.2. *Hydrodynamic diameters of shRNA plasmid (expression vector)-loaded nanoassemblies at different shRNA plasmid (ng) to nanoassembly (optical density in a.u.) ratios measured using dynamic light scattering (DLS). Data represent mean of the hydrodynamic size in nanometers (nm) ± standard error (n=3).*

Cytotoxicity of Expression Vector-Loaded Nanoassemblies. Nanoassemblies, set to an optical density of 0.0025 a.u. in SFM, were loaded with 0-100 ng of Luc25, Luc29, pEGFP or shEGFP. 22Rv1-Luc cells were treated with these expression vector-loaded nanoassemblies for 72 hours, after which, cell viability was determined using the MTT assay. Minimal loss of cell viability was observed in all cases of loaded nanoassemblies (**Figure 3.3**); a loss of cell viability of less than 30% was deemed as the upper limit of cytotoxicity that could be tolerated in our experiments. For the case of Luc25-loaded nanoassemblies, the greatest loss of cell viability was approximately 15% at a loading amount of 25 ng. Luc29-loaded nanoassemblies demonstrated the greatest loss of cell viability with ~18% loss at a loading amount of 20 ng. Both pEGFP and shEGFP loaded nanoassemblies also exhibited the greatest loss of cell viability

(approximately 25% and 22%, respectively) for 20 ng loading. However, no single treatment condition exhibited a decrease in cell viability above 30% and thus, all conditions were employed in further studies. Since losses in cell viability may result in decrease in gene expression, luciferase expression values were normalized to the percentage of viable cells following shRNA plasmid delivery using nanoassemblies in all cases.

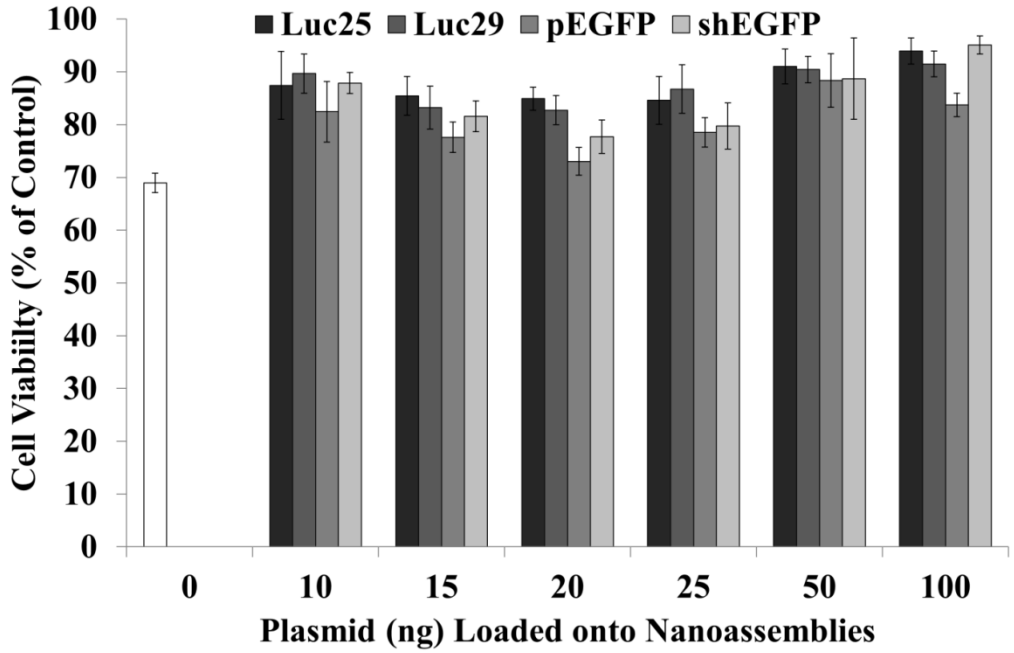

Figure 3.3. *Viability of 22Rv1-Luc cells following treatment of 0.0025 a.u. nanoassemblies loaded with 0-100ng of different expression vectors (indicated in the legend). Cell viability was determined 72 hours post treatment using the MTT assay. Data represent mean of experimentally determined cell viability values relative to untreated control ± standard error (n ≥ 3 independent experiments).*

Nanoassembly-mediated Delivery of shRNA plasmid Expression Vectors.

Nanoassemblies, set to an optical density of 0.0025 a.u. in SFM, were loaded with 0-100 ng of Luc25, Luc29, pEGFP, or shEGFP, similar to the cytotoxicity experiments described above. 22Rv1-Luc cells were treated with nanoassemblies, and luciferase expression was determined 72 hours post treatment in order to investigate the efficacy of

the gene silencing treatment. Luciferase expression is expressed as a percentage of the untreated control following correction for cell viability. Nanoassemblies loaded with 10 ng, 15 ng, 20 ng, 25 ng and 50 ng Luc29 shRNA plasmid showed a statistically significant decrease in luciferase expression (**Figure 3.4a**). However, cells treated with nanoassemblies loaded with Luc25 showed statistically significant decrease only at loading amounts of 10ng, 25 ng, and 50 ng. The maximum decrease in luciferase expression was seen for Luc29 loading of 20 ng, which resulted in approximately 53% luciferase gene knockdown, compared to untreated control. These results are consistent with reports in the literature in which, mice injected with Luc29 expression vectors demonstrated rapid and effective luciferase repression, whereas luciferase repression following Luc25 injection was comparatively lower(Grimm, et al., 2006). Statistically significant differences were not observed for cells treated with nanoassemblies loaded with control plasmids (EGFP expressing plasmid or shRNA plasmid against EGFP), or unloaded nanoassemblies, when compared to the untreated control. Higher qualitative EGFP expression was observed for loading amounts of50 ng and less when compared to 100ng, similar to the observed decrease in luciferase expression.

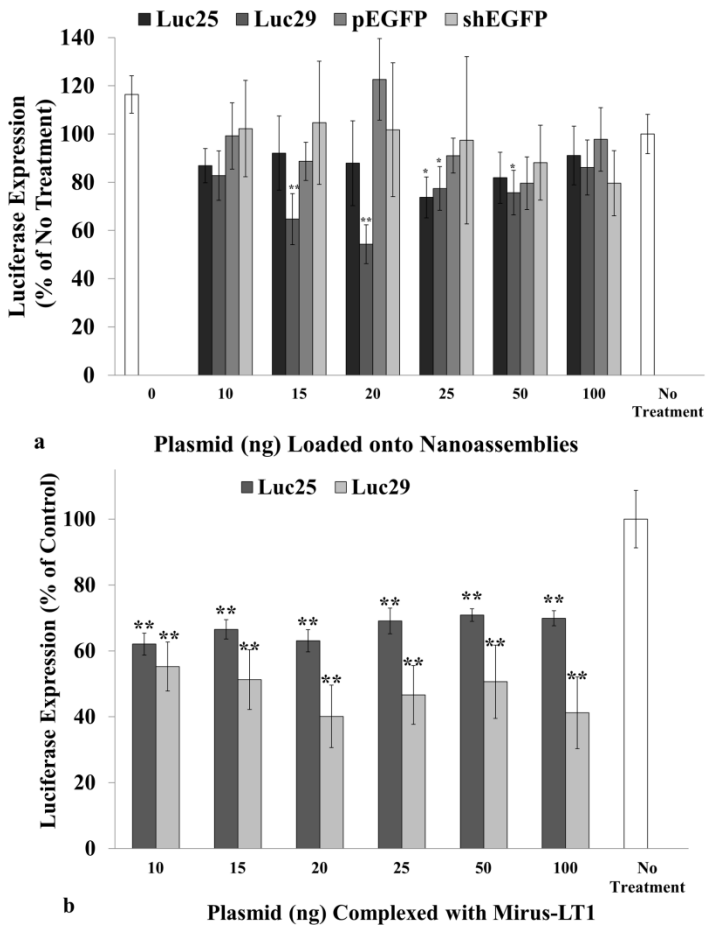

Figure 3.4. (a) *Luciferase expression in 22Rv1-Luc cells following (a) treatment of nanoassemblies loaded with different plasmid amounts, and (b) treatment with Mirus TransIT®-LT1 at manufacturer's recommended complexation ratios. Statistical significance is reported relative to the untreated control and is denoted by asterisks (* $p<0.05$; ** $p<0.01$; Student t-test). Luciferase expression was determined 72 hours post treatment, and is expressed as a percentage of untreated controls following correction for loss of cell viability. Data represent mean ± standard error ($n \geq 3$ independent experiments).*

22Rv1-Luc cells were also treated with Mirus *Trans*IT®-LT1-shRNA plasmid complexes. Mirus *Trans*IT®-LT1 is a commercially available, broad spectrum, transfection reagent that has previously been used for delivery of shRNA(Dallas et al., 2012). These studies enabled us to compare the efficacy of our nanoassemblies with a commercially available transfection reagent. Approximately 30-40% decrease in

luciferase expression was observed following delivery of Luc25 shRNA plasmid using different doses of the Mirus *Trans*IT®-LT1 agent (**Figure 3.4b)**. These values are similar to the maximum luciferase silencing levels obtained using nanoassemblies (0.0025 a.u.) loaded with 25 ng Luc 25 shRNA plasmid. A decrease in luciferase expression of approximately 50-60% was observed following Mirus *Trans*IT®-LT1-mediated delivery of Luc29 shRNA plasmids. Similar values were obtained with our nanoassemblies loaded with 15 ng and 20 ng Luc 29 shRNA plasmid. Although the Mirus *Trans*IT®-LT1 agent was effective over a larger shRNA plasmid dose range, the levels of maximal luciferase silencing were similar for both cases.

As described previously, a dose-dependent trend in luciferase silencing was observed for cells treated with Luc29-loaded nanoassemblies; luciferase protein expression decreased as the amount of Luc29 shRNA plasmid delivered increased to 20 ng, after which, it returned to the expression level observed for the untreated control. A similar dose-dependent trend in efficacy was observed in our previous studies when using PAE-GNR assemblies for transgene delivery and expression(Ramos & Rege, 2012b). This dose dependence can be correlated with changes in zeta potential values observed for nanoassemblies loaded with different amounts of expression vectors. Unloaded nanoassemblies demonstrated a zeta potential value of ~37± 8 mV (**Figure 3.5**). Loading Luc25 and Luc29 shRNA plasmids at ratios of 10 ng shRNA plasmid to 0.0025 a.u. nanoassemblies, 15 ng shRNA plasmid to 0.0025 a.u. nanoassemblies, 20 ng shRNA plasmid to 0.0025 a.u. nanoassemblies, 25 ng shRNA plasmid to 0.0025 a.u. nanoassemblies and 50 ng shRNA plasmid to 0.0025 a.u. nanoassemblies, did not result in statistically significant differences in zeta potential values; positive zeta potential

values, ranging from 14-31 mV were observed in all cases (**Figure 3.5**). However zeta potential values greatly decreased to -0.7 mV and +2.9 mV for Luc25 and Luc29-loaded nanoassemblies, respectively, at a loading ratio of 100 ng shRNA plasmid to 0.0025 a.u. nanoassemblies. This is likely due to the increased loading of the anionic shRNA plasmid molecules on the nanoassemblies, which shields the positive charge of the 1,4C-1,4Bis polymer coating.

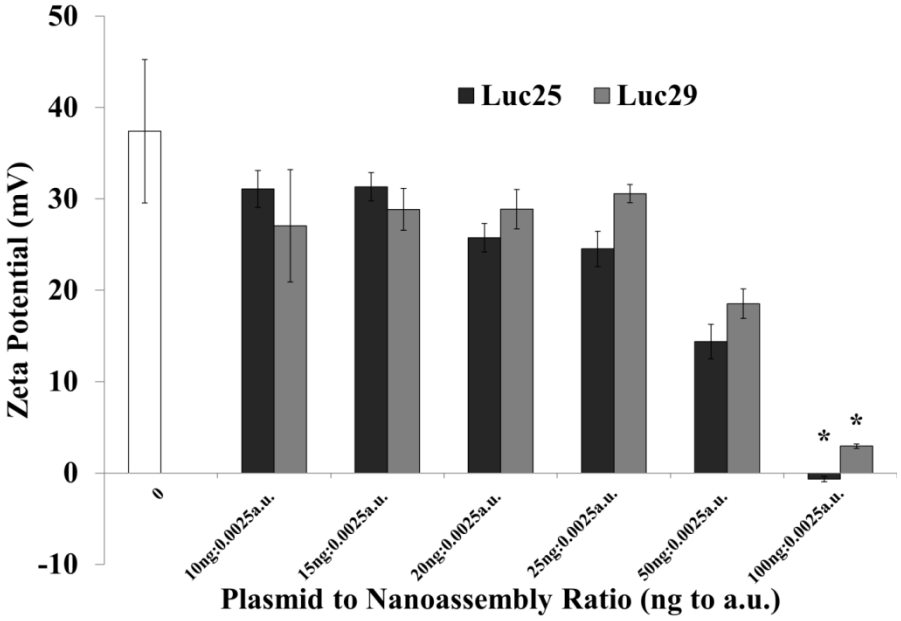

Figure 3.5. *Zeta potential values of nanoassemblies loaded with different amounts of Luc25 and Luc29 shRNA plasmids. Statistical significance is reported compared to unloaded nanoassemblies (i.e. without shRNA plasmid), and is denoted by asterisks (*p < 0.05, Students t-test). Data represent mean zeta potential ± standard error (n=3 independent experiments).*

It is well established that there is a strong correlation between nanoparticle surface potential and cellular uptake efficacy; uptake is greater for nanoparticles with strongly positive charged surfaces as it facilitates interactions with cell surfaces that possess negative surface potential(Liang. Chen, Joseph M. Mccrate, James C-M. Lee, &

Hao. Li, 2011; Zhao et al., 2012). Thus, the greatly reduced zeta potential of nanoassemblies with higher shRNA plasmid loadings is likely to reduce their cellular uptake. This results in decreased delivery of the shRNA plasmid payload which, in turn, may be attributed to lower luciferase silencing efficacies. Taken together, the efficacy of nanoassembly-mediated gene silencing can be tailored by a careful balance between cytotoxicity, shRNA plasmid loading, and surface charge.

Nanoassembly-mediated Delivery of Increased shRNA plasmid Payloads

The above results indicated that 22Rv1-Luc cells treated with 15 ng, 20 ng, and 25 ng Luc29 shRNA plasmid loaded on 0.0025 a.u. nanoassemblies, displayed the most significant silencing efficacies, likely due to retention of positive surface charge. Based on these findings, these ratios of shRNA plasmid to nanoassemblies were held constant, while nanoassembly-shRNA plasmid concentrations used for treating 22Rv1-Luc cells was increased by 2, 3, 4, 5, and 10 fold, in order to deliver higher amounts of the shRNA plasmids to cells. Based on cytotoxicity data (**Figure 3.6**), Luc25 and Luc29 loaded nanoassemblies with ODs greater than 0.0075 (i.e. three-fold higher concentration of the nanoassemblies in the original screening experiment) resulted in >30% loss of cell viability, and were thus not studied further. Interestingly, nanoassemblies loaded with pGL3 and shEGFP nucleic acids exhibited greater loss of cell viability than those loaded with luciferase shRNA, although the reasons behind this are not explicitly clear.

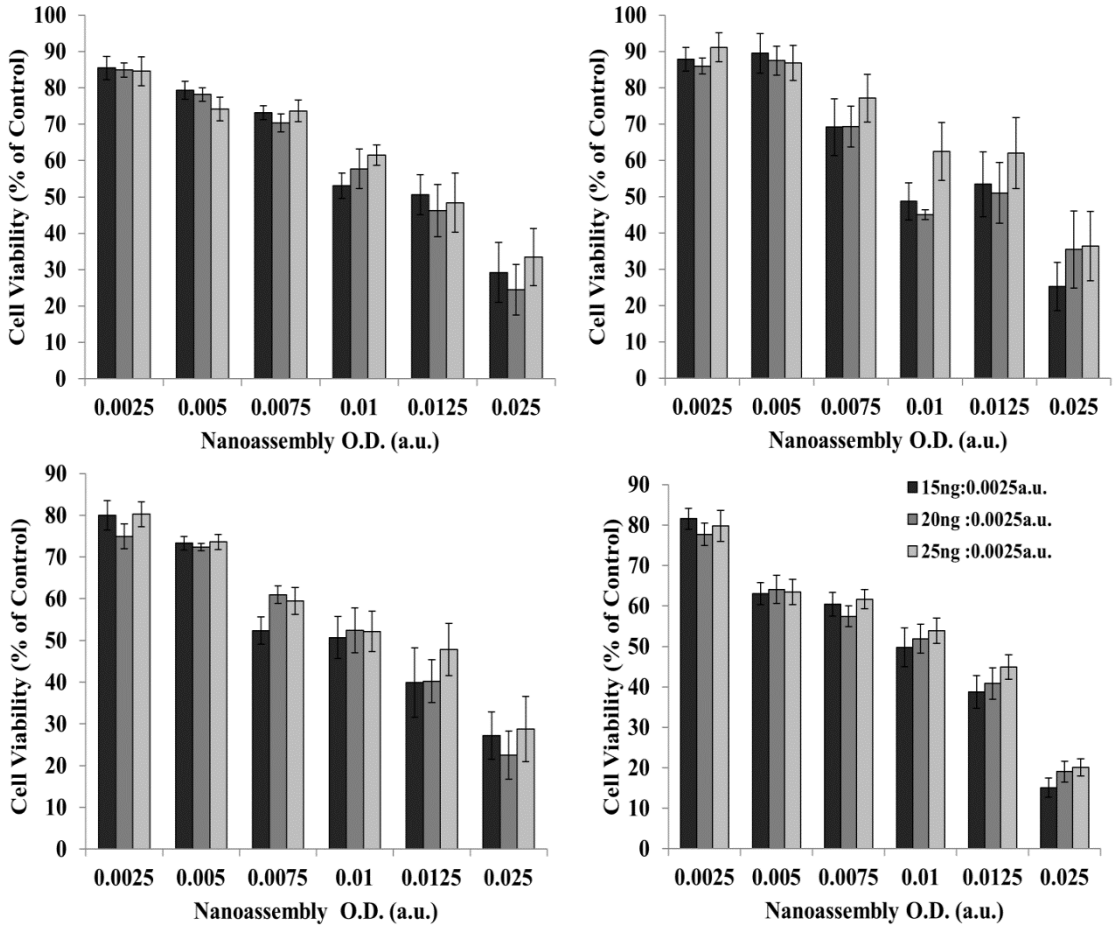

Figure 3.6. *Viability of 22Rv1-Luc cells following treatment with increased concentrations of nanoassemblies at loading ratios of 15ng, 20 ng, and 25 ng expression vector to 0.0025 nanoassembly ratios for Luc25 (**top left**), Luc29 (**top right**), pEGFP (**bottom left**) and shEGFP (**bottom right**). X-axis values indicate different amounts (O.D.) of nanoassemblies, which are loaded with different amounts of expression vectors in order to maintain the loading ratios. Cell viability was determined 72 hours post treatment using the MTT assay. Loss of > 30% cell viability was deemed too toxic for further investigations. Consequently, only 0.0025a.u., 0.005a.u., and 0.0075a.u. were investigated subsequently. Data represent mean of experimentally determined cell viability values relative to untreated control ± standard error (n ≥ 3 independent experiments).*

Based on the above cytotoxicity data, 22Rv1-Luc cells were treated with nanoassemblies with GNR ODs = 0.005 and 0.0075 (i.e. 2 and 3 times the concentration of nanoassemblies in the original screening shown in **Figure 3.5**) keeping the original 15 ng, 20 ng, and 25 ng shRNA plasmid to 0.0025 a.u. nanoassembly ratios constant. A

statistically significant decrease in luciferase expression was originally observed in case of 25ng shRNA plasmid to 0.0025a.u. nanoassemblies loading ratio for Luc25 (**Figure 3.7 top left**). At this ratio, ~32% decrease in luciferase expression was observed upon delivery of the nanoassembly at an O.D. of 0.0025. However, further decrease in luciferase expression, i.e. ~38% and ~45%, was observed when the nanoassembly concentration (or OD) was increased by 2- and 3-fold respectively at the same shRNA plasmid to nanoassembly ratio. Cells treated with the other loading conditions showed no significant decrease in luciferase expression.

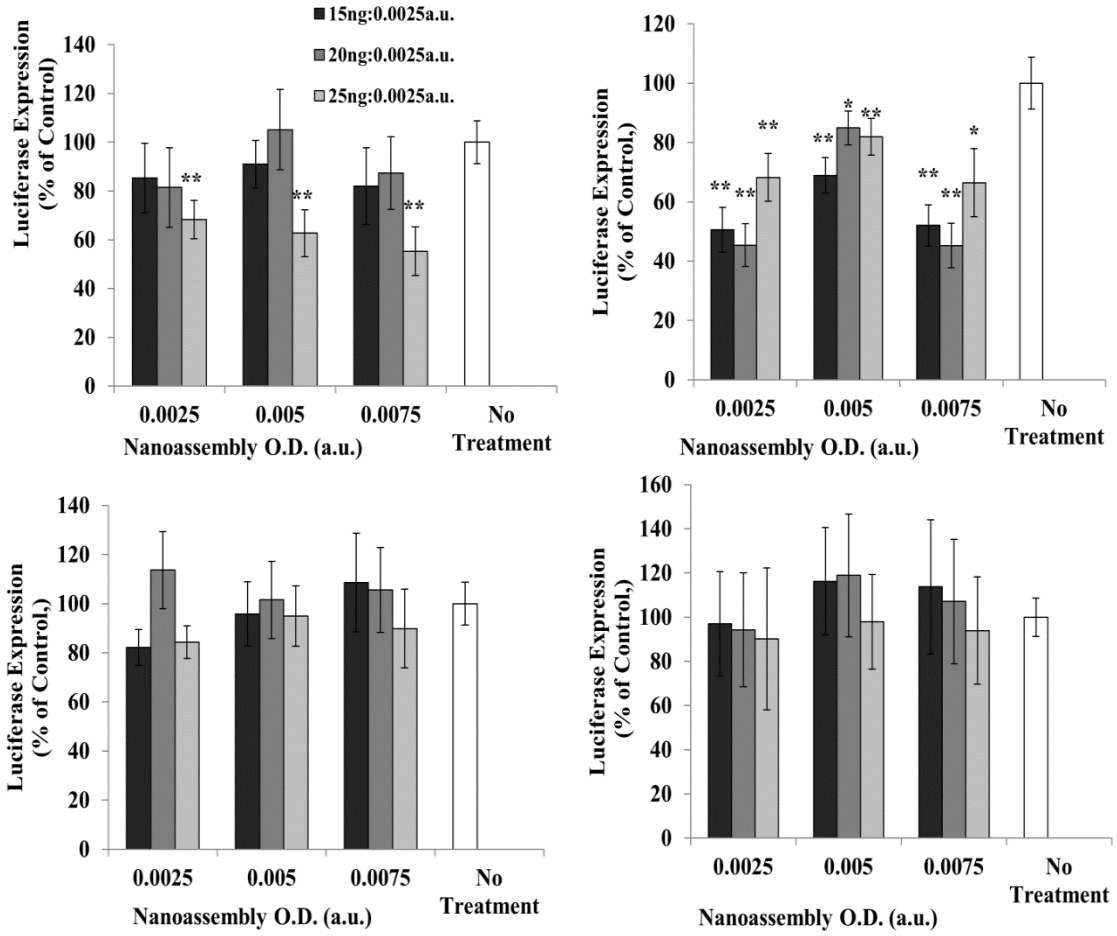

Figure 3.7. *Luciferase expression in 22Rv1-Luc cells following treatment of increased concentrations of 1,4C-1,4Bis-GNRs at loading ratios of 15ng shRNA plasmid:0.0025a.u. 1,4C-1,4Bis-GNRs, 20ng shRNA plasmid:0.0025a.u. 1,4C-1,4Bis-GNRs, and 25ng shRNA plasmid:0.0025a.u. 1,4C-1,4Bis-GNRs with Luc25 (**top left**), Luc29 (**top right**),*

*pEGFP (**bottom left**) and shEGFP (**bottom right**). Statistical significance to the untreated ('no treatment') control, and is denoted by asterisks (* $p<0.05$; ** $p<0.01$; Student t-test). Luciferase expression was determined 72 hours post treatment, and is expressed as a percentage of untreated controls following correction for loss of cell viability. Data represent mean ± standard error ($n \geq 3$).*

In case of the Luc29 shRNA plasmid (**Figure 3.7 top right**), a maximum decrease of luciferase expression of approximately 55% was observed, at the three-fold higher concentration (i.e. 0.0075a.u.). In all cases, no statistically significant change in luciferase expression was observed when either pEGFP or shEGFP (**Figure 3.7 bottom left and bottom right respectively**)-loaded nanoassemblies were delivered at increased concentrations, indicating that silencing was observed only in cases of plasmids expressing shRNA targeted against the luciferase protein.

Polymeric and lipid-based delivery systems demonstrate between 20%-90% gene silencing after delivery of siRNA or shRNA expression vectors in vitro(S. H. Kim, Jeong, Cho, Kim, & Park, 2005; J.-M. Lee, Yoon, & Cho, 2013; Navarro, Sawant, Essez, Tros de Ilarduya, & Torchillin, 2011; Waite & Roth, 2009). In addition, gold nanoparticle based delivery systems have reported gene suppression between ~40%-90% following siRNA (A. Bonoiu, et al., 2011; A. C. Bonoiu, et al., 2009; Braun, et al.; Song, et al., 2010) and shRNA delivery(Ryou, et al., 2010; Ryou, et al., 2011). However, investigations for the delivery of plasmid shRNA with gold nanoparticle systems are uncommon, indicating that our approach demonstrates comparable efficacy and is a novel delivery vehicle for shRNA plasmids.

Visualization of Luc29-Nanoassembly Uptake in 22Rv1-Luc Cells using Two-Photon induced Luminescence Imaging. GNRs demonstrate highly efficient two-

photon induced luminescence both in vitro and in vivo(Durr, et al., 2007). In particular, the ability of GNRs to absorb excitation wavelengths in the near infrared (NIR) region of the absorption spectrum can allow minimal tissue scattering and phototoxicity compared to other fluorescent based imaging techniques(J.-L. Li & Gu, 2010; H. F. Wang, et al., 2005). Cellular uptake of Luc29 shRNA plasmid-loaded nanoassemblies in 22Rv1-Luc cells was visualized using two-photon luminescence in order to demonstrate their theranostic potential. Following treatment of 22Rrv1-Luc cells with unloaded nanoassemblies and with 10 ng, 15 ng, 20 ng, 25 ng, 50 ng, and 100 ng shRNA plasmid loaded on 0.0025a.u. nanoassemblies, live cells, in the absence of additional stains, dyes, or fixatives, were imaged using two-photon induced luminescence. No signal was seen in case of 22Rv1-Luc cells untreated with nanoassemblies. Excellent two photon luminescence signal was seen from 22Rv1-Luc cells in treated with nanoassemblies (**Figure 3.8**). Unfortunately, due to the set-up of the two-photon microscope used, we were unable to acquire any phase-contrast or DIC microscopy images for simultaneous overlay with the two-photon microscopy images. 22Rv1 cells grew in clusters, and the two-photon luminescence signal from the nanoassemblies can be observed throughout the cluster. Larger spots are likely clusters or aggregates of the nanoassemblies.

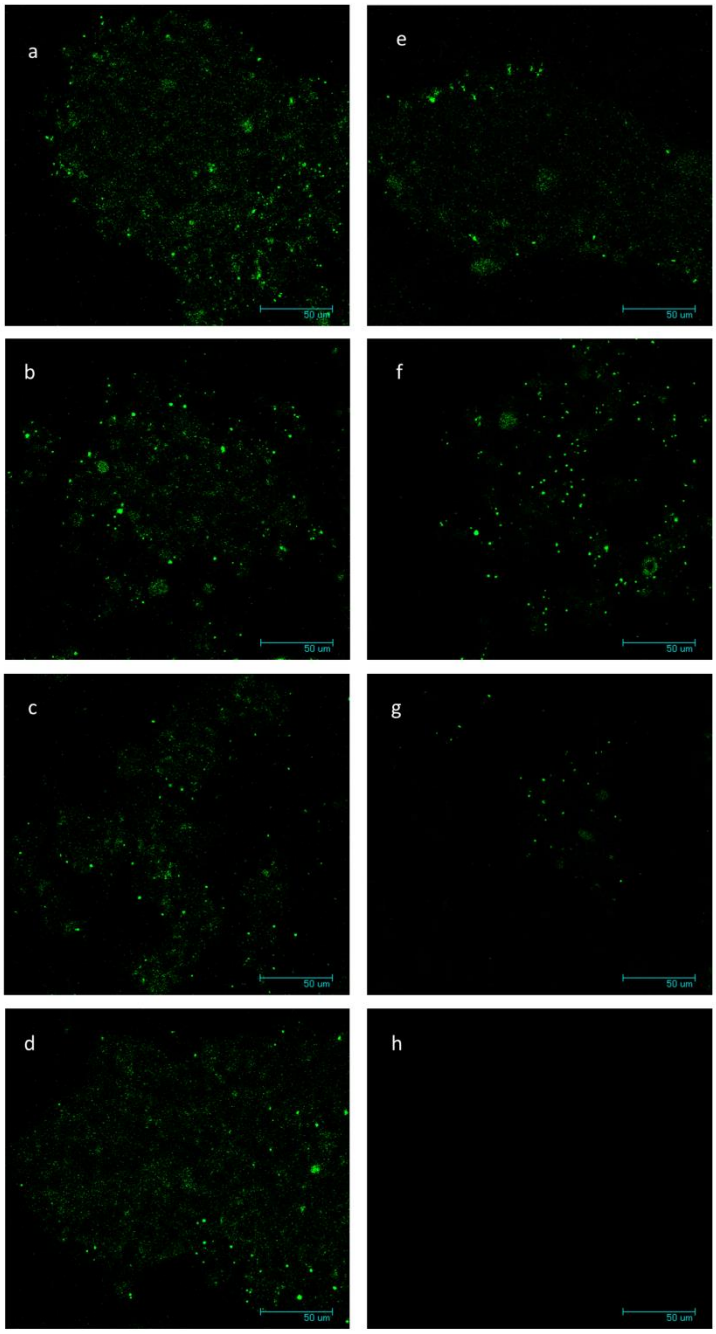

Figure 3.8. *Live cell, two-photon induced luminescence (pseudo-colored green) images of 22rv1-Luc cells after treatment with nanoassemblies (a) without shRNA plasmids, and loaded with Luc29 shRNA plasmid at ratios of (b) 10ng, (c) 15ng, (d) 20ng, (e) 25ng , (f) 50ng, (g) 100ng shRNA plasmid to 0.0025 a.u. nanoassemblies and (h) untreated cells. Scale bar = 50 µm. No luminescence signal was seen in untreated 22Rv1 cells (h).*

The use of two-photon luminescence for visualization of our nanoassemblies highlights the theranostic potential of these delivery vehicles for simultaneous imaging and gene silencing. When compared to commercially available transfections agents, such as the Mirus *Trans*IT®-LT1, the nanoassemblies investigated in this study possess advantages. They were found to have similar maximum silencing efficacies when compared to Mirus *Trans*IT®-LT1, however they are also able to be used for live cell imaging. This theranostic capability of the nanoassemblies can be used for tracking, diagnosis, or targeted/triggered delivery of payloads for specific cell types or diseases. Additionally, due to the ease of modification and/or surface functionalization of gold nanoparticles, aspects of the polymer/surface coating can be tuned and further investigated to further enhance the delivery efficacies. These modification include using targeting molecules to facilitate their delivery to specific cell types. The use of gold nanoparticles for optical coherence tomography(T. Wang, Mancuso, Sapozhnikova, et al., 2012), photoacoustic tomography(Y. W. Wang, et al., 2004; X. M. Yang, et al., 2007), and X-Ray-CT opens up different theranostic possibilities with these vehicles. In addition to gene silencing, it is possible to use GNR-based nanoassemblies for hyperthermic ablation of cancer cells using near infrared lasers(Dickerson, et al., 2008; Niidome et al., 2009), as has been investigated for primary and metastatic liver(Gough-Palmer & Gedroyc, 2008; Vogl, Straub, Eichler, et al., 2004; Vogl, Straub, Zangos, et al., 2004) and lung cancer diseases(Rosenberg, et al., 2009).

CONCLUSIONS

We generated 1,4C-1,4Bis-GNR poly(amino ether)-based nanoassemblies loaded with shRNA plasmids for silencing luciferase protein expressed constitutively in 22Rv1-

Luc human prostate cancer cells. We also demonstrated two-photon luminescence based imaging of these nanoassemblies in live cells. Our studies indicate the utility of this platform for delivering plasmid-based expression vectors that encode shRNA molecules for gene silencing applications. Up to 55% silencing of the original luciferase signal was observed when shRNA plasmid-loaded nanoassemblies were used, and these efficacies were similar to those observed with a commercially available plasmid DNA transfection agent. Nanoassembly-mediated silencing efficacies were consistent with observations related to their cellular uptake and surface charge.

Several strategies may be employed for further enhancing gene silencing efficacies of these nanoassemblies, one of which involves the judicious selection and optimization of effective shRNA sequences and expression vectors. Further enhancements in gene silencing may also be observed when these assemblies are used to treat cells in combination with chemotherapeutics or other drugs that can help overcome intracellular resistance to plasmid delivery (S. Barua & K. Rege, 2010). Additionally, it is possible to design expression cassettes that express multiple shRNA sequences under the control of the same or different promoters in a single vector. This allows for a combinatorial RNA interference (co-RNAi) approach in which an increase in gene suppression is achieved via the targeting of single and/or multiple genes via preventing escape of mutation-prone transcripts and/or addressing increased expression of a supplementary gene in response to suppression of another(Lambeth, Van Hateren, Wilson, & Nair, 2010; Motegi et al., 2011; Nagao et al., 2008). This is a significant advantage over siRNA-based approaches. Further optimization may be possible by investigating different polymers coated on GNR surfaces. Combinatorial synthesis and

parallel screening approaches(S. Barua, et al., 2011b), like those employed in our laboratory, can lead to the identification of polymer candidates that demonstrate higher silencing efficacies when interfaced with GNRs. Taken together, imaging, hyperthermia and gene silencing properties of shRNA plasmid-loaded nanoassemblies make them attractive in image-guided gene silencing and photothermal treatments for different diseases, including cancer.

CHAPTER 4

PARALLEL SYNTHESIS OF POLY (AMINO ETHER)-TEMPLATED PLASMONIC NANOPARTICLES FOR TRANSGENE DELIVERY

Plasmonic metal-based nanomaterials have been widely investigated as therapeutics and imaging agents(Ghosh, et al., 2008; H. C. Huang, et al., 2011; T. Wang, Mancuso, Kazmi, et al., 2012) in biomedical studies, and have also found applications in sensing and catalysis. In particular, gold nanoparticles (GNPs) have been increasingly investigated for separations(Gross, Nelson, Grate, & Synovec, 2003), sensing(Dos Santos, Goulet, Pieczonka, Oliveira, & Aroca, 2004; Faulds, Littleford, Graham, Dent, & Smith, 2004), delivery of chemotherapeutic drugs(Ramos, et al., 2012) / nucleic acids(Conde, et al., 2012; Chu Hu, et al., 2010; S. T. Kim, et al., 2012b; Ramos & Rege, 2012a; Mini Thomas & Alexander M Klibanov, 2003) and bioimaging(Bardhan, Lal, Joshi, & Halas, 2011; Huang-Chiao Huang, Ramos, Grandhi, Potta, & Rege, 2010; Sokolov et al., 2003). In addition, they exhibit high surface-area-to-volume ratios and biocompatibility, are candidates for facile surface modification / functionalization and possess unique optical properties(X. Huang, et al., 2009). Silver nanoparticles (AgNPs) demonstrate antibacterial activity resulting in potential application in treatments against microbial infections, burns, diabetic skin ulcers, and medical devices; the antimicrobial spectrum of AgNPs is considered to be broader than that of most common antibiotics(C. You, et al., 2012). AgNPs have also been investigated as antifungal agents(Esteban-Tejada, et al., 2009) and as effective virucidal agents(Panacek, et al., 2009). However, broad use of silver

nanoparticles is somewhat limited due to concerns regarding their toxicity(S. Singh, et al., 2010; Sotiriou & Pratsinis, 2011).

Both, GNPs and AgNPs have been synthesized using diverse methods including chemical(Al-Thabaiti, Al-Nowaiser, Obaid, Al-Youbi, & Khan, 2008; Nguyen, Kim, So, & Kim, 2010; Shimmin, Schoch, & Braun, 2004) / photochemical(Eustis & El-Sayed, 2006; Eustis, Hsu, & El-Sayed, 2005; Jia, Zeng, Song, An, & Zhao, 2006) reduction, and one-pot synthesis methods where a polypeptide(Walker et al., 2013) or polymer acts as both, a reducing as well as a capping agent(J.D.S. Newman & Blanchard, 2006; Sakai & Alexandridis, 2005; Song, et al., 2010). Combinatorial / parallel synthesis methods allow exploration of diverse chemical space, leading to the rapid generation of molecular species for diverse applications. Although combinatorial methods have been widely employed for synthesis of small and macromolecules, their utility for nanoparticle synthesis is underexplored.

Amine-containing compounds, including amino acids and polymers, have been utilized as both, reducing as well as stabilizing agents, for the synthesis of GNPs(Bhargava, Booth, Agrawal, Coloe, & Kar, 2005; J.D.S. Newman & Blanchard, 2006; J.D.S Newman & Blanchard, 2007; Selvakannan et al., 2004). We have recently reported the synthesis and use of polyamine-based poly(amino-ether) (PAE) cationic polymers(S. Barua, et al., 2009b; S. Barua, et al., 2011b; L. Vu, J. Ramos, T. Potta, & K. Rege, 2012) for transgene expression following delivery of plasmid DNA, and for enhancing adenoviral delivery to cells resistant to viral transduction(Gosnell et al., 2014; Kasman, et al., 2009a). In this report, we investigate the efficacy of a small set of cationic PAEs to template the formation of gold and silver nanoparticles in a one-pot, parallel synthesis reaction scheme under

ambient conditions, and compare nanoparticle formation efficacy to that observed with 25 kDa poly(ethylene imine) of pEI25k. The identification of polymers that can template nanoparticle synthesis under ambient conditions, without the necessity of additional reducing agents, derivatization chemistries, or harsh synthesis conditions, is a significant advantage over other existing methods, particularly over pEI25k. Poly(amino ether)-templated gold nanoparticle assemblies were also employed for transgene delivery and expression in mammalian cells. Taken together, our current approach resulted in the identification of poly(amino ethers) that can simultaneously template nanoparticle formation and stabilize them in aqueous media, resulting in the formation of PAE-GNP nanoassemblies, which, in turn, can deliver nucleic acids to mammalian cells.

MATERIALS AND METHODS

Poly(amino ether) (PAE) Polymer Synthesis. A small set of eight PAE polymers, synthesized as described previously(S. Barua, et al., 2009b; L. Vu, et al., 2012), was used to demonstrate the combinatorial synthesis approach. Briefly 1,4-cyclohexanedimethanol diglycidyl ether (1,4C) was reacted in equimolar amounts with 1,4-bis(3-aminopropyl) piperazine (1,4Bis), 3,3'-diamino-n-methyldipropylamine (3,3'), pentaethylenehexamine (PHA), 1,3-diaminopropane (1,3DPP), and 2-methylpentane-1,5-diamine (2M1,5P), resulting in the formation of 1,4C-1,4Bis, 1,4C-3,3', 1,4C-PHA, 1,4C-1,3DPP, and 1,4C-2M1,5P poly(amino ethers), respectively. Neopentylglycol diglycidyl ether (NPDGE) was reacted in equimolar amounts with 1,4Bis, 3,3', PHA, and 1,3DPP to generate NPGDE-1,4Bis, NPGDE-3,3', NPGDE-PHA, and NPGDE-1,3DPP respectively. Amine monomers employed in this study are shown in **Figure 4.1a**. The polymerization reaction was carried

out in 20 ml glass scintillation vials for 16 hours. Following the reaction, polymers were dissolved at a concentration of 10 mg/mL in phosphate-buffered saline (0.01 X PBS), and the solution pH was adjusted to 7.4 using 30% hydrochloric acid in deionized (DI) water, in order to compensate for the basicity of the cationic PAEs. The extent of polymerization was determined by comparing reactive amine concentrations at initial mixing of monomer reagents (time – 0h) and after 16 hours polymerization using the ninhydrin assay as described previously(S. Barua, et al., 2009b; Kasman, et al., 2009a).

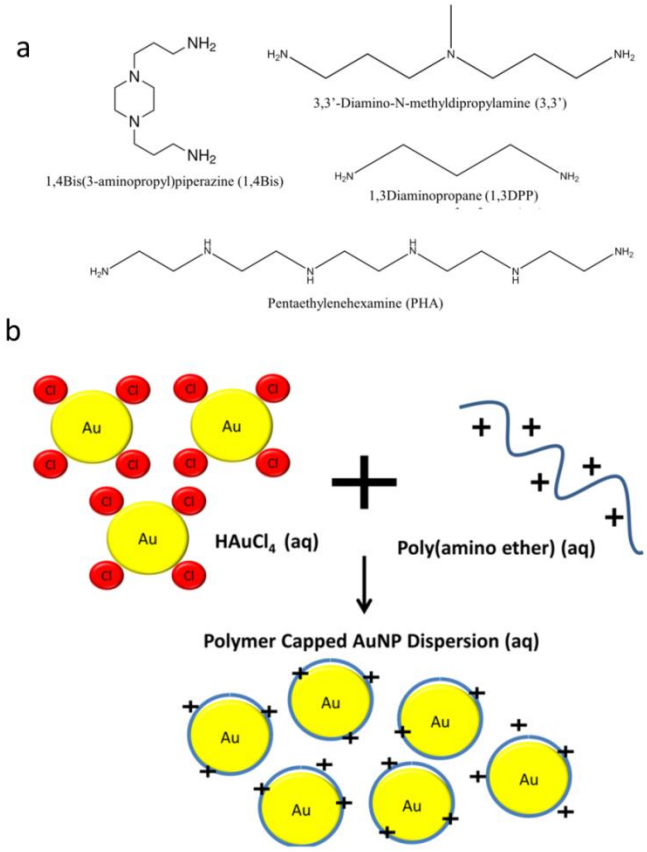

Figure 4.1. *(a) Chemical structure of amine containing monomers used in synthesis of Poly(amino ether) polymers for nanoparticle formation. Abbreviations used in this study are in parenthesis. (b) Simplified schematic of GNP synthesis using Poly(amino ether) polymers.*

Synthesis of Poly(amino ether)-Gold Nanoparticles (PAE-GNPs) and Poly (amino ether)-Silver Nanoparticles (PAE-AgNPs) Synthesis. PAE-GNP and PAE-AgNP syntheses was carried out in a one-pot reaction under ambient conditions. Briefly, 1 mg of $HAuCl_4$ or 0.1 mg of $AgNO_3$ was co-incubated with each of the PAE polymers or branched pEI25k [25 kDa poly(ethyleneimine)] at polymer to metal salt weight ratios of 25 to 1, 50 to 1, and 100 to 1. Reactions were allowed to proceed in the dark at room temperature for 5 or 4 days for GNP and AgNP, respectively. Nanoparticle synthesis was monitored by measuring the solution absorption spectra from 300 nm to 999 nm in 5 nm increments at various time points during the nanoparticle synthesis. After monitoring, PAE-nanoparticle dispersions were centrifuged for 20 min at 10,000 rcf in order to remove excess polymer and $HAuCl_4$, re-dispersed in nanopure water, and filtered with a 0.22 μM filter for further characterization.

UV irradiation. In order to determine the effect of UV irradiation on nanoparticle formation, 1 mg of $HAuCl_4$ or 0.1 mg $AgNO_3$ were co-incubated with each of the PAEs or branched pEI25k at polymer to metal salt weight ratios of 25 to 1, 50 to 1, and 100 to 1. Dispersions were then irradiated with a UV light using a handheld UV lamp (366 nm, 6 W) for 24 or 3 hours at room temperature for GNP and AgNP respectively. Following irradiation, dispersions were allowed to sit for an additional 4 days or 21 hours in the dark at room temperature for GNP and AgNP, respectively. The solution absorption spectra were monitored from 300nm to 999 nm in 5 nm increments at various time points, in order to monitor nanoparticle formation. After 5 days or 24 hours for GNP and AgNPs respectively, dispersions were centrifuged for 20 min at 10,000 rcf in order to remove

excess polymer and $HAuCl_4$, redispersed in nanopure water, and filtered with a 0.22 μM filter for further characterization.

Transmission Electron Microscopy. Following synthesis, PAE-GNP and PAE-AgNPs were visualized using Transmission Electron Microscopy (TEM), carried out using a JEOL-JEM-2000FX microscope, operating at 200 kV. Specimen samples for TEM were prepared by casting a drop of PAE-GNP or PAE-AgNP dispersions onto a carbon film on a 200 mesh copper mesh (Global Electron Microscopy Technology Co.) and dried in air. Dried samples were examined by TEM at 200 kV.

Determination of Hydrodynamic Diameter and Zeta Potential of PAE-GNPs and PAE-AgNPs. The hydrodynamic diameters of PAE-GNPs and PAE-AgNPs were determined via dynamic light scattering (DLS) using a particle sizer (Corrvus Advanced Optical Instruments). Hydrodynamic diameters are reported in nanometers (nm). 1,4C-1,4Bis-GNPs were synthesized at a ratio of 100 to 1 of 1,4C-1,4Bis to $HAuCl_4$ under UV irradiation. Templated GNPs were set to concentrations of 4.9, 9.8, 24.4, 48.8, or 97.5 μg/mL and loaded with between 0-250 ng of pGL3 plasmid DNA. Dispersions were transferred into folded capillary zeta cells (Malvern, Westborough, MA). Zeta potential values were determined using a Zetasizer Nano ZS (Malvern).

Determination of Primary and Secondary Amine Concentration of PAE-GNPs. Ninhydrin (2,2-Dihydroxyindane-1,3-dione) reacts with free primary and secondary amines with a resulting deep blue or purple color, which can be measured and

compared to a standard for quantifying reactive (i.e. primary and secondary) amine concentrations. Glycine standards, with known amine concentrations (0, 50, 150, and 300 µM), were prepared in nanopure water with a total volume of 200 µl. GNPs were synthesized as described above. Following synthesis, GNPs were dispersed in nanopure water, and their optical density was determined at the maximum absorbance wavelength. GNP dispersions of 200, 100, and 75 µL were prepared and filled up to 200 µL with nanopure water. Following addition of the ninhydrin reagent (100 µl), all samples were incubated in water at 100^{o}C for ten minutes, following which, they were allowed to cool to room temperature. 500 µl of 95% ethanol was then added to each sample and the absorbance was measured at 570nm. Reactive amine concentrations were determined by comparing measured values to the glycine standard curve. Amine concentrations were then normalized to the respective GNP maximum absorbance (pseudo-concentration).

Plasmid DNA Delivery using 1,4C-1,4Bis-GNPs

Plasmid DNA. The pGL3 control vector (Promega Corp., Madison, WI), which encodes for the modified firefly luciferase protein under the control of an SV40 promoter, was used for transgene expression studies. E. coli (XL1 Blue) cells containing the pGL3 plasmid DNA were cultured overnight (16 h, 37°C, 150 rpm) in 15 mL tubes (Fisher) in 5 mL of Terrific Broth (MP Biomedicals, LLC). The cultures were then centrifuged at 5400*g* and 4°C for 10 min. Plasmid DNA was purified according to the QIAprep Miniprep Kit (Qiagen) protocol. DNA concentration and purity were determined based on absorbance at 260 and 280 nm using a NanoDrop spectrophotometer (ND-1000; NanoDrop Technologies). Plasmid DNA concentrations of 200-300 ng/µL were typically obtained,

and volumes were adjusted in order to load between 10-200 ng of pGL3 plasmid DNA on 1,4C-1,4Bis-GNP**s** prior to transfections.

Cell culture. 22Rv1 human prostate cancer cells and MB49 murine bladder cancer cells were both generous gifts from Professor Christina Voelkel-Johnson of the Medical University of South Carolina as part of an existing collaboration. RPMI-1640 with L-glutamine and HEPES (RPMI-1640 medium), DMEM with high glucose, L-Glutamine, and HEPES, Pen-Strep solution: 10000 units/mL penicillin and 10000 µg/mL streptomycin in 0.85% NaCl, and fetal bovine serum (FBS), were purchased from Hyclone. Serum-free medium (SFM) consisted of RPMI-1640 or DMEM medium plus 1% Pen-Strep (1000 units/mL penicillin and 1000 µg/mL). Serum-containing medium (SCM) consists of SFM plus 10% FBS. 22Rv1 cells, as received, were cultured in a 5% CO_2 incubator at 37^{o}C using RPMI-1640 medium containing 10% heat-inactivated FBS and 1% antibiotics (Pen-Strep). MB49 cells, as received, were cultured in a 5% CO_2 incubator at 37^{o}C using DMEM containing 10% heat-inactivated FBS and 1% antibiotics (Pen-Strep).

***Cytotoxicity*.** Cytotoxicity of 1,4C-1,4Bis-GNPs was determined in 22Rv1 and MB49 cells. Cells were seeded at a density of 8,400 cells/well in 150 µL serum-containing medium in a 96-well plate and allowed to attach overnight. Plasmid DNA encoding the luciferase protein, pGL3, was diluted to a concentration of 50 ng/µL using Tris EDTA buffer (10 mM Trizma and 1mM EDTA, Thermo Fisher Scientific, Rockford, IL). 1,4C-1,4Bis-GNPs were dispersed in SFM at concentrations of 4.9, 9.8, 24.4, 48.8, or 97.5 µg/mL 1,4C-1,4Bis-GNP dispersions were then co-incubated with 0, 25, 50, 75, 100, 125, 150, 200, or 250 ng of pGL3 plasmid DNA for 30 min. Following incubation, pGL3 plasmid-loaded 1,4C-1,4Bis-GNPs were used to treat 22Rv1 or MB49 cells in serum-free

media for 6 hours, in an incubator under humidified air containing 5% CO_2 at 37°C. Subsequently, the medium was replaced with fresh serum-containing medium. Lipofectamine3000 complexes were prepared according to manufacture's protocol at same plasmid DNA amounts used for 1,4C-1,4Bis-GNP experiments and used to treat cells. Following incubation for 48 hours, cell viability was determined using the 3-(4,5-dimethylthiazol-2-yl)-2,5-diphenyltetrazolium bromide (MTT) cell proliferation assay kit (ATCC). This assay involves the enzymatic conversion of the MTT substrate to purple-colored formazan in metabolically active cells. This activity is widely employed as an indicator of cell viability and proliferation(Hayon, et al., 2003); loss of metabolic activity was used as an indirect indicator of loss of cell viability. Following addition of the MTT reagent (2 h at 37°C), cells were treated with a lysis buffer from the kit and kept at room temperature in the dark for 2 h in order to lyse cells and solubilize the MTT product. The absorbance of each well was measured using a plate reader (BioTek Synergy 2) at 570 nm to assay for the blue MTT product. Absorbance readouts were normalized to the live (untreated) and dead (5 µL of 30% hydrogen peroxide treated) controls in subsequent data analyses.

Transgene Delivery and Expression. MB49 and 22RV1 cells were transfected using pGL3 plasmid loaded 1,4C-1,4Bis-GNPs as described above. Prior to transfection, cells were seeded at a density of 8,400 cells/well in 150 µL serum-containing medium in a 96-well plate and allowed to attach overnight. The pGL3 plasmid, encoding the luciferase protein, was diluted to a concentration of 50 ng/µL using Tris EDTA buffer (10 mM Trizma and 1mM EDTA, Thermo Fisher Scientific, Rockford, IL). 1,4C-1,4Bis-GNPs were dispersed in SFM at concentrations of 4.9, 9.8, 24.4, 48.8, or 97.5 µg/mL. 1,4C-1,4Bis-

GNP dispersions were then co-incubated with 0, 25, 50, 75, 100, 125, 150, 200, or 250 ng of pGL3 plasmid DNA for 30 min. Following incubation, pGL3 loaded 1,4C-1,4Bis-GNPs were used to treat 22Rv1 or MB49 cells in serum free media for 6 hours in an incubator under humidified air containing 5% CO_2 at 37°C. Subsequently, the medium was replaced with fresh serum-containing medium and allowed to incubate for an additional 48 hours. Lipofectamine3000 complexes were prepared according to manufacture's protocol at same plasmid DNA amounts used for 1,4C-1,4Bis-GNP experiments and used to treat cells. Luciferase protein expression, expressed in terms of relative luminescence units or RLU, was determined using the luciferase assay kit according to the manufacturer's protocol, 48 hours after transfection; luminescence measurements were carried out using a plate reader (Bio-Tek Synergy 2). The protein content (mg protein) in each well was determined using the BCA Protein Assay Kit. Transgene (luciferase) expression in all cell lines was calculated, normalized with the protein content and expressed as RLU per milligram (mg) protein (RLU/mg protein). Transfection experiments were performed at least in triplicate.

Statistical Analysis. For cytotoxicity and transgene delivery single factor ANOVA with Bonferroni correction was performed for data across each individual plasmid DNA loading conditions. For zeta potential experiments single factor ANOVA with Bonferroni correction was performed across each individual GNP concentration. Similar letters denote no significant statistical significance.

RESULTS AND DISCUSSION

A focused library of poly(amino ethers) was previously synthesized, characterized, and investigated for their transgene delivery capabilities(S. Barua, et al., 2009b; L. Vu, et al.,

2012). It was found that several of the novel poly(amino ethers) synthesized in our laboratory demonstrated higher transgene expression efficacy compared to 25kDa poly(ethylene imine) or pEI25k. In addition, due to the facile synthesis of this class of polymer and the ease with which amine containing monomers can be substituted to obtain poly(amino ethers) with varying chemical structures we employed these polymers for the combinatorial synthesis of plasmonic nanoparticles (GNP and AgNPs) under ambient conditions, without the need for energy intensive conditions. Poly(amino ethers) were able to template and cap nanoparticles, leading to stable dispersions in aqueous media. The diversity in poly(amino ether) chemistry translates to differences in the yield and kinetics of formation of these nanoparticles. Poly(amino ether)-templated gold nanoparticles were employed for transgene delivery and expression in mammalian cells.

Kinetics of Nanoparticle Formation. ***Gold Nanoparticle (GNP) Formation.*** GNP formation was observed for all polymers and conditions following incubation of PAEs with $HAuCl_4$ for 5 days (**Figure 4.2**). Nanoparticle formation was visualized by a change in color from a pale yellow solution to red-maroon-colored dispersion. This color change was corroborated by a light absorption peak maximum at approximately 520 nm, which is characteristic of spherical GNPs(Song, et al., 2010). The mechanism of gold nanoparticle formation is hypothesized to occur by metal ion binding to the amines present in PAEs. Following binding, transfer of electrons from the amines to metal ions(J.D.S. Newman & Blanchard, 2006) causes reduction of the latter to zero-valent ions. This leads to nucleation, growth and subsequent nanoparticle formation. As a result, PAEs are integral to this

process since they can template as well as cap nanoparticle formation, leading to the formation of stable dispersions in aqueous media. (**Figure 4.1b)**.

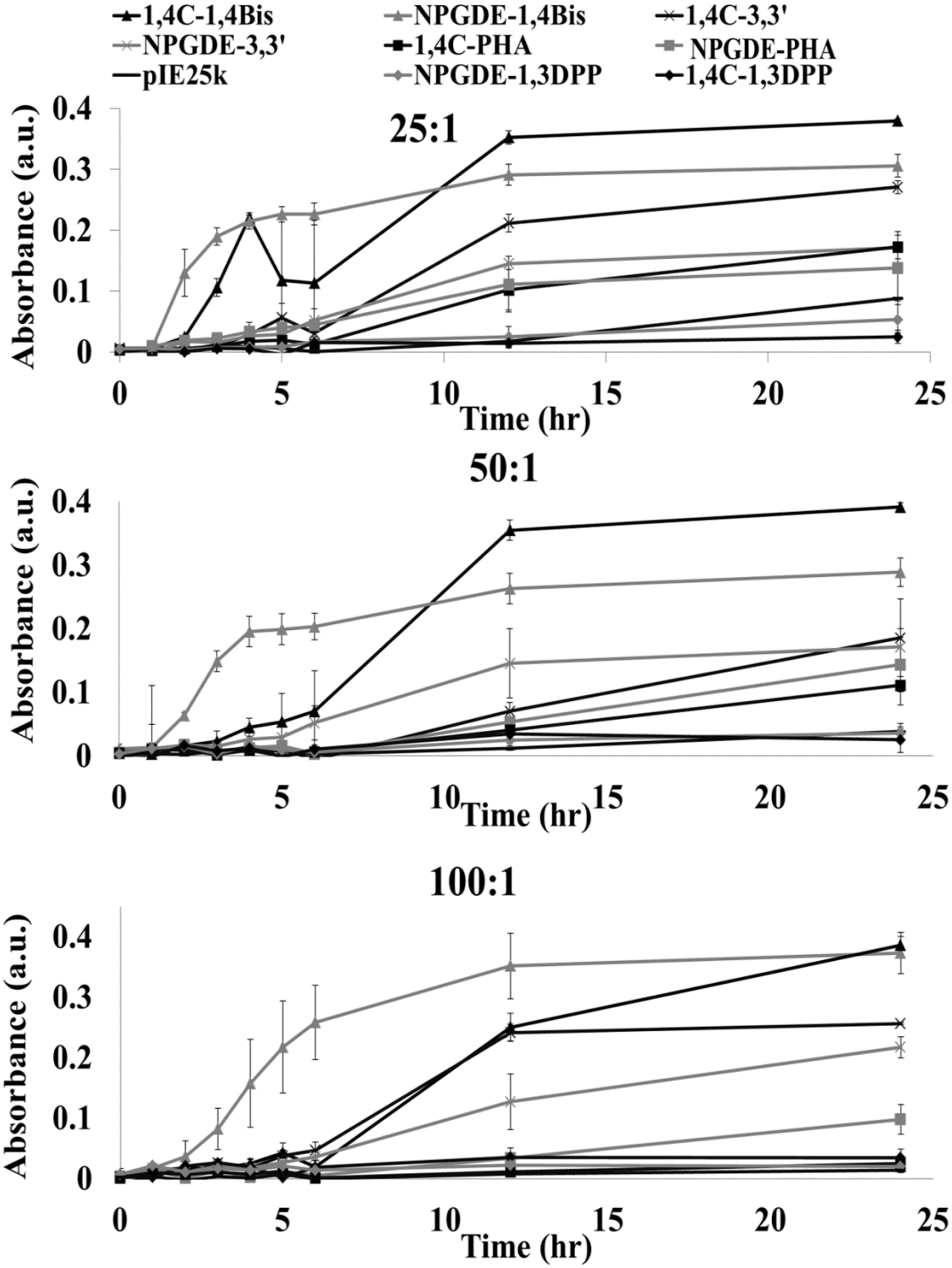

***Figure 4.2**. Comparison of PAE-GNP kinetics of formation monitored at maximum absorption peak (between 500-540 nm) by weight ratio and the difference in nanoparticle kinetics of formation with and without UV-irradiation for PAEs based on 1,4C. Nanoparticles were monitored for 5 days, however only the first 24 hours are shown. Data points represent the mean absorbance ± standard error (n=3). Lines connecting data points are included for visualization only.*

As seen in **Figure 4.2**, the extent of nanoparticle formation depends on the polymer chemistry employed. These observed differences in PAE-templated nanoparticle formation rates can, in turn, be correlated to the chemical composition of the amine monomers used for the polymer synthesis (**Figure 4.1**). Both, 1,4Bis and 3,3'-based polymers exhibited the fastest rates of nanoparticle formation. The 1,4Bis, monomer contains two primary amines (with one or both converted to a secondary amine following polymer synthesis), as well as two tertiary amines. Similarly, 3,3' contains two primary amines (with one or both converted to a secondary amine following polymer synthesis) as well as a tertiary amine. It is accepted that tertiary amine binding to metals is weaker compared to primary or secondary amines(Golub, Zilbermann, Cohen, & Meyerstein, 1996). The presence of tertiary amines in these polymers likely results in faster dynamics of binding, reduction, and release of gold ions. Faster nucleation and growth of gold nanoparticles is therefore likely observed in cases of polymers that have moderate affinities of interacting with gold, or those with an increased number of tertiary amines. PHA, and pEI25k, are both dominated by primary and secondary amines, whereas 1,3DPP has two primary amines. The high amine / charge density in pEI25k and PHA, and the presence of primary amines in 1,3DPP may result in stronger binding to gold ions, resulting in decreased de-solvation and thus decreased nucleation explaining the decreased kinetics of nanoparticle formation. In addition, complexation has been found to lower the redox potential of metal ions

resulting in decreased reducibility (Tan, Lee, & Wang, 2010). Thus increased complexation times compared to the polymers that possess higher amounts of tertiary amines will also result in decreased reducibility. These results suggest that polymers that are dominated with strong metal binding moieties (primary and secondary amines will result in decreased kinetics of nanoparticle synthesis. This is due to their decreased de-solvation resulting in a decrease in the metal ion reducibility and the reduced metal ions nucleation. By identifying or synthesizing amine-containing polymers or molecules with an increased ratio of tertiary amine, it is likely that enhanced nanoparticle kinetics can be observed. The tertiary amines will increase the de-solvation of the metal ions which will allow for faster nucleation kinetics as well as increased reduction. It is also possible that by modifying polymers such as pEI25k with weaker metal binding moieties can result in increased nanoparticle synthesis kinetics. These observations also allow for the synthesis of polymers with controllable reducing properties for tunable nanoparticle growth kinetics. However, sophisticated molecular modeling methods (e.g. molecular dynamics simulations) will be necessary to delve deeper into the mechanisms of PAE-templated nanoparticle formation.

Increase in the polymer to metal salt ratio resulted in retardation in the kinetics of nanoparticle formation, indicating that additional reduction / templating and capping sites did not promote faster kinetics (**Figure 4.3**). This difference in nanoparticle formation was observed during the first 12 hours of incubation, whereas after 24 hours, the effective concentrations of the GNP dispersions were comparable for a given templating polymer. This decrease in nanoparticle formation kinetics is likely due to polymer entanglement at higher concentrations. It has been reported that entanglement of polymer chains can decrease complexation rate of polymers with metal ions(Sakai & Alexandridis, 2005),

which in turn, can result in decreased reduction rates of metal ions and therefore, subsequent nanoparticle formation. This indicate that not only the identification of an ideal amine containing polymer with suitable chemical composition is necessary for optimal nanoparticle formation, but the reaction conditions need to be carefully controlled as well. Reaction conditions can also be used as an additional method to tune nanoparticle growth kinetics. It has been observed that increasing the reaction temperature can result in faster nanoparticle formation,(Yan, Blacklock, Li, & Mohwald, 2012) and modifying the reaction pH(C. Li, Li, Wan, Xu, & Hou, 2011) or reagent addition rate(Mualidharan, Subramanian, Nallamuthu, Santhanam, & Kumar, 2011) can result in different formation mechanism. Here we see that by controlling polymer concentration nanoparticle kinetics can be modified. Reaction conditions add additional tunability to control of nanoparticle growth rates.

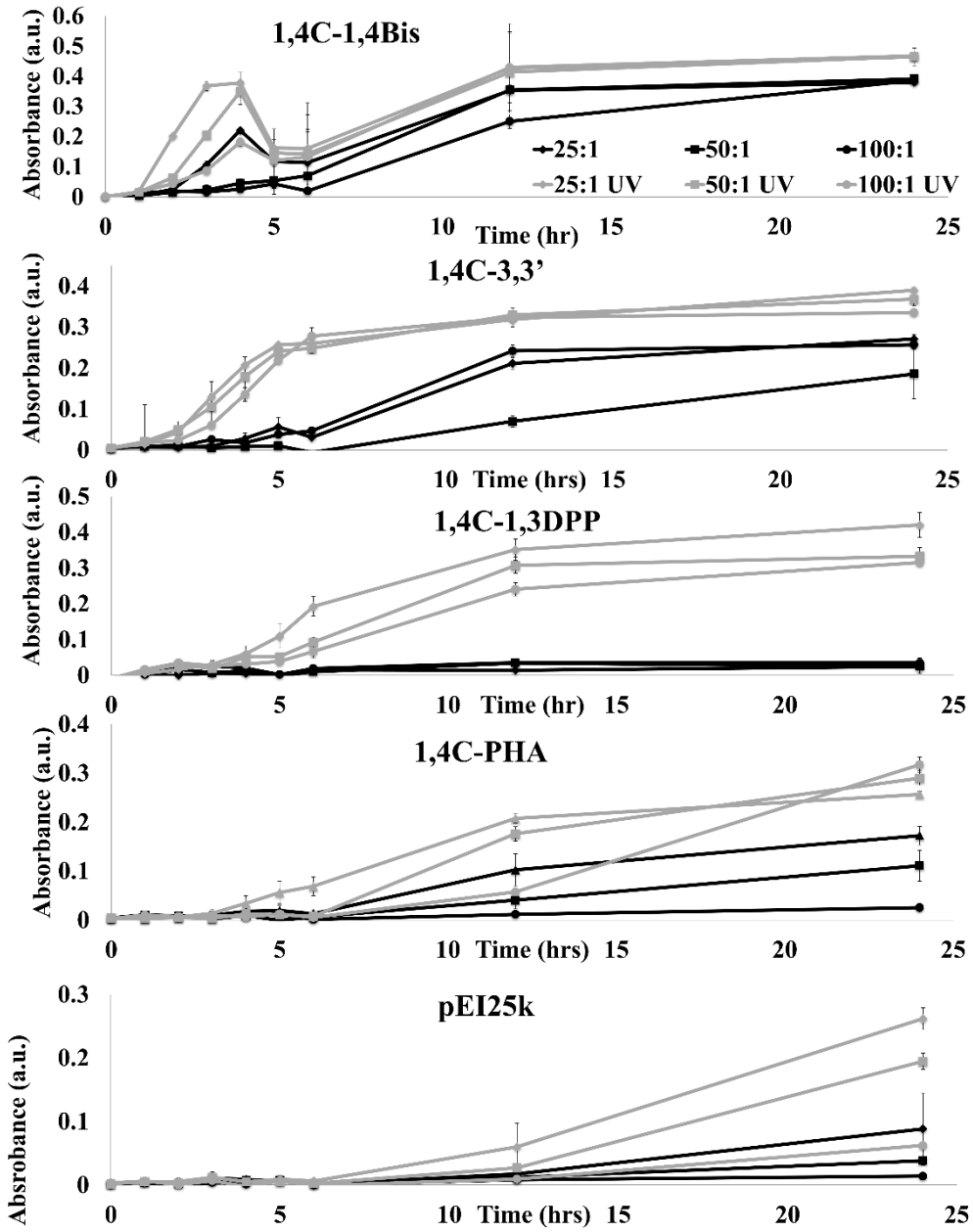

Figure 4.3. *Comparison of PAE-GNP kinetics of formation monitored at maximum absorption peak (legend parenthesis) by weight ratio and the difference in nanoparticle kinetics of formation with and without UV-irradiation. Nanoparticles were monitored for 5 days, however only the first 24 hours are shown. All particles were synthesized in triplicate and data points represent the mean absorbance ± standard error. Lines were included for visualization only.*

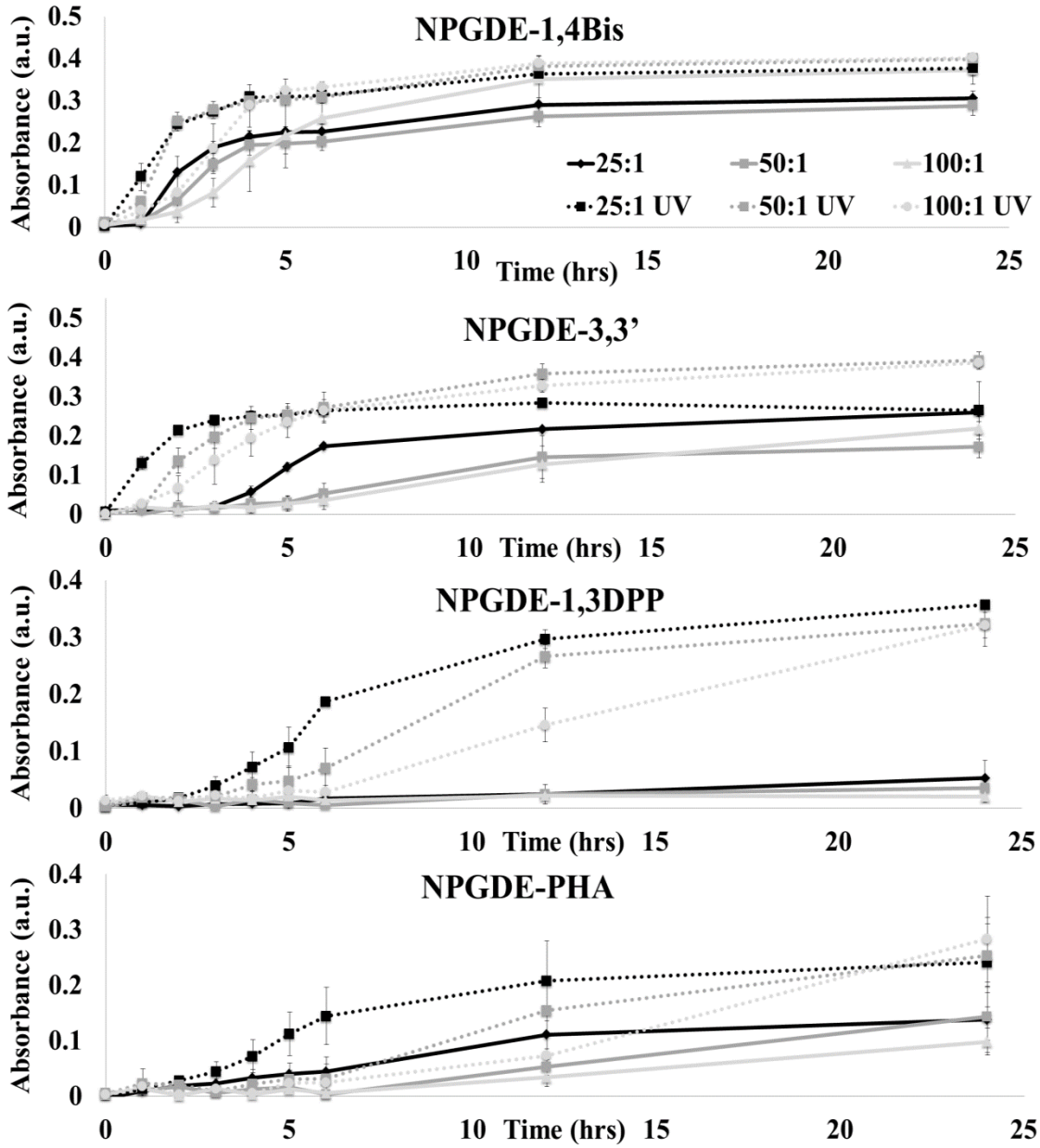

Figure 4.3 continued

Ultraviolet (UV) irradiation has been employed for photochemical reduction of both, gold and silver ions for nanoparticle formation(Eustis & El-Sayed, 2006; Eustis, et al., 2005; Harada, Inada, & Nomura, 2009; H. Zhang et al., 2012). Exposure to UV irradiation for 24 hours indeed resulted in an increase in GNP formations in case of all PAEs employed, but was particularly effective in the case of 1,3DPP and pEI25k polymers

(**Figure 4.3**). In presence of UV irradiation, formation of GNPs likely occurs through a co-reduction mechanism, where gold ions are simultaneously reduced by both, photo and chemical means. It has been proposed that nanoparticle formation following UV exposure occurs in a multi-step process(Kurihara, Kizling, Stenius, & Fendler, 1983). The proposed mechanism begins with excitation of Au^{3+} by the incident UV radiation, which is followed by subsequent reduction to an unstable Au^{2+} form. This results in disproportionation of Au^{2+} resulting in the formation of Au^{1+} and Au^{3+}. The Au^{1+} ions then absorb an additional photon and is again photo-reduced to Au^{0} or zero-valent gold ions, which nucleate and grow to form gold nanoparticles.

It is likely that UV radiation enhances the kinetics of PAE-templated nanoparticle formation via mechanisms similar to those previously proposed(Eustis & El-Sayed, 2006; Eustis, et al., 2005). We also investigated the formation of nanoparticle formation in presence of an anionic polymer, poly(styrene sulfonate) or PSS. To the best of our knowledge, PSS has no known inherent metal reducing capabilities, although the polymer has been employed as a stabilizing reagent in the presence of a reducing agent for nanoparticle synthesis(Dorris, Rucareanu, Reven, Barrett, & Lennox, 2008; Cw Hu, Huang, & Tsiang, 2009; Kumar, Kumar, Mathiyarasu, & Phani, 2007). Gold nanoparticle formation was observed following UV-based photo-reduction of $HAuCl_4$ in presence of PSS after 24 hours; no change in color (i.e. no nanoparticle formation) was observed when the gold salt was incubated with PSS in the absence of UV light. These results indicate UV irradiation can induce nanoparticle formation (metal reduction) in presence of a suitable capping agent, and that the observed increase in PAE nanoparticle formation during UV irradiation is most likely due to additional metal reduction via UV-photoreduction. In

contrast to PSS, PAEs can template the formation of gold nanoparticles by themselves in the absence of UV radiation. However, GNP kinetics and yield, is further enhanced by exposure to UV radiation via a co-reduction effect. All else being same, exposure to UV radiation resulted in higher yields of GNPs than PAEs alone, as demonstrated by higher final optical densities (surrogate for nanoparticle concentration).

Control over the presence or absence of UV irradiation adds further tunability over nanoparticle growth rate. This is most evident, as previously mentioned, in the case of pEI25k and the 1,3DPP-based polymers which both exhibited slow nanoparticle formation kinetics. However, by exposing them to UV irradiation, nanoparticle synthesis kinetics were vastly improved. This suggests that it if an appropriate capping agent, with slow or no nanoparticle synthesis kinetics, is wanted on the surface of the nanoparticle UV irradiation can be used to enhance nanoparticle synthesis. UV irradiation can also be used as an alternative to chemical reducing agents for nanoparticle synthesis with capping agents that have no reducing properties.

Silver nanoparticle (AgNP) formation. AgNP formation was observed for all PAE polymers and conditions following incubation of PAEs with $AgNO_3$ for three days at polymer to $AgNO_3$ weight ratios of 25 to 1, 50 to 1 and 100 to 1; interestingly AgNP formation was not observed in case of (**Figure 4.4**). Formation of silver nanoparticles was visually observed by a change in solution color from clear to a yellow color, which was reflected in the appearance of a maximum absorption peak at approximately 420 nm. However, the yields of AgNPs were lower than that of GNPs, and the times required for nanoparticle formation were significantly longer. This may be a result of amines showing

stronger affinities to silver compared to gold(Nath et al., 2006) resulting in stronger binding, decreased de-solvation, and decreased nanoparticle nucleation. Additionally, silver has lower reduction potential and higher electro-chemical potential compared to gold which may also explain the decreased nanoparticle formation(Hoppe, Lazzari, Pardinas-Blanco, & Lopez-Quintela, 2006). With the exception of 1,4C-3,3', PAE-based system showed moderate increase in absorbance at approximately 420 nm; in fact, a reduction maximal absorbance was observed from 24 to 48h, likely due to aggregation and precipitation of the nanoparticles. Interestingly, color change or appearance of an absorbance peak indicative of AgNP formation was not observed for pEI25k under any of the conditions investigated. It is likely that this is due to strong binding of the metal ions to the primary and secondary amines of pEI25k, which does not allow for subsequent de-solvation and nanoparticle nucleation. Previous reports on pEI25k-templated AgNP formation employed a strong reducing agent (e.g. $NaBH_4$)(H. Lee et al., 2001) or high incubation temperatures(Shin & Kim, 2011). Here, we demonstrate that PAEs generated in our laboratory are capable of synthesizing AgNPs in a one-pot synthesis method at room temperature without the use of an additional reducing agent. Again the importance of identifying a polymer or amine containing system is highlighted. Due to no observed AgNP synthesis for pEI25k under ambient conditions it is unsuitable for this application. Identification of polymers with weaker metal binding, or modification ofpEI25k to allow for weaker binding may allow for pEI25k templated AgNP synthesis.

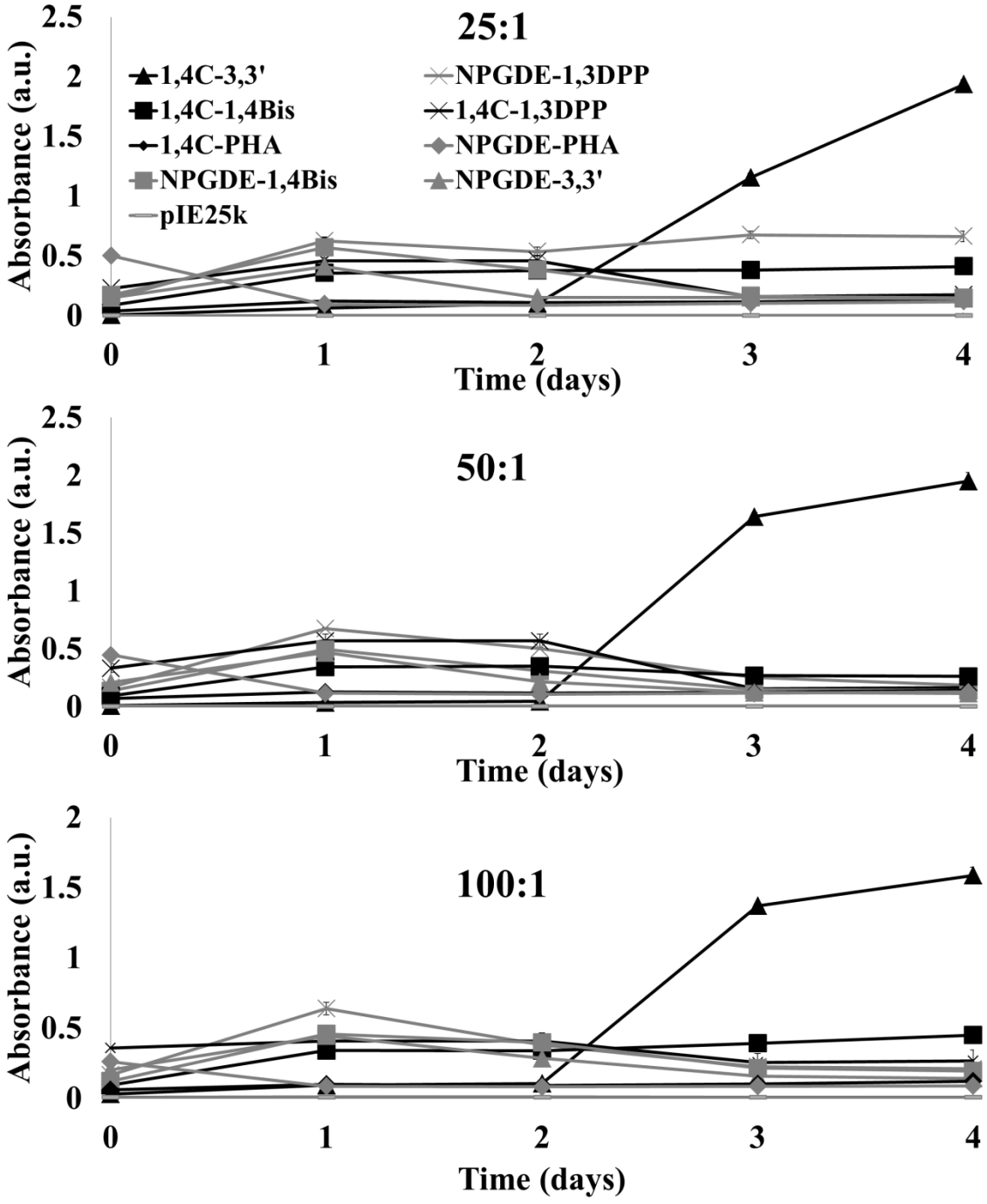

Figure 4.4. *Kinetics of PAE-AgNP synthesis monitored at maximum absorption peak (between 400-430 nm) at polymer to $AgNO_3$ weight ratios of* ***(top)*** *25 to 1,* ***(middle)*** *50 to 1, and* ***(bottom)*** *100 to 1. Nanoparticles were monitored for 4 days. Data points represent the mean absorbance ± standard error (n=3). Lines connecting data points are included for visualization only.*

As with GNPs, PAE-mediated AgNP synthesis was investigated in presence of UV-irradiation to determine if photo-reduction could increase the kinetics and yield of nanoparticles. Whereas observable PAE-AgNP synthesis took 1-2 days without UV-irradiation, AgNP formation began within 1-5 minutes in presence of UV irradiation (**Figure 4.5**). Interestingly, AgNP formation was not observed in case of pEI25K even in presence of UV irradiation, as indicated by a lack of color change, as well as lack of an absorption peak at 420 nm in the spectrum. In order to study effects over a longer period of time and to allow for maximal AgNP formation, PAE-$AgNO_3$ solutions were exposed to UV radiation for a maximum of 3 hours (**Figure 4.5**), during which, AgNP formation proceeded with fast kinetics. However, negligible levels of nanoparticle formation were observed once the UV irradiation was removed and the nanoparticles were kept in the dark for an additional 21 hours. These results indicate that the efficacy of photoreduction is significantly higher than that of chemoreduction for AgNP formation. However, similar to observations with GNPs, AgNP formation occurred most rapidly at lower polymer-to-metal salt weight ratios. All PAEs demonstrated similar efficacies for templating and capping AgNPs, and aggregation / precipitation of AgNPs was not observed when UV-irradiation was employed, unlike in the absence of radiation.

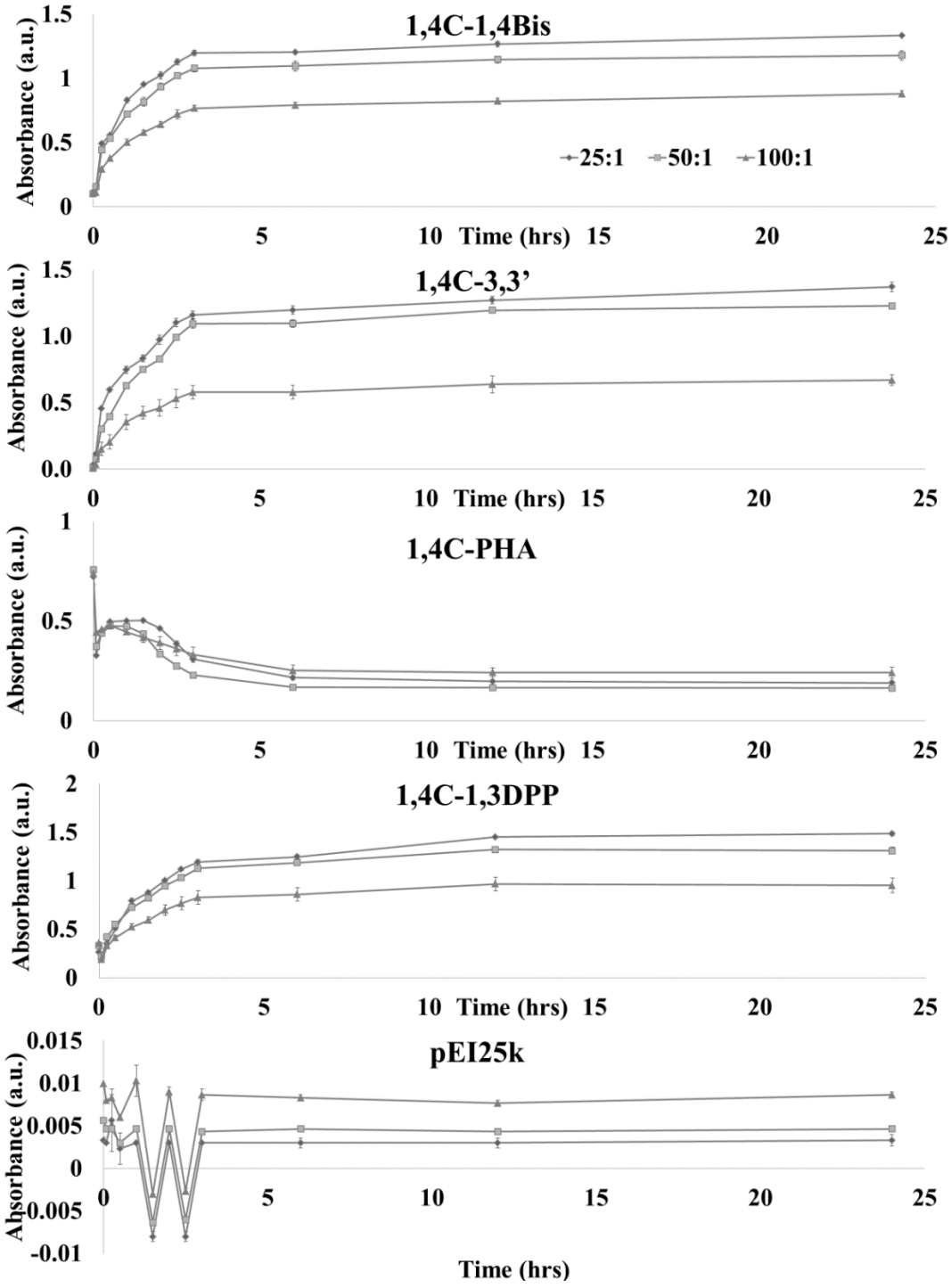

Figure 4.5. *Kinetics of PAE-AgNP synthesis monitored at maximum absorption peak (legend parenthesis) at different polymer to $AgNO_3$ weight in the presence of UV-irradiation. Nanoparticles were monitored for 24 hours with the initial 3 hours under UV*

irradiation. All particles were synthesized in triplicate and data points represent the mean absorbance ± standard error. Lines are included for visualization only.

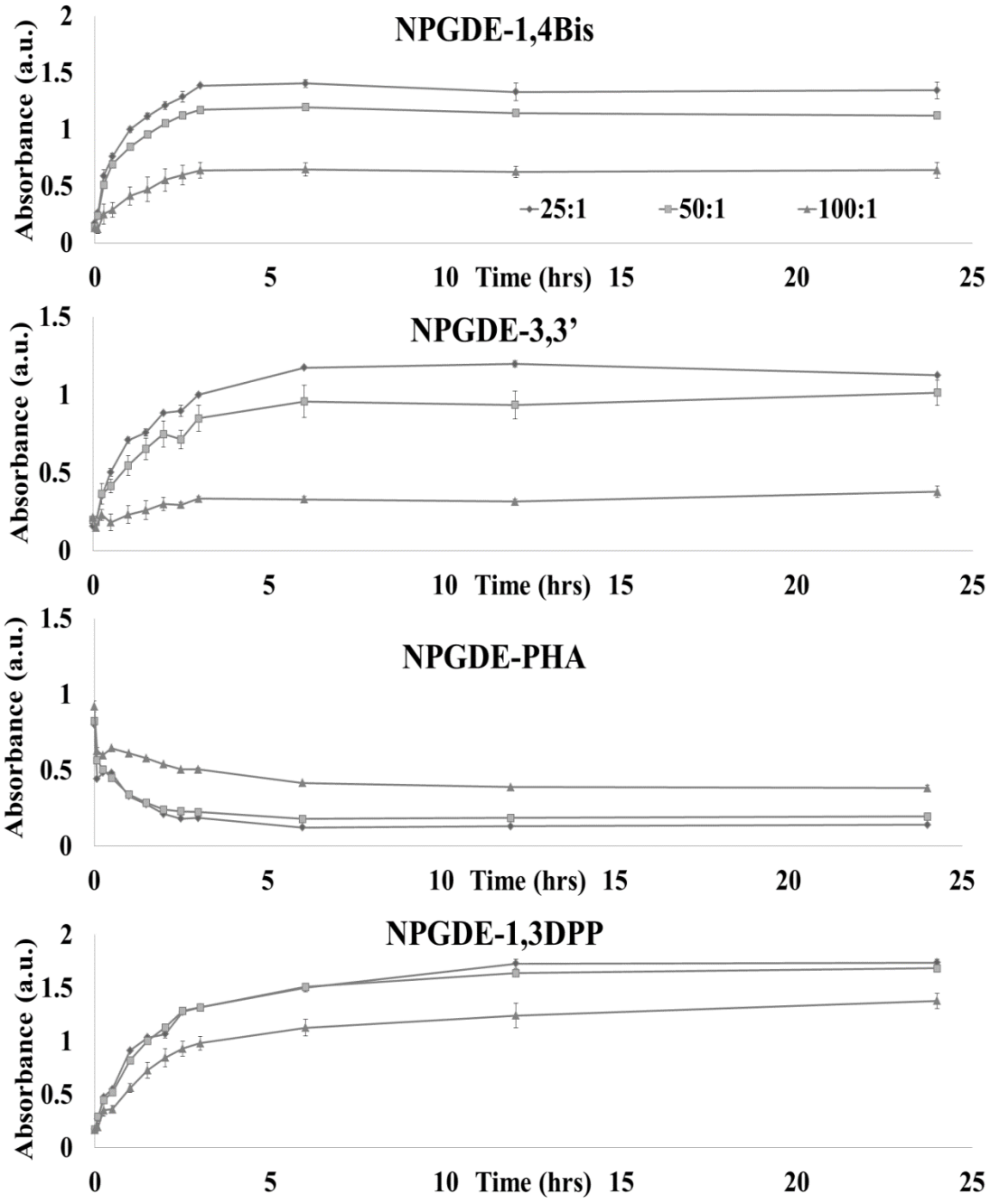

Figure 4.5. *Continued*

PAE-Nanoparticle Characterization. ***Transmission Electron Microscopy.*** Following synthesis in the absence of UV-irradiation and removal of excess polymer and metal salts via centrifugation 1,4C-1,4Bis-GNPs, NPGDE-1,4Bis-GNPs, pEI25k-GNPs, and NPGDE-1,4Bis-AgNPs were characterized by transmission electron microscopy (TEM); these polymers were chosen since 1,4Bis-based PAEs demonstrate the fastest kinetics or GNP formation. 1,4C-1,4Bis-GNPs, NPGDE-1,4Bis-GNPs, and pEI25k-GNPs possessed spherical metal cores in the sub-20 nm range (**Figure 4.6 a-i**). Despite the observed differences in the initial kinetics of nanoparticle formation, the metal cores exhibit similar sizes across the three different weight ratios tested. However, aggregation/bridging of some metal cores was observed in case of pEI25k-GNPs. NPGDE-1,4Bis-AgNPs demonstrate metal cores that are larger than 20 nm, with similar sizes across the three different tested weight ratios (**Figure 4.6 j, k, and l**). Some aggregation and interestingly, formation of nanorods, was observed in case of NPGDE-1,4Bis-AgNPs.

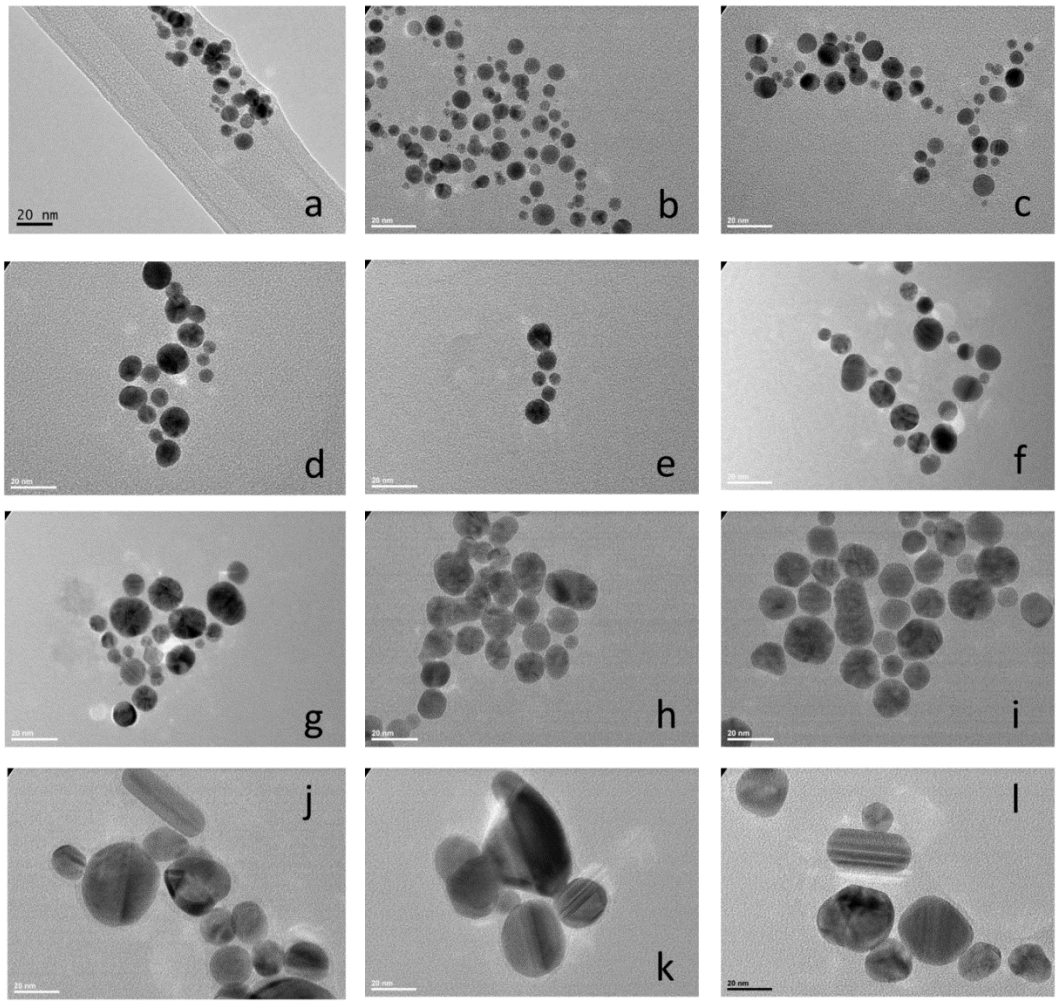

Figure 4.6. *TEM images of 1,4C-1,4Bis-GNPs at a weight ratio of (a) 25 to 1, (b) 50 to 1, (c) 100 to 1; NPGDE-1,4Bis-GNPs at weight ratios of (d) 25 to 1, (e) 50 to 1, (f) 100 to 1; PEI25k-GNPs at weight ratios of (g) 25 to 1, (h) 50 to 1, (i) 100 to 1; and NPGDE-1,4Bis-AgNPs at weight ratios of (j) 25 to 1, (k) 50 to 1, (l) 100 to 1 polymer to* $HAuCl_4$*. All scale bars indicate 20 nm.*

Hydrodynamic Diameter. The hydrodynamic diameters of all PAE-GNPs were in the sub-150 nm range (**Figure 4.7a**). The hydrodynamic diameter for a given PAE-GNPs did not vary significantly with different PAE to gold salt weight ratios. However, the hydrodynamic diameter increased moderately with an increase in the weight ratio for 1,4C-1,4Bis and 1,3DPP PAE-based gold nanoparticles. Interestingly, the hydrodynamic

diameters decreased with increasing weight ratios for PHA based polymers. With the exception of 1,4C-1,4Bis-GNPs the hydrodynamic diameters of PAE-GNPs synthesized with and without UV-irradiation are comparable. pEI25k-GNPs exhibited the smallest hydrodynamic diameters in the 25-35 nm range, which was similar to the size observed via TEM. The hydrodynamic diameters of 1,4C-1,4Bis-GNPs and NPGDE-1,4Bis-GNPs (non-UV-irradiated) were much larger than the metal cores observed via TEM. This is likely due to the presence of the polymer / PAE coat, which was not observed in TEM analysis.

All PAE-AgNPs exhibited hydrodynamic diameters in the sub-120 nm range (**Figure 4.7b**); no measurements were obtained in case of pEI25K due to lack of nanoparticle formation. As opposed to GNPs, less clear trends in hydrodynamic diameter size were seen with respect to synthesis conditions (i.e. change in weight ratios or UV irradiation) in case of PAE-AgNPs. For example, in case of 1,4C-1,4bis, 1,4C-1,3DPP, and NPGDE-PHA polymers, AgNPs synthesized in presence of UV-irradiation are smaller in size than those synthesized in absence of the radiation. However, the opposite trend was observed in case of other PAEs such as, 1,4C-3,3' and NPGDE-1,3DPP. Finally, diameters of AgNPs were comparable for some PAEs including, 1,4C-PHA, NPGDE-1,4Bis, and NPGDE-3,3'.

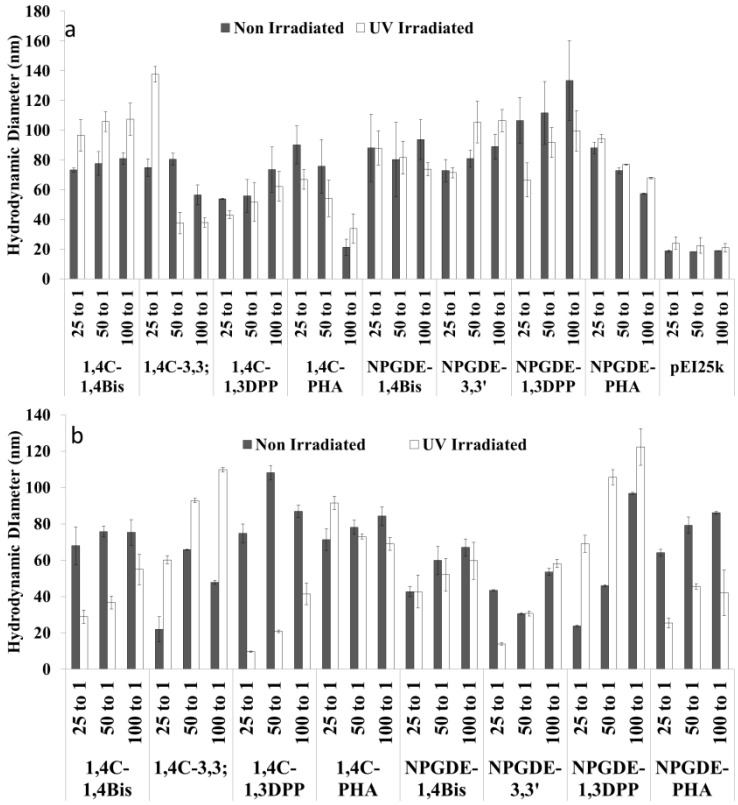

Figure 4.7. *Hydrodynamic diameter of (a) PAE-GNPs and (b) PAE-AgNPs following synthesis at different weight ratios, with and without UV-irradiation, and purified via centrifugation. Hydrodynamic diameters were measured in triplicate and data points represent the mean hydrodynamic diameter ± standard error.*

Amine Content. PAE-GNPs were further characterized for amine content using the ninhydrin assay in order to further confirm the presence of the cationic polymer; higher amine content is used as an indicator of increased polymer content. Similarly to the trend in hydrodynamic diameters, at increased weight ratios of PAE to $HAuCl_4$, 1,4C-1,4Bis-GNPs exhibited slightly increased amine content (i.e. increased polymer coating) (**Figure 4.8**). In addition, the amine content for PHA-based polymers decreased with an increase in weight ratios, which is in agreement with the decrease in hydrodynamic diameters observed for these polymers (**Figure 4.7**). Taken together, the amine content can be used as an

indicator of extent of polymer coating, and follows similar trends as that of the measured hydrodynamic diameters.

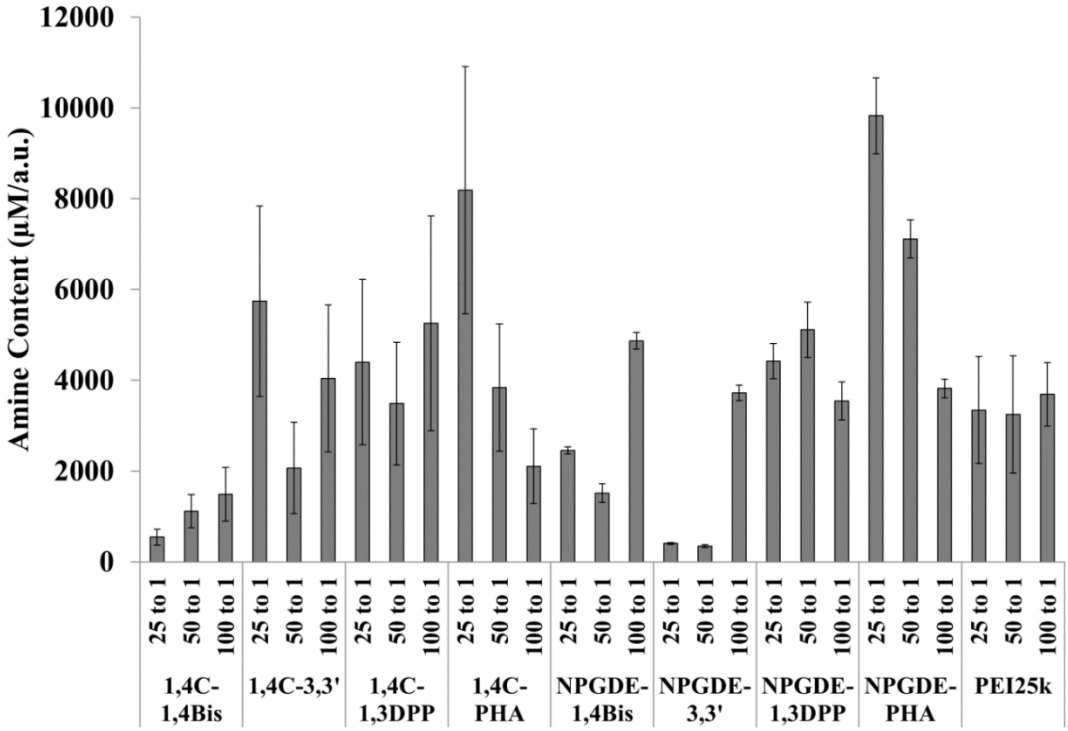

Figure 4.8. *Primary and secondary amine concentration of PAE-GNPs determined by ninhydrin assay. Amine concentration (µM) is normalized by the maximum absorbance (a.u.) of the PAE-GNPs. All measurement were done in triplicate and data points represent the mean measurement ± standard error.*

Biological Activity of PAE-Templated Nanoparticles: Transgene Delivery and Expression. Previous studies from our laboratory demonstrated that 1,4C-1,4Bis polyplexes(S. Barua, et al., 2009b; S Barua & K Rege, 2010), and 1,4C-1,4Bis-coated gold nanorods(Ramos & Rege, 2012a), were able to deliver plasmid DNA leading to transgene expression or gene silencing(Ramos & Rege, 2013b) in mammalian (e.g. cancer) cells. In these previous investigations 1,4C-1,4Bis polyplexes exhibited decreased cytotoxicity and up to 80 fold enhancement in transfection efficacies in PC3-PSMA cells. Additionally,

PAEs were employed to coat pre-made gold nanorods using a layer-by-layer deposition approach. These nanoparticles exhibited up to 165-fold enhancement compared to similarly modified pEI25k gold nanorods. Due to previous investigations identifying 1,4C-1,4Bis-based polymer systems s highly efficient non-viral gene delivery vehicles, 1,4C-1,4Bis-GNPs (i.e. PAE-templated GNPs) were investigated for their ability to deliver plasmid DNA leading to transgene expression. 1,4C-1,4Bis-GNPs were synthesized at a weight ratio of 100 to 1 (1,4C-1,4Bis to $HAuCl_4$) in presence of UV irradiation. They were then dispersed in serum-free media (SFM) at different concentrations, and loaded with 1-250 ng of pGL3 plasmid DNA, which expresses the luciferase protein. Plasmid-loaded 1,4C-1,4Bis-GNPs or 'nanoassemblies' were delivered to 22Rv1 human prostate cancer and MB49 murine bladder cancer cells. Lipofectamine 3000 (Lipo3000) was also investigates as a commercially available delivery vehicle. The nanoassemblies exhibited greater cytotoxicity in 22Rv1 cells (**Figure 4.9a**) when compared to MB49 cells (**Figure 4.9b**). Lower concentrations of 1,4C-1,4Bis-GNPs were therefore used for delivery to 22Rv1 cells (concentrations of 4.9, 9.8, 24.4, and 48.8 μg/mL) than in the case of MB49 cells (concentrations of 9.8, 24.4, 48.8, and 97.5 μg/mL). Lipo3000 was found to significantly less toxic in 22Rv1 cell when compared to the 24.4 and 48.8 μg/mL concentration. In MB49 cells it exhibited similar cytotoxicity for the majority of conditions, though it was significantly more toxic than some conditions in the 50-200 ng plasmid DNA range.

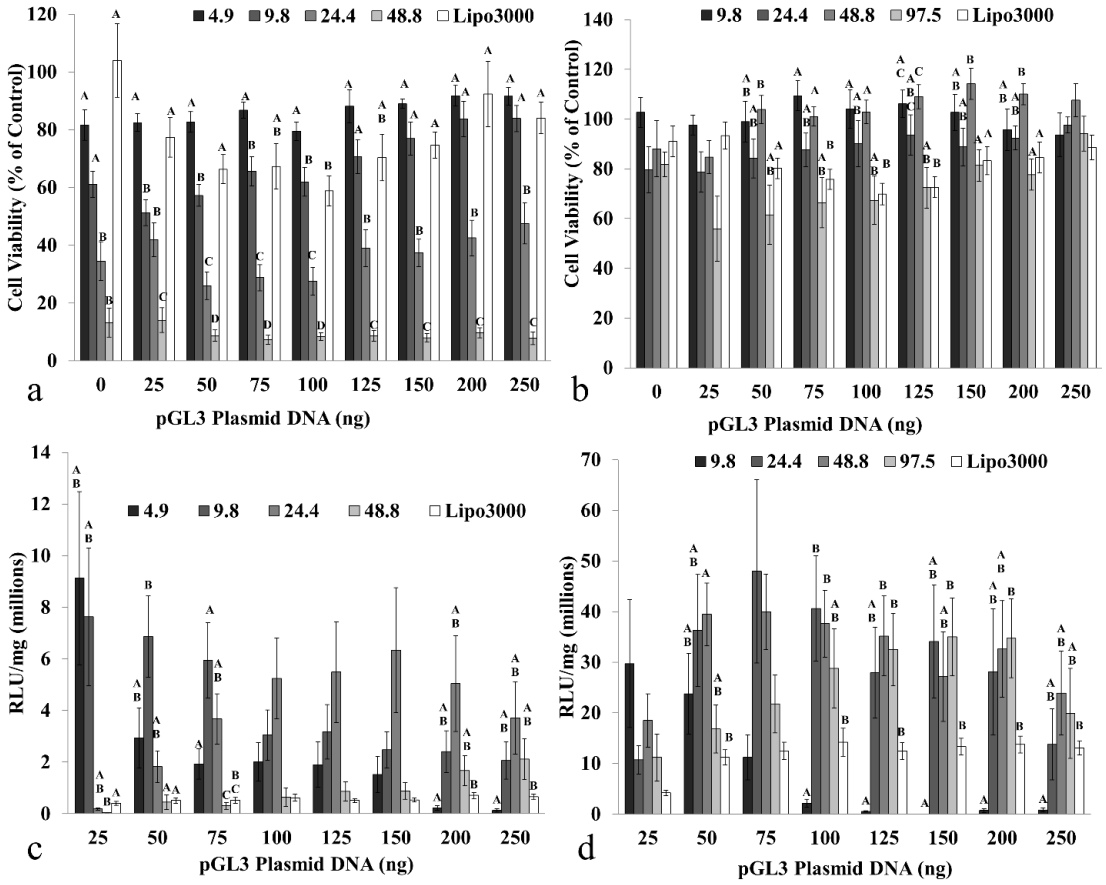

Figure 4.9. *Cell viability of* ***(a)*** *22Rv1 and* ***(b)*** *MB49 cells, and luciferase expression (RLU/mg) in* ***(c)*** *22Rv1 and* ***(d)*** *MB49 cells following delivery of 1,4C-1,4Bis-GNPs synthesized at a weight ratio of 100 to 1 1,4C-1,4Bis to $HAuCl_4$ with UV irradiation. The* ***concentrations*** *of 1,4C-1,4Bis-GNPs were adjusted to 4.9, 9.8, 24.4, or 48.8 µg/mL for 22Rv1 cells and 9.8, 24.4, 48.8 or 97.5 µg/mL in MB49 cells, and loaded with varied amount of pGL3 plasmid DNA for transgene expression. Lipo3000 was also investigated as a control. Cell viability and luciferase expression were determined 48 hours following transfection. Data points represent the mean measurement ± standard error (n≥3). Same letters within a loading condition indicate no statistical significant difference, absence of letter indicated no statistical significant difference within the loading condition for all concentrations and Lipo3000 (ANOVA w/Bonferroni correction).*

The highest observed luciferase transgene expression was at ~9.2 million RLU/mg, at a treatment condition of 4.9 µg/mL of 1,4C-1,4Bis-GNPs and plasmid loading of 25 ng in 22Rv1 cells (**Figure 4.9c**) and was found to not be statistically significant from Lipo3000 at this loading conditions. Luciferase expression decreased with increasing

plasmid loading on the nanoparticles. A similar trend was observed when 9.8 µg/mL GNPs were employed for delivering plasmid DNA. However, at this concentration, the nanoparticles were significantly higher than Lipo3000 at loading conditions of 50 and 75 ng. It is likely that the decrease in luciferase expression is due to a decrease in the nanoassembly zeta potential since negatively charged plasmids can shield the positively charged polymer coating with increasing loading amounts, as seen previously(Ramos & Rege, 2012a). Zeta potential measurements of 1,4C-1,4Bis-GNPs were found to decrease for all nanoparticle concentrations as the amount of plasmid DNA loaded increased to 250 ng (**Figure 4.10**). In some instances a reversal of the positive charge was observed, likely due to excess negative charge of the plasmid DNA shielding the positive charges from the amines in these PAEs.

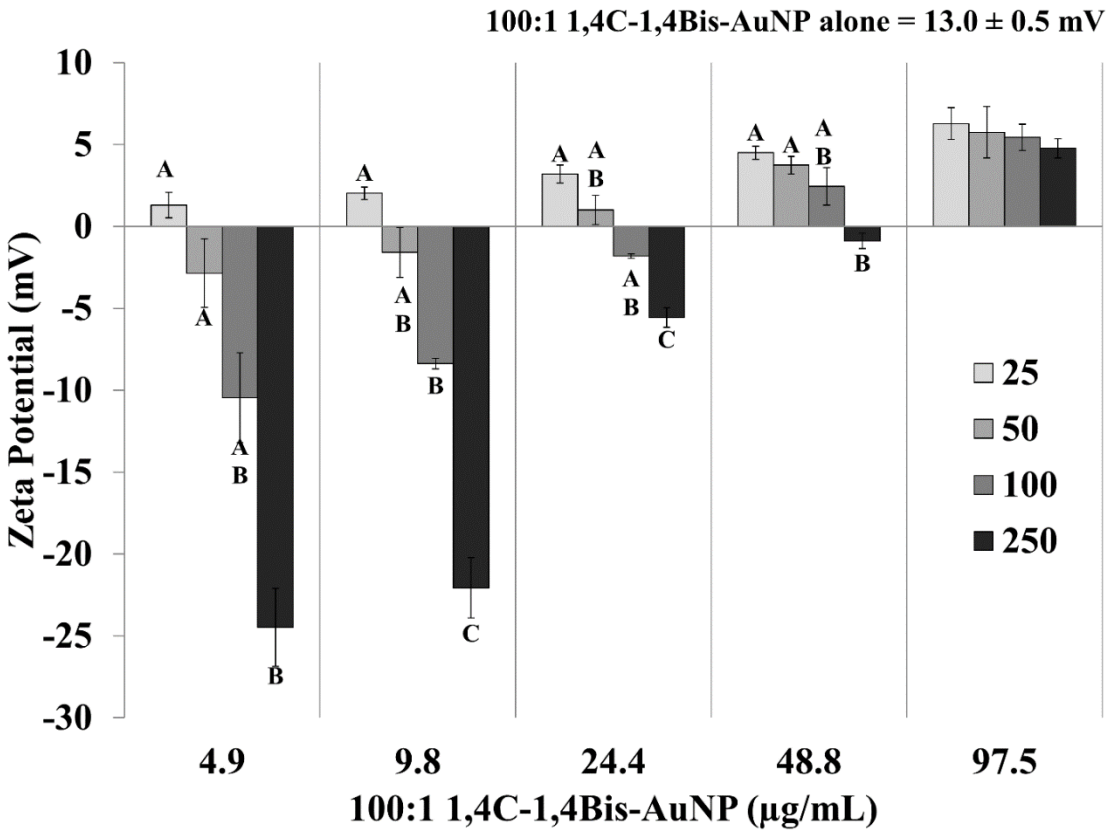

Figure 4.10. *Zeta potential values of 1,4C-1,4Bis-GNPs synthesized at a weight ratio of 100 to 1 1,4C-1,4Bis to $HAuCl_4$ with UV irradiation, and subsequently loaded with varying amounts of pGL3 plasmid DNA (ng plasmid DNA indicated in the figure legend). Values represent the mean zeta potential ± standard error (n=3). All plasmid loading conditions were found to be statistically significant to the unloaded condition (student t-test $p<0.05$). Same letters within a loading condition indicate no statistical significant difference, absence of letter indicated no statistical significant difference within the loading condition for all concentrations and Lipo3000 (ANOVA w/Bonferroni correction).*

Use of higher concentrations of 1,4C-1,4Bis-GNPs (i.e. 24.4, 48.8, and 97.5 µg/mL) can result in increased luciferase expression, most likely due to an increase in the effective polymer concentration. Although increased polymer concentration can allow for increased interactions with cells leading to greater uptake, cell viability was observed to be less than 50% under these conditions. As a consequence of this toxicity at higher doses, luciferase expression levels did not reach the maximum observed in case of the 4.9 µg/mL dose condition.

In MB49 cells, the highest observed luciferase expression was ~50 million RLU/mg at a GNP concentration of 24.4 µg/mL and plasmid loading of 75 ng (**Figure 4.9d**) However this was not found to be statistically significant from Lipo3000. At a concentration of 48.8 µg/mL and 50 ng plasmid loading, GNPs exhibited a significantly higher transfection efficacy than Lipo3000. Additionally, the levels of luciferase expression observed in MB49 cells were significantly higher than those observed in 22Rv1 cells. Similar to 22Rv1 cells there was an observed decrease in luciferase expression at higher plasmid loading conditions. This is likely due to the observed decrease in zeta potential (**Figure 4.10**) as a result of shielding of the positive charges on the PAEs(Ramos & Rege, 2012a). It is likely that intermediate loadings of pGL3 (25-100ng) are likely ideal

conditions where zeta potential is positive enough to allow for cell interaction and uptake, and enough plasmid DNA is loaded for effective transgene delivery and expression.

The facile synthesis method and chemical diversity of the poly(amino ether) polymers have elucidated certain design principles that could help in engineering future amine containing polymeric systems for efficient one-pot synthesis of gold and silver nanoparticle systems. As can be observed from our results, polymers with higher amounts of tertiary amines resulted in the fastest nanoparticle growth. Similar observations have been reported, where when increasing the ratio of tertiary amines to gold-salt resulted in a decrease in time for observable gold nanoparticle synthesis using PAMAM succinamic acid dendrimers(Vasile et al., 2014). The ability of tertiary amines to result in faster nanoparticle formation kinetics is likely due to two reasons. First, the binding of tertiary amines bind to metal ions is weaker than that of secondary or primary amines. This is important as it allows for binding, reduction, and quick release of the metal ions for nucleation and nanoparticle growth. Second, tertiary amines have a higher oxidation potential than secondary or primary amines(Lewis & Crompton, 2004) which allows for them to more readily give up electrons resulting in faster reduction of the metal ions. Though tertiary amines are favorable for reduction, release, of metal ions, secondary and primary amines have the same function, only at slower rates. Thus optimization of primary, secondary, and tertiary amines within a polymer can allow for tunability of nanoparticle growth, depending on specific requirements. It has been reported that change in nanoparticle reduction/nucleation rates can affect the size and optical properties of nanoparticles(X. Sun, Dong, & Wang, 2005). This change in nanoparticle formation rate can also be a result of reaction conditions. As observed here, an increase in

polymer concentration led to the decrease in nanoparticle formation kinetics (Figure 3). This also shows the importance of using an appropriate capping agent that can not only stabilize nanoparticles in aqueous media, but also impart the desired functionality for a given application. Specifically, PAE-templated gold nanoparticles synthesized in this study were used for transgene delivery; thus, PAEs were simultaneously able to template nanoparticle formation, stabilize them in aqueous media, carry and deliver plasmid DNA to mammalian (cancer) cells.

PAE-templated gold and silver nanoparticle formation reported here is a facile and attractive method for synthesis of these plasmonic nanoassemblies, and is either competitive to or better than other existing methods employed for nanoparticle generation. Polypeptides have also been used as reducing and capping agents for facilitating nanoparticle formation from metal salts; it was found that the formation of metal nanoparticles by short peptides depends on both the reducing capability and the capping / binding properties of the peptide(Tan, et al., 2010). Polypeptide-nanoconjugates have been used to template the synthesized of gold nanoparticles for in a one-pot method and have been used for transgene delivery(Yan, et al., 2012) as well as antiviral- and anticancer drug delivery(Shirazi et al., 2012) *in vitro*. We have previously demonstrated that cysteine-containing elastin-like polypeptides can be employed for templating the formation of gold nanoparticle synthesis within 18h, although upwards of 175Gy of ionizing (X-ray) radiation are required for obtaining significant levels of nanoparticles(Walker, et al., 2013).

Polymers have also been investigated for the synthesis of gold nanoparticles. For example, PVP has been used as a capping agent for nanoparticles synthesized via reduction

by gycerol(Grace & Pandian, 2006). Thiol-modified pEI2 (pEI with a molecular weight of 2kDa) was used for capping of gold nanoparticles following chemical reduction and demonstrated efficient gene delivery(Mini Thomas & Alexander M Klibanov, 2003). Excessive modifications were necessary in order to thiolate the pEI and $NaBH_4$ was required to induce nanoparticle formation. In addition, pEI25k-silvernanoaprticles have been synthesized, however, they required chemical reduction or high temperatures for efficient nanoparticle synthesis(H. Lee, et al., 2001; Shin & Kim, 2011). PEI25k has been investigated previously for the one-pot synthesis of gold nanoparticles(X. Sun, et al., 2005) and pEI25k- gold nanoparticles demonstrated efficient delivery of siRNA for gene silencing(Song, et al., 2010). However, as demonstrated here, and previously by us, several poly (amino ethers) demonstrate either higher transgene expression efficacies(Ramos & Rege, 2012a), (S. Barua, et al., 2009b; L. Vu, et al., 2012) or nanoparticle templating activities or both compared to pEI25k.

CONCLUSIONS

In this report, we demonstrated a facile, one-pot, combinatorial synthesis method for the generation of both, gold and silver nanoparticles under ambient conditions using a small set of poly(amino ethers) generated in our laboratory. PAEs were able to simultaneously act as both, reducing and capping agents for nanoparticle synthesis, and did not require the use of any additional reagents (e.g. reducing agents) or subsequent derivatization, which are significant advantages over several existing methods. Poly(amino ethers) from our library demonstrated faster kinetics of gold nanoparticle formation compared to 25 kDa branched poly(ethylene imine) or pEI25k. Significantly, all PAEs

were able to template formation of silver nanoparticles, whereas this was not observed with pEI25k.

The rate of nanoparticle formation is dependent on the chemical composition of the polyamine monomers used in the polymer synthesis. Particularly, 1,4-bis(3-aminopropyl) piperazine (1,4Bis), and 3,3'-diamino-n-methyldipropylamine (3,3') - based polymers, which are likely to have high content tertiary amines, demonstrated the fastest kinetics of nanoparticle formation, possibly due to increased solvation of amine-metal complexes that facilitates nanoparticle nucleation(Tan, et al., 2010). Nanoparticle synthesis was dependent on the polymer concentration relative to the metal ion concentration. Exposure to UV irradiation significantly enhanced the kinetics of nanoparticle formation; of particular significance, the time required for silver nanoparticle synthesis was greatly reduced from several days to only a few minutes in presence of UV radiation. Hydrodynamic diameters of less than 150 nm were seen for all nanoparticles, while the metal cores were spherical and approximately 20 nm in diameter in most cases. We demonstrated that 1,4C-1,4Bis-templated gold nanoparticles were able to deliver plasmid DNA leading to transgene (luciferase) expression in two different cancer cell lines. The ease of synthesis of PAE-templated plasmonic nanoparticles, stability in biologically relevant media, presence of amines for further functionalization, and biological activity (e.g. nucleic acid delivery), make this an attractive approach for several applications in biotechnology and medicine.

CHAPTER 5

COMPARISON OF IN VITRO POLYMER AND NANOPARTICLE SYSTEMS FOR TRANSGENE DELIVERY: POLYPLEXES, GOLD NANOROD NANOPLEX, AND GOLD NANOSPHERE NANOPLEX

Viruses have been employed for transgene delivery to various cell lines, both *in vitro* (Kasman, Barua, Lu, Rege, & Voelkel-Johnson, 2009b; Y. Park et al., 2010; Simeone, Cascarelli, & Logsdon, 1997; Varga et al., 2005) and *in vivo* (Jounaidi, Chen, Veal, & Waxman, 2006; Jounaidi & Waxman, 2004) due to high levels of transgene expression. However, concerns with immunogenicity and insertional mutagenesis(Merdan, Kopecek, & Kissel, 2002) have motivated investigations into non-viral vectors, including cationic polymers, as potentially safer alternatives. In addition, ease of synthesis, scale up, versatility, and in some cases, biocompatibility and biodegradability (Elsabahy, Nazarali, & Foldvari, 2011), make cationic polymers attractive delivery vehicles. Cationic polymers are able to bind and complex with negatively charged plasmid DNA (pDNA), resulting in the formation of polymer/pDNA complexes also known as polyplexes. These polyplexes typically retain a positive charge and are thus able to interact with negatively charged cell membranes and other surface proteins. Polyplex-membrane interactions facilitate endocytosis into cell and delivery to intracellular endosomal compartments. Successful delivery vehicles are then able to escape endosomes, presumably in part due to endosomal buffering by cationic polymers(Akinc, Thomas, Klibanov, & Langer, 2005; Berthold, Shiraishi, & Nielsen, 2010; Boussif et al., 1995). Following uncomplexing in the cytoplasm, a fraction of the

delivered pDNA in the cytoplasm enters the nucleus where they are transcribed leading to translation in the cytoplasm, and ultimately expression of the transgene. Polyethylenimine (PEI), (Boussif, et al., 1995; Cherng, Hung, & Kao, 2011; Chumakova et al., 2008; Coll et al., 1999; Gabrielson & Pack, 2009; Kang, Kang, & Bae, 2011; M. Lee, 2007; Mishra, Kang, & Bae, 2011; Y. H. Wang, et al., 2011), poly amido-amines (Emilitri, Ranucci, & Ferruti, 2005; S. T. Guo et al., 2011), and chitosan (Jean, Alameh, Buschmann, & Merzouki, 2011; Sarkar, Srivastava, Chatterji, & Kundu, 2011) are among the commonly employed cationic polymers for plasmid DNA delivery. However, observed low efficacies of polymer-mediated transgene expression has resulted in engineering of novel polymer and polymeric-based delivery vehicles with higher efficacies.

In addition to polymeric vehicles, inorganic nanoparticles, including gold nanoparticles, have been widely explored for drug and gene delivery to cells(Conde, et al., 2012; H.-C. Huang, et al., 2010; H. C. Huang, et al., 2011; S. T. Kim et al., 2012a; Masood, et al., 2012; Ramos, et al., 2012; Zhao, et al., 2012). Particle properties play a significant role in determining the efficacy of vehicles for transgene delivery and expression. However, despite the significance of particle physicochemical properties(Champion, Ktare, & Mitragotri, 2007), a head-to-head comparison of different gene delivery vehicles, specifically polymeric and nanoparticle-derived vehicles has been elusive. We have previously employed ring-opening polymerization of diglycidyl ethers and polyamines for the combinatorial generation of a library of poly(amino ethers) (PAEs) for transgene delivery and expression (S. Barua, et al., 2009b; S. Barua et al., 2011a). The1,4 C-1,4 Bis polymer, generated from 1,4-cyclohexanedimethanol diglycidyl

ether (1,4C) and 1,4-bis(3-aminopropyl) piperazine) (1,4Bis) monomers demonstrated higher levels of transgene expression than 25 kDa PEI depending on the polymer:pDNA weight ratios (S. Barua, et al., 2009b; S. Barua & K. Rege, 2010). Additionally, the 1,4C-1,4Bis polymer has been employed for gold nanorod modification for effective transgene and shRNA plasmid delivery, resulting in both exogenous transgene expression and endogenous gene silencing efficacies(Ramos & Rege, 2012a, 2013a). We recently have employed the 1,4C-1,4Bis polymer for the one-pot synthesis of gold nanoparticles. These previous studies offer us a unique opportunity to compare different gene delivery systems in a head-to-head fashion. Here, we investigate the transgene expression efficacies of 1,4C-1,4Bis polymer, 1,4C-1,4Bis-templated gold nanoparticles, and 1,4C-1,4Bis-coated gold nanorods in different cancer cell lines.

MATERIALS AND METHODS

1,4C-1,4Bis Poly(amino ether) Polymer Synthesis. Polymer synthesis was carried out as described previously (S. Barua, et al., 2009b). Briefly 1,4-cyclohexanedimethanol diglycidyl ether (1,4C) was reacted in equimolar amounts to 1,4-bis(3-aminopropyl) piperazine (1,4Bis), to generate 1,4C-1,4Bis, The polymerization reaction was carried out in 20 ml glass scintillation vials for 16 hours. Following the reaction, polymers were dissolved at a concentration of 10 mg/mL in phosphate-buffered saline (1 X PBS) and the solution pH was adjusted to 7.4 using 30% hydrochloric acid in deionized (DI) water in order to compensate for the basicity of the cationic polymer. The extent of polymerization was determined by comparing reactive amine concentrations at initial mixing of monomer reagents (time – 0h) and after 16 hours polymerization using the ninhydrin assay as described previously (S. Barua, et al., 2009b; Kasman, et al.,

2009a). Following polymerization, purification was carried out by dialysis using a 1000 Da molecular weight cut off (MWCO) membrane. The polymers were dialyzed against Nanopure water for 48 hours and fresh water was replaced every 12 hours. After 48 hours of purification, the polymer solutions were lyophilized, reconstituted in 1X PBS.

Generation of Gold Nanorods (GNRs). The seed-mediated method(Johnson, et al., 2002; Nikoobakht & El-Sayed, 2003) was used for the synthesis of cetyltrimethyl ammonium bromide (CTAB) or CTAB-templated gold nanorods (CTAB-GNRs). Briefly, a seed solution was prepared by adding 5 ml of 0.2 M CTAB to 5 ml of 0. 5 mM auric acid ($HAuCl_4.3H_20$). The addition of 0.6 ml of iced water-cooled 10mM sodium borohydride was used to reduce the solution. The growth solution was prepared by adding 5 ml of 1mM auric acid to 5 ml of 0.2 M CTAB containing 250 µl of 4mM silver nitrate. The growth solution was reduced by the addition of 70 µl of 0.0788 M L-ascorbic acid. Seed solution (12 µl) was added to the growth solution and continuously stirred for four hours to allow for the generation of the gold nanorods. The concentration of silver nitrate in the growth solution was modulated in order to generate CTAB-GNRs, with absorbance maxima at different wavelengths (750-900 nm) in the near infrared (NIR) region of the absorption spectrum.

Generation of 1,4C-1,4Bis-GNR Nanoassemblies ('GNRs'). Dispersions of GNRs with an optical density of 0.5 at the maximal absorbance wavelength in 1.5 mL microcentrifuge tubes were centrifuged at 6000 rcf for 10 minutes using a Microfuge 18 centrifuge (Beckman Coulter, Brea, CA), in order to remove excess CTAB surfactant.

The supernatant was removed and the GNRs were redispersed in 100 µL of a poly(styrene sulfonate) (PSS) solution (10 mg/mL in 0.01X PBS; ~1.5 mM salt concentration). This dispersion was immediately sonicated for 30 minutes to allow for the formation of PSS-coated GNRs (PSS-CTAB-GNRs). Excess PSS was removed by centrifugation at 6000 rcf for 10 minutes and the supernatant was discarded. PSS-CTAB-GNRs were then re-dispersed in 300 µL nanopure water, and 200 µL 1,4C-1,4Bis polymer (10 mg/mL in 0.01X PBS) were added to the dispersions. These were immediately sonicated for 30 min to allow for the formation of the 1,4C-1,4Bis-PSS-CTAB-GNR nanoassemblies. Excess 1,4C-1,4Bis polymer was removed by centrifugation at 6000 rcf for 10 minutes and the supernatant was discarded. The nanoassemblies were finally resuspended in serum-free media (SFM) for use in *in vitro* experiments.

1,4C-1,4Bis-Gold Nanospheres (GNS) Synthesis. 1,4C-1,4Bis-Gold Nanosphere synthesis was carried out in a one pot reaction under UV irradiation (366 nm, 6 W) and otherwise ambient conditions. Briefly, 1 mg of $HAuCl_4$ was co-incubated with 100 mg of 1,4C-1,4Bis. Reactions were allowed to proceed for 16 hours. GNP synthesis was confirmed by a reddish color and maximal absorption at approximately 520 nm, characteristic of gold nanospheres. After synthesis 1,4C-1,4Bis-Gold Nanosphere dispersions were centrifuged for 20 min at 10,000 rcf in order to remove excess polymer and $HAuCl_4$ and redispersed in nanopure water.

Ninhydrin Assay for Amine Content Determination. Following synthesis of 1,4C-1,4Bis, 1,4C-1,4Bis-GNRs, and 1,4C-1,4Bis-GNS samples were prepared for a ninhydrin assay to determine amine content. Ninhydrin (2,2-Dihydroxyindane-1,3-dione) reacts with free primary and secondary amines with a resulting deep blue of purple color which can be measured and compared to a standard for amine concentration quantification. Glycine standards with known amine concentrations (0, 50, 150, and 300 µM) were prepared in 1XPBS at a pH of 7.4 with a total volume of 200 µl. 1,4C-1,4Bis in 1XPBS at a pH of 7.4 was prepared at concentrations of 0.1 mg/ml, 0.05 mg/ml, and 0.025 mg/ml with a total volume of 200 µl. 1,4C-1,4Bis-GNRs and GNS were synthesized as previously described and dispersed in 200 µl nanopure water. Their absorbance spectra of the samples was measured in order to determine maximum absorbance. To these samples, 100 µl of ninhydrin reagent was added and samples were incubated in water at 100^{o}C for ten minutes, following which they were allowed to cool to room temperature. 500 µl of 95% ethanol was added to each sample and the absorbance measured at 570nm. Following correction for absorbance of gold nanoparticles at 570nm for the appropriate samples, primary and secondary amine concentration was determined via comparing measured values to the glycine standard curve.

Transgene Delivery. ***Plasmid DNA.*** The pGL4.5 control vector (Promega Corp., Madison, WI), which encodes for the modified firefly luciferase protein was used for transgene expression studies. E.coli (XL1 Blue) cells containing the pGL4.5 plasmid DNA were cultured overnight (16 h, 37 °C, 150 rpm) in 15 mL tubes (Fisher) in 5 mL of

Terrific Broth (MP Biomedicals, LLC). The cultures were then centrifuged at 5400*g* and 4°C for 10 min. Plasmid DNA was purified according to the QIAprep Miniprep Kit (Qiagen) protocol and DNA concentration and purity were determined based on absorbance at 260 and 280 nm, determined using a NanoDrop spectrophotometer (ND-1000; NanoDrop Technologies). Plasmid DNA concentrations of 200-300 ng/µL were typically obtained and volumes were adjusted in order to load between 10-200 ng of plasmid DNA on PAE-GNRs prior to transfections.

Cell culture. 22Rv1 bone-metastatic prostate cancer cells and MB49 murine bladder cancer cells were both generous gifts from Professor Christina Voelkel-Johnson of the Medical University of South Carolina. MDA-MB-231 breast cancer cells were a generous gift from Dr. Josh Lebear of Arizona State University. RPMI-1640 with L-glutamine and HEPES (RPMI-1640 medium), DMEM with high glucose, L-Glutamine, and HEPES, Pen-Strep solution: 10000 units/mL penicillin and 10000 µg/mL streptomycin in 0.85% NaCl, and fetal bovine serum (FBS), were purchased from Hyclone. Serum-Free medium (SFM) consisted of RPMI-1640 or DMEM medium plus 1% Pen-Strep (1000 units/mL penicillin and 1000 µg/mL). Serum containing medium (SCM) consists of SFM plus 10% FBS. 22Rv1 cells, as received, were cultured in a 5% CO_2 incubator at 37ºC using RPMI-1640 medium containing 10% heat-inactivated FBS and 1% antibiotics (Pen-Strep). MB49 and MDA-MB-231 cells, as received, were cultured in a 5% CO_2 incubator at 37ºC using DMEM containing 10% heat-inactivated FBS and 1% antibiotics (Pen-Strep).

Cytotoxicity. Cells were seeded at a density of 8,400 cells/well in 150 µL serum-containing medium in a 96-well plate and allowed to attach overnight. Plasmid DNA

encoding the luciferase protein, pGL4.5, was diluted to a concentration of 50 ng/μL using Tris EDTA buffer (10 mM Trizma and 1mM EDTA, Thermo Fisher Scientific, Rockford, IL). 1,4C-1,4Bis, 1,4C-1,4Bis-GNRs, and 1,4C-1,4Bis-GNS were adjusted to a reactive amine concentration of either 0.5 or 1 μM in 1XPBS. These were then added to between 0 and 300 ng of pGL4.5 plasmid DNA. Complexes were incubated for 20 minutes at room temperature prior to use. Cells were treated with delivery vehicles in serum containing media for 6 hours in an incubator under humidified air containing 5% CO_2 at 37°C. Subsequently, the medium was replaced with fresh serum-containing medium. Following 48 hour incubation, cell viability was determined using the 3-(4,5-dimethylthiazol-2-yl)-2,5-diphenyltetrazolium bromide (MTT) cell proliferation assay kit (ATCC). This assay involves the enzymatic conversion of the MTT substrate to purple-colored formazan in metabolically active cells. This activity is widely employed as an indicator of cell viability and proliferation(Hayon, et al., 2003); loss of metabolic activity was used as an indirect indicator of loss of cell viability upon polyplex treatment. Following addition of the MTT reagent (2 h at 37 °C), cells were treated with a lysis buffer from the kit and kept at room temperature in the dark for 2 h in order to lyse cells and solubilize the MTT product. The absorbance of each well was measured using a plate reader (BioTek Synergy 2) at 570 nm to assay for the blue MTT product. For data analysis, absorbance readouts were normalized to the live (untreated) and dead (5 μL of 30% hydrogen peroxide treated) controls.

Transgene Delivery. MB49, MDA-MB-231, and 22RV1 cells were transfected using DNA/polymer complexes (polyplexes) and DNA/nanoparticle complexes (nanoplexes) consisting of pGL4.5 plasmid DNA and the synthesized polymers. Prior to

transfection, cells were seeded at a density of 8,400 cells/well in 150 μL serum-containing medium in a 96-well plate and allowed to attach overnight. Plasmid DNA encoding the luciferase protein, pGL4.5, was diluted to a concentration of 50 ng/μL using Tris EDTA buffer (10 mM Trizma and 1mM EDTA, Thermo Fisher Scientific, Rockford, IL). 1,4C-1,4Bis, 1,4C-1,4Bis-GNRs, and 1,4C-1,4Bis-GNS were adjusted to a reactive amine concentration of either 0.5 or 1 μM in 1XPBS. These were then added to between 0 and 300 ng of pGL4.5 plasmid DNA. Complexes were incubated for 20 minutes at room temperature prior to use. Cells were then treated with the delivery vehicles in serum-containing medium for 6 hours in an incubator under humidified air containing 5% CO_2 at 37°C. Subsequently, the medium was replaced with fresh serum-containing medium and allowed to incubate for an additional 48 hours. Luciferase protein expression, expressed in terms of relative luminescence units or RLU, was determined using the luciferase assay kit according to the manufacturer's protocol 48 hours after transfection; luminescence measurements were carried out using a plate reader. The protein content (mg protein) in each well was determined using the BCA Protein Assay Kit. Transgene expression in all cell lines was calculated and normalized with the protein content and expressed as RLU per milligram (mg) protein (RLU/mg protein). Transfection experiments were performed at least in quadruplicate using 2 separate batches of synthesized polymers.

Determination of Hydrodynamic Diameter of PAE-GNPs and PAE-AgNPs. Polyplexes, GNRs and GNS's were generated as described above and set to a reactive amine concentration of 1 μM and co-incubated with 0, 50, 100, 200, or 300 ng of pGL4.5 plasmid DNA. Dispersions (in 1XPBS) were measured for hydrodynamic diameters via

dynamic light scattering (DLS) using a Delsa™ Nano Submicron Particle Size and Zeta Potential Particle Analyzer (Beckman Coulter, Brea, CA). The hydrodynamic diameter was reported in nanometers (nm).

Determination of Zeta Potential of Nanoassemblies. Polyplexes, GNRs and GNS's were generated as described above and set to a reactive amine concentration of 1 μM and will be co-incubated with 0, 50, 100, 200, or 300 ng of pGL4.5 plasmid DNA. Dispersions (in 1XPBS) were transferred to the manufacturer's reusable zeta cell (Beckman Coulter, Brea, CA) and zeta potential values were determined using a Delsa™ Nano Submicron Particle Size and Zeta Potential Particle Analyzer (Beckman Coulter, Brea, CA). Zeta Potential values were reported in millivolts (mV).

Statistical Analyses. All experiments will be carried out at least in triplicate unless mentioned otherwise. Statistical significance was determined using a single factor ANOVA with Bonferroni correction across groups at specific plasmid DNA loading amounts. Reported values represent the mean ± standard error.

RESULTS AND DISCUSSION

Previous studies from our laboratory demonstrated that polyplexes based on the 1,4C-1,4Bis poly(amino ether) polymer(S. Barua, et al., 2009b; S Barua & K Rege, 2010) were efficient transgene delivery vehicles. 1,4C-1,4Bis polyplexes exhibited up to 80 fold enhancement in transfection efficacies in PC3-PSMA cells compared to pEI25k at polymer:pDNA weight ratio of 25:1(S. Barua et al., 2009a). In related studies, the 1,4C-1,4Bis polymer was employed to coat pre-made gold nanorods using a layer-by-layer deposition approach. The 14C-1,4Bis-GNRs were able to deliver plasmid DNA leading

to transgene expression exhibited up to 165-fold enhancement compared to pEI25k gold nanorods(Ramos & Rege, 2012a). Similarly 1,4C-1,4Bis-GNRs were investigated for delivery of shRNA expressing plasmid and demonstrated efficient gene silencing in mammalian (e.g. cancer) cells(Ramos & Rege, 2013a). The 1,4C-1,4Bis polymer also demonstrated the ability to template the synthesis of gold nanospheres using a one-pot synthesis approach similar to previously reported methods(Song, et al., 2010). 1,4C-1,4Bis polymer-templated gold nanospheres also demonstrated transgene delivery in different cancer cell lines. Following up on the versatility of the 1,4C-1,4Bis polymer, we generated three unique non-viral gene delivery vehicles, each of which has individually demonstrated efficient transgene delivery. These three delivery vehicles, 1,4C-1,4Bis polyplexes, 1,4C-1,4Bis-gold nanorod-nanoplexes (GNRs), and 1,4C-1,4Bis-gold nanosphere-nanoplexes (GNS's), were investigated and compared for their transgene expression efficacy. Physicochemical differences including the presence of a metal core vs. a polymer system, as well as in shape between GNRs and GNS's we reasoned that a head-to-head comparison could enable a thorough understanding of the efficacy of these different gene delivery systems.

The concentration of reactive amines was used as the basis of comparison between transgene delivery efficacies of polyplexes, GNRs, and GNS's. Protonation of amines results in cationic character of these delivery vehicles, which is important for electrostatic binding with anionic pDNA molecules (Rege et al., 2005b); higher nanoparticle zeta potential values can result in stronger binding to nucleic acids(Munier, Messai, Delair, Verrier, & Atamon-Onal, 2005), which can also protect them from nuclease degradation. The amines will also be responsible for the vehicle surface charge

which can greatly influence cell-vehicle binding and uptake. Due to non-specific delivery of these vehicles (i.e. no antibodies present), electrostatic based uptake will be largely influenced by the surface amines. Retaining a positive charge is desired as nanoparticles with stronger positive charges have demonstrated higher transfection efficacies in *in vitro* studies5(Chen et al., 2007; Munier, et al., 2005). It is well-established that there is a strong correlation between nanoparticle surface potential and cellular uptake efficacy; where cellular uptake is greater for nanoparticles with strongly positive charged surfaces as it facilitates interactions with cell surfaces that possess negative surface potential, and subsequent endocytosis (Liang Chen, Joseph M Mccrate, James C-M Lee, & Hao Li, 2011; Frohlich, 2012; Yue et al., 2011; Zhao, et al., 2012). Though lower charged, neutral, or negatively charged particles have been observed to be taken up by cells, most observations conclude that strongly positive nanoparticles are more readily internalized by cells (J. Liu et al., 2010). Additionally, the surface charge of the vehicles can also play a role in the cytotoxicity of the vehicles. In consideration of their higher uptake efficacies, in some cases, it has been reported that strongly cationic nanoparticles result in higher cytotoxicity in cells *in vitro*, when compared to similar neutral or negative forms. This can be attributed to toxicity resulting from positively charged functional groups (i.e. amines) that give the particle its positive charge, or as a result of higher uptake tending to greater biological effects(Frohlich, 2012). Additionally, one study has reported that when comparing similar particles with different charges (strongly negative, strongly positive, and near-neutral), following cellular internalization, positively charged nanoparticles were able to escape the endosomes, while the negatively charged and neutral particles were found preferentially in lysosomes(Yue, et al., 2011). Endosomal

escape is a crucial step for delivery of nucleic acids for transfection studies(S. Barua & K. Rege, 2010). Thus, the available amines on the delivery vehicles will play a critical role in their transfection efficacies.

The ninhydrin assay was used in order to quantify the concentration of reactive amines for the three individual delivery vehicles. Following quantification, a linear relationship describing the amine concentration versus the polymer concentration and the GNR and GNS optical densities (pseudo concentration) was identified (**Figure 5.1**). Using these linear relationships, an amine concentration can be chosen and the corresponding concentration or optical density of the delivery vehicles can be calculated.

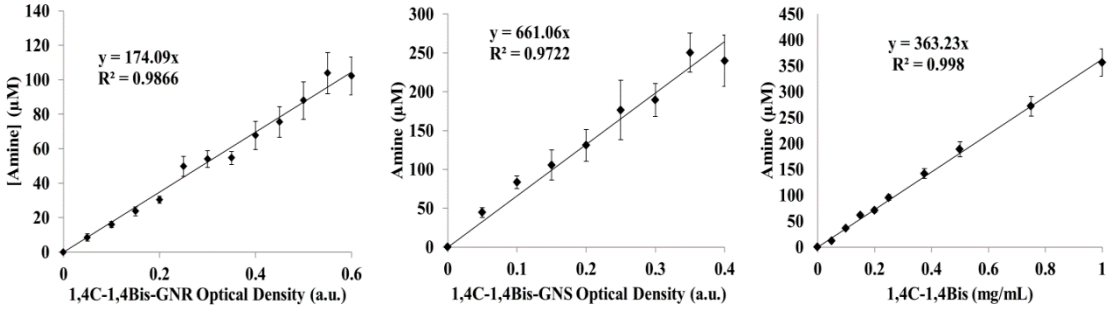

Figure 5.1. *Relationship between (left) 1,4C-1,4Bis-GNR, (middle) 1,4C-1,4Bis-GNS, and (right) 1,4C-1,4Bis polymer pseudo/concentration and amine concentration determined via ninhydrin assay (n≥9across at least 3 independent polymer batches)*

Amine concentrations of 0.5 µM and 1 µM were chosen in order to investigate the cytotoxicity and transgene delivery efficacies of the delivery vehicles. The different vehicles were set to these concentrations and complexed with varying amounts of pGL4.5 plasmid DNA. Following complexation, they were used to treat 22Rv1 human prostate cancer cells, MDA-MB-231 human breast cancer cells, and MB49 murine bladder cancer cells. Following 48 hours of treatment, the three different vehicles were observed to have similar cytotoxicity profiles at similar treatment conditions in each cell lines (**Figure 5.2**).

For no cell line did the cell viability drop below ~65% of the control and the majority of conditions were found to be between 70-100% of the control. These was deemed suitable values for further investigations for transgene delivery. The similarities in the cytotoxicity profiles are likely due to the similar amount of amines present for each delivery vehicle. In addition, due to the lack of any major differences in the cytotoxicity profile, it will be safe to conclude that any differences in the transgene delivery efficacies will not be due to excessive toxicity of a particular delivery vehicle.

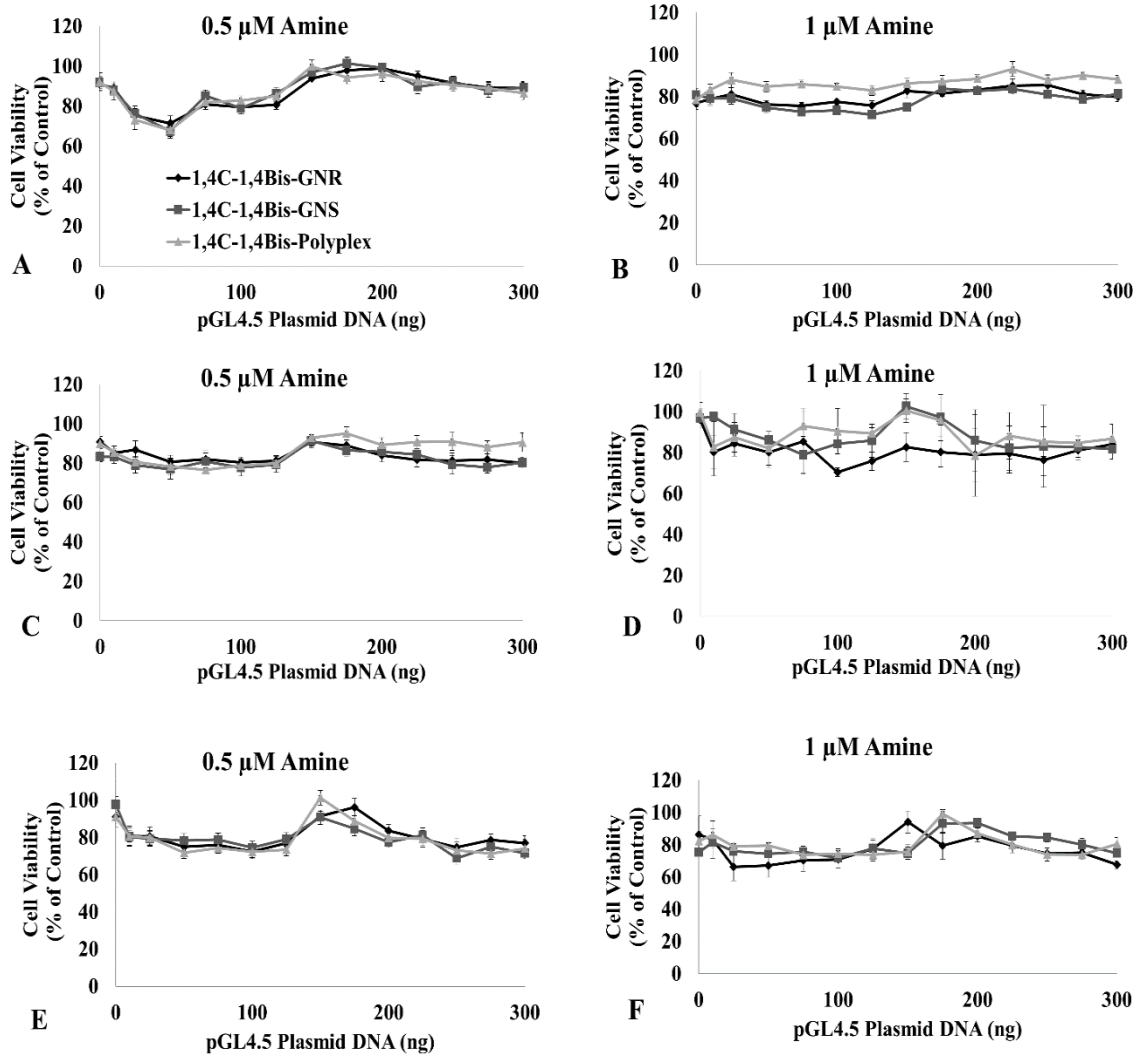

Figure 5.2. *Cytotoxicity of 1,4C-1,4Bis-based poly/nanoplexes loaded with between 0-300 ng of pGL4.5 plasmid DNA in 22Rv1 cells at (A) 0.5 µM amine concentration and (B) 1 µM amine concentration, in MDA-MB-231 cells at (C) 0.5 µM amine concentration and (D) 1 µM amine concentration, and in MB49 cells at (E) 0.5 µM amine concentration and (F) 1 µM amine concentration. Cell viability was determined 48 hours following treatment with the plasmid DNA loaded delivery vehicles (n=9 across 3 independently synthesized polymer batches). Lines were added for visualization only*

At each amine concentration, the three cell lines exhibited similar transgene dose-dependent responses based on the amount of plasmid DNA loaded (**Figure 5.3**). At the 0.5 µM amine concentration, luciferase expression appeared to be highest for the three different delivery systems in between the 25-50 ng range with a decrease in luciferase expression observed at loading conditions above 150 ng. At the 1 µM concentration, maximum luciferase expression was observed in the 75-100 ng plasmid DNA range, with a less pronounced decrease in luciferase expression as the amount of plasmid DNA complexed with the delivery vehicles increased.

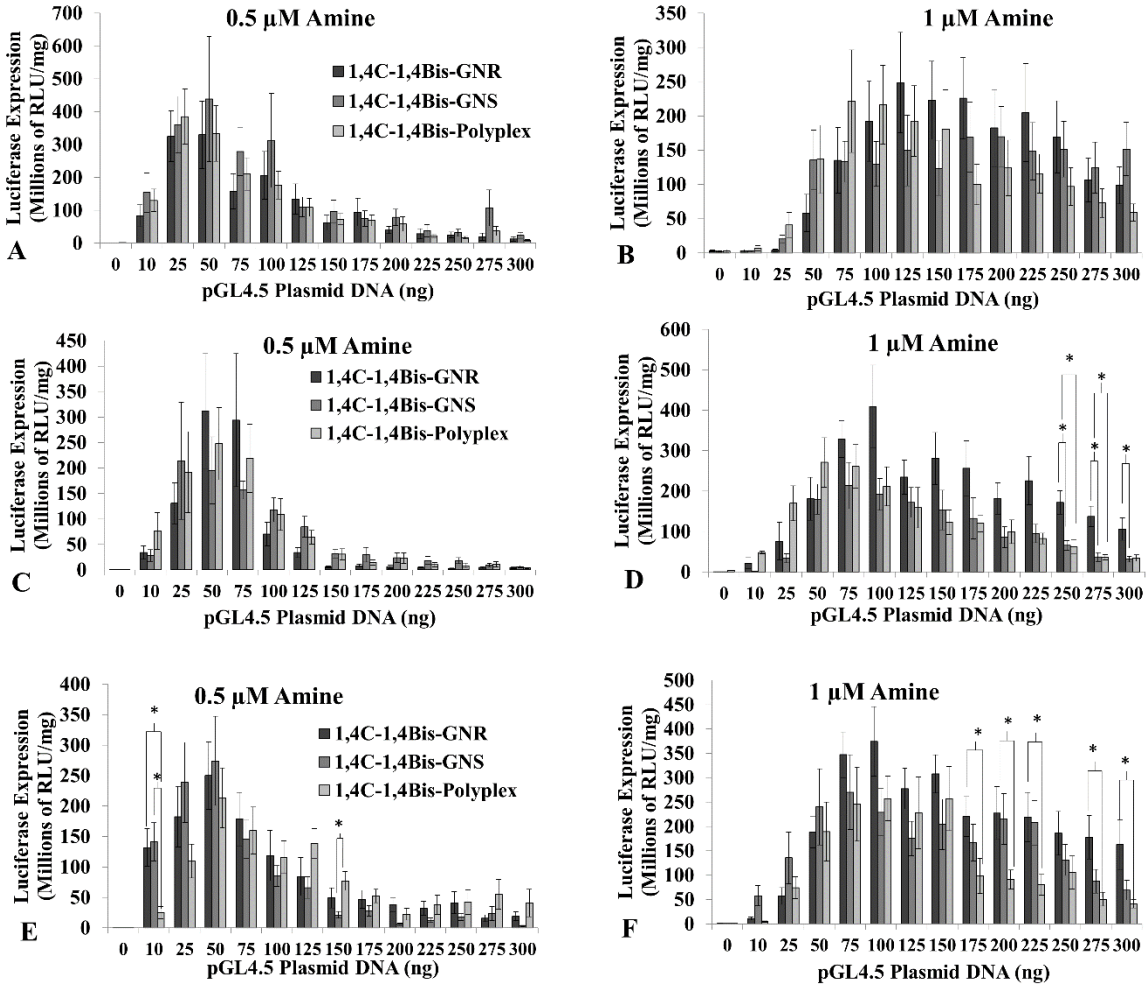

Figure 5.3. *Transgene delivery of 1,4C-1,4Bis-based poly/nanoplexes loaded with 0-300 ng of pGL4.5 plasmid DNA in 22Rv1 cells at (A) 0.5 µM amine concentration and (B) 1 µM amine concentration, in MDA-MB-231 cells at (C) 0.5 µM amine concentration and (D) 1 µM amine concentration, and in MB49 cells at (E) 0.5 µM amine concentration and (F) 1 µM amine concentration. Transgene delivery was determined 48 hours following treatment with the plasmid DNA loaded delivery vehicles (n=9 across 3 independently synthesized polymer batches). Asterisks denotes statistical significance (single factor ANOVA with Bonferroni correction).*

Statistically significant differences in transgene expression efficacies were not observed between the three different vehicles in 22Rv1 cells at any of the different plasmid loading conditions at either amine concentration (**Figure 5.3 A and B**). The same was observed in MDA-MB-231 cell at the 0.5 µM amine concentration (**Figure 5.3**

C), however at the 1 μM amine concentration (**Figure 5.3 D**) at plasmid loading amounts of 250-300 ng, the GNRs were found to be statistically significantly different than both the polyplexes and the GNS's with higher luciferase expression values. MB49 cells demonstrated statistically significant difference between the three vehicles at the 0.5 μM amine concentration (**Figure 5.3 E**), with both, GNRs and GNS's demonstrating higher luciferase expression values than the polyplexes at a loading amount of 10 ng, and the polyplex having a higher value than the GNS's at a loading of 150 ng. At the 1 μM amine concentration in MB49 cells (**Figure 5.3 F**), GNRs were found to be significantly higher than the polyplexes at loading conditions of 175, 200, 225, 275, ad 300 ng. Though there were some significant differences, for the majority of the conditions tested in the three different cell lines the three delivery vehicles had similar efficacies. These results indicate that there is, for the most part, no decrease in efficacy of the transgene delivery capabilities of the 1,4C-1,4Bis polymer following its use for synthesis or modification of nanoparticles. Several classes of polymers have been used for the synthesis or modification of gold nanoparticles for several different applications(A. C. Bonoiu, et al., 2009; Cui et al., 2011; Ghosh, et al., 2008; Song, et al., 2010). However there has been a lack of investigations detailing or comparing efficacies following the step from a purely polymeric system to a nanoparticle system. To the best of our knowledge, here we show one of the first comprehensive comparisons of purely polymeric to nanoparticle systems from transgene delivery. The minimal differences in transgene delivery between the three systems suggest that using efficient gene delivery polymeric systems to modify or synthesis metal nanoparticles will not result in a loss of efficacy. At certain conditions it may even increase efficacies as seen in MB49 and MDA-MB-231 cells.

Though, there was minimal change in efficacies, we wished to determine factors that may influence the observed significant differences. Though not widely investigated until recently, differences in morphology of nanoparticle delivery systems has been found to play an important role in influencing cellular uptake and efficiency of delivery of desired payload(Sutapa Barua et al., 2013; Champion, et al., 2007; Chithrani, Ghazani, & Chan, 2006; X. Huang, Teng, Chen, Tang, & He, 2010; Y. Liu, Tan, Thomas, Ou-Yang, & Muzkantov, 2012). In addition to geometry, orientation of the delivery vehicle's interaction with cells have been found to play a role in uptake. Differences in polyplex aspect ratios has been found to affect cellular internalization and transfection efficacy as well, where polyplexes with smaller aspect ratios outperforming those with larger aspect ratios(Shi et al., 2013). Previous studies have demonstrated that antibody coated nanorods had higher cellular uptake efficacies than nanospheres(Sutapa Barua, et al., 2013; Kolhar et al., 2013). However, the same studies reports that uncoated nanospheres were found to have higher cellular entry than uncoated nanorods likely due to unspecific binding interaction such as hydrophobic binding of polystyrene to the cell membrane(Sutapa Barua, et al., 2013). Though the delivery vehicles in our investigation are not targeted to the cell, they do interact with the cells via electrostatics. For instances where electrostatics are the primary influence on cell binding and uptake it has been found that rod shapes have an advantage. This is likely due to the large surface area to volume ratio allowing for multivalent cationic interaction with the cell surface(Gratton et al., 2008). For conditions where GNRs (Rod shaped) outperformed the GNS and polyplex (sphere shaped) it is reasonable to conclude that there is some shape-induced enhancement for transgene delivery at certain conditions. However, there are likely other factors that also

influence the increased transgene efficacy of the GNRs at the higher pDNA loading conditions.

The three delivery vehicles were also characterized for zeta potential values. As previously mentioned surface properties, including surface charge have been found to play a major role in nanoparticle – cellular interactions. It has been found that for efficient binding to cellular surfaces, which are primarily negatively charged, a delivery system with a strong positive charge is desirable(Liang Chen, et al., 2011; Frohlich, 2012; Osaka, Nakanishi, Shanmugam, & Zhang, 2009; Yue, et al., 2011). Following complexation of all vehicles with between 0-200 ng all vehicles were found to have positive zeta potential values for loading conditions between 0-200 (**Figure 5.4**). For all three delivery vehicles, as the amount of plasmid DNA loaded increased the zeta potential was found to decrease. This decrease continued to the 300 ng loading amount where all the vehicles exhibited a charge reversal to a negative value. This observed decrease in zeta potential and the subsequent charge reversal is likely due to the negative charge of the plasmid DNA shielding the positive charge of the cationic polymer-based systems(Ramos & Rege, 2012a). For pDNA loading conditions between 0-100 ng and the loading condition of 300 ng there was found to be no significant differences. However, at a loading condition of 200 ng, the GNRs were found to be statistically significant to both the GNS's and the polyplexes with a higher zeta potential value. This may also influence the observed differences in the transgene delivery efficacies of the three systems. Likely due to the increased surface area to volume ratio for the rod shaped vehicles there is less surface coverage with the plasmid. This results in retaining a stronger positive charge as they are complexed with increased amounts of plasmid. As previously discussed stronger

positive charged are desired in order to facilitate cellular binding and subsequent uptake. In the conditions below ~200 ng where all three vehicles exhibit the no significant differences in zeta potential we see a similar trend in transfection efficacies. However at loading conditions at higher than 200 (in MB49 and MDA-MB-231 cells) the GNRs are observed to maintain a stronger positive charge at higher plasmid loading amounts, these are similar to the conditions where the GNRs outperform either the GNS's the polyplex or both. Maintaining this positive charge likely results in the GNRs having more efficient cell binding as cell internalization. Shape may not be the only factor influencing the differences that were observed, but zeta potential also will play an important role.

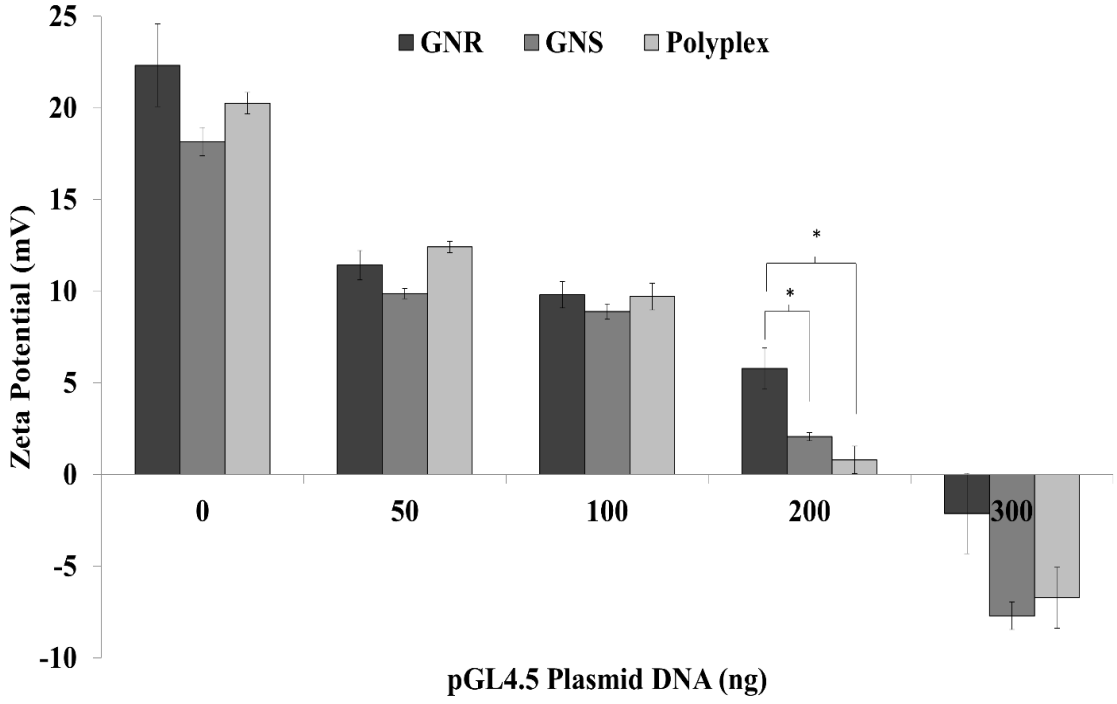

Figure 5.4. *Zeta Potential (mV) of 1,4C-1,4Bis-based poly/nanoplexes (1µM) with different amounts of pGL4.5. Measurements were taken in 1XPBS in order to mimic cell growth media salt conditions. Asterisks denotes statistical significance (single factor ANOVA with Bonferroni correction).*

The three systems were further characterized for hydrodynamic diameter following complexation with varying amounts of plasmid DNA (**Figure 5.5**). Size of delivery systems has been shown to influence cellular uptake, with sizes below 200 nm being desirable for efficient cellular uptake of nanoparticles(He, Hu, Yin, Tang, & Yin, 2010; K. Huang et al., 2012). For the vehicles alone the GNRs, GNS's, and polymer were found to have hydrodynamic diameters of approximately 60, 100, and 150 nm respectively, though there was found to be no statistically significant difference across the group. It should be noted that due to the non-particle nature of the polymer alone high polydispersity was observed. Additionally, it is acknowledged that DLS reports for spherical morphologies, and therefore, the hydrodynamic diameters of the GNRs were primarily used as indicators of size change.

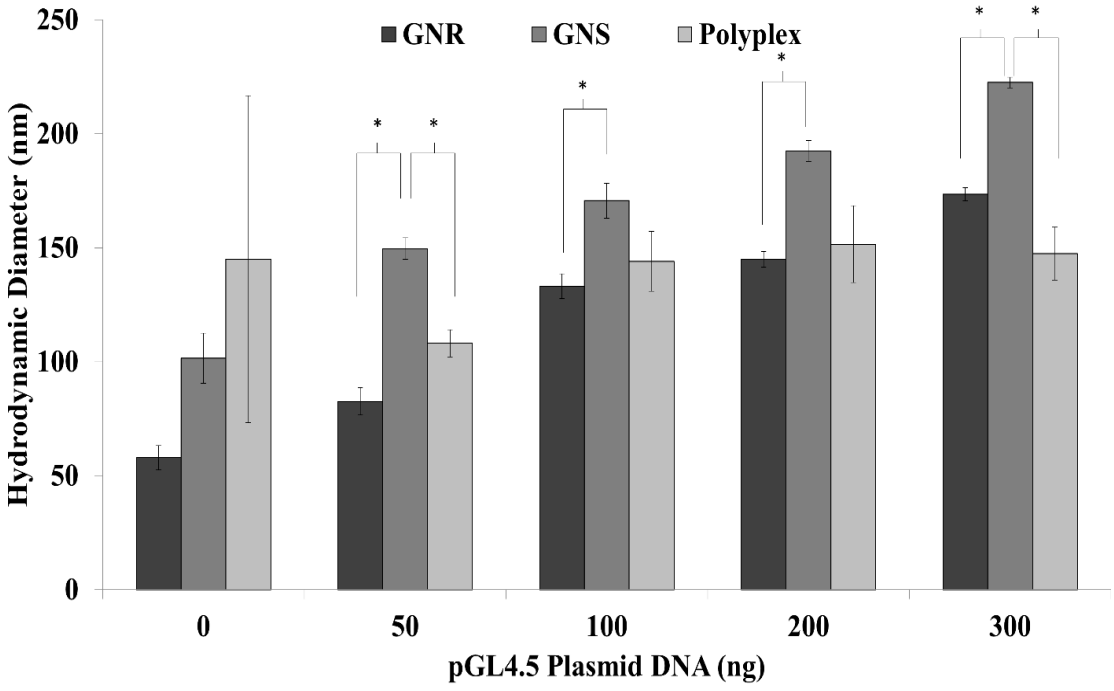

Figure 5.5. *Hydrodynamic diameter (nm) of 1,4C-1,4Bis-based poly/nanoplexes (1μM) with different amounts of pGL4.5. Measurements were taken in 1X PBS in order to mimic*

cell growth media salt conditions. Asterisks denotes statistical significance (single factor ANOVA with Bonferroni correction).

At increasing plasmid loading of 50-300 nm the GNRs were found to be significantly different than the GNS's, with smaller hydrodynamic diameters. At both 50 and 300 nm the polyplexes were also significantly different than the GNS with smaller hydrodynamic diameters. Though we do see significant differences in size change, it is likely that the change in size have less influence on the transgene delivery efficacies for the different systems. We see that all delivery vehicles remain primarily in the sub-200 nm range. However, the differences observed in the hydrodynamic diameter do not correlate with the similarities or differences observed for the transgene delivery efficacy, thus it is likely that the zeta potential and the shape are the two factors influencing any differences observed in transfection efficacies.

In comparing the three unique delivery systems, there was no significant difference in their transgene delivery capabilities, with the exception of a few conditions. This is largely attributed to similar trends observed in the zeta potential values at similar conditions. These results are promising as they demonstrate that using polymeric system that have previously been shown to be efficient for modification of gold nanoparticles does not result in a loss of efficacy. In some cases its efficacy increased in addition to introducing the polymer system to a new realm of applications.

Differences in morphology of nanoparticle delivery systems has been found to play an important role in influencing cellular uptake and efficiency of delivery of desired payload(Sutapa Barua, et al., 2013; Champion, et al., 2007; Chithrani, et al., 2006; X.

Huang, et al., 2010; Y. Liu, et al., 2012). Using the polymer system described here, nanoparticles of different shapes can be synthesized or modified in order to increase the transgene delivery efficacy. In addition to geometry, orientation of the delivery vehicle's interaction with cells have been found to play a role in uptake. Differences in polyplex aspect ratios has been found to affect cellular internalization and transfection efficacy as well, where polyplexes with smaller aspect ratios outperforming those with larger aspect ratios(Shi, et al., 2013). In addition, for instances where electrostatics primarily influence cell binding and uptake it has been found that rod shapes have an advantage. This is likely due to the large surface area to volume ratio allowing for multivalent cationic interaction with the cell surface(Gratton, et al., 2008). Using the 1,4C-1,4Bis polymer to modify and maintain a rod shape and adjusting the aspect ratio can also result in increasing the transgene efficacy.

Nanoparticles systems possess an inherent advantage over the pure polymeric system in that they can be used as a theranostic platform. Polymers have been employed for the synthesis or modification or several classes of nanoparticles. For example, magnetic nanoparticles have been synthesized or modified with polymers for use as imaging agents (Kumagai et al., 2010) as well as for targeted gene delivery in magnetofection, where an electro-magnetic field is used to guide the nanoparticles to a desired location(Chertok, David, & Yang, 2010; Plank, Zelphati, & Mykhaylyk, 2011). Polymers have also been employed for the synthesis of silver nanoparticles(H. Lee, et al., 2001; Shin & Kim, 2011; Tam, Erol, Attygelle, Du, & Sukhishvili, 2007) which have been found to have attractive antibacterial(C. You, et al., 2012), antifungal (Esteban-Tejada, et al., 2009), and anti-viral(Panacek, et al., 2009) properties. Additionally,

plasmonic gold nanoparticles exhibit unique optical properties such as surface plasmon resonance which allows them to strongly absorb and scatter incident light(Link & El-Sayed, 1999). This, has led to them being attractive as contrast agents since they can overcome detection limits, chemical and photo-stability typically associated with conventional contrast agents(Hahn, et al., 2011). Due to greater tissue depth penetration, minimal tissue scattering, and decreased phototoxicity NIR laser based imaging modalities have been increasingly investigated and gold nanoparticles, tuned to absorb NIR light, have been widely explored for use in multiple imaging modalities(Durr, et al., 2007; J.-L. Li & Gu, 2010; H. F. Wang, et al., 2005). Some classes of gold nanoparticle are also able to convert resonant energy to heat following exposure of near infrared (NIR) light, electron-phonon and phonon-phonon interactions can convert incident light into heat (Jain, et al., 2007; Oldenburg, Jackson, et al., 1999). Thermal or hyperthermic therapy is an attractive alternate or co-approach for the ablation of diseased (e.g. cancer) tissue. Due to their unique optical properties several classes of gold nanoparticles have been engineered for use in NIR-based hyperthermic therapy(Chatterjee, et al., 2011; El-Sayed, et al., 2005, 2006; Glazer & Curley, 2010; H.-C. Huang, et al., 2009; H.C. Huang, et al., 2010; Kennedy, et al., 2011; Ma, et al., 2009) for ablation of cancer cells (Cao, 2004) and bacteria(Cortie, 2004). As the results of this study suggest, polymer efficacy was mainlined following synthesis or modification of nanoparticles. This allows for effective polymeric systems, such as 1,4C-1,4Bis, to be used for the modification or synthesis of nanoparticle systems and still maintain their efficacy. By introducing effective polymers to nanoparticle systems, their impact in biomedicine is enhanced as they will possess multi-modal capabilities.

CONCLUSIONS

In this report, we investigated the head-to-head comparison of three unique non-viral gene delivery vehicles based on the novel 1,4C-1,4Bis polymer that has previously been shown to be an efficient non-viral gene delivery vehicle. 1,4C-1,4Bis-polyplexes, -gold nanorods, and -gold nanospheres were synthesized and compared for transgene delivery efficacies. Following treatment of three different cell lines the different systems were found to possess similar cytotoxicity profiles. In addition, a majority of treatment conditions demonstrated no significant difference in transgene delivery efficacies. The few conditions that did demonstrate a significant difference were likely due to similar trends in the difference observed in the zeta potential of the three systems. This results suggest that polymeric systems can be used for synthesis or modification of nanoparticle systems without compromising their efficacy. This allows for the use of successful polymeric systems for the generation of attractive theranostic systems.

CHAPTER 6

FUTURE DIRECTIONS: NIR LASER ENHANCED TRANSGENE DELIVERY FOR 1,4C-1,4BIS-GNRS

INTRODUCTION

The primary objective of the presented research is to investigate and engineer efficient non-viral gene delivery vehicles. In previous reports we have demonstrated the efficient transgene delivery of the 1,4C-1,4Bis poly(amino ether) polymer. Furthermore, 1,4C-1,4Bis has been used to modify gold nanorods and found to not lose its delivery efficacy. The theranostic potential of polymer modified GNR nanoplexes has also been highlighted through its use in bioimaging(Lucas Vu, et al., 2012). Being able to deliver a therapeutic payload and couple it with live bioimaging give the nanorod based transfection vehicle a clear advantage over traditional polyplex based systems. Additional, gold nanorods have unique optical properties that allows them to strongly absorb and scatter incident light, such as their ability to absorb near infrared (NIR) light. This gives them further advantage over other nanoparticle based systems lacking NIR adsorption properties. In addition to imaging, the ability of NIR adsorbing nanoparticles to transform photons into heat energy has resulted in investigation using them for triggered release or relevant therapeutic payloads including drugs and nucleic acids(Agasti et al., 2009; Braun, et al.; Han et al., 2006; Wijaya, Schaffer, Pallares, & Hamad-Schifferli, 2009).

Here we hypothesis that by using 1,4C-1,4Bis-GNRs for delivery of transgenes as we have previously shown, delivery efficacies can be increased via irradiating the treated cells with pulsed NIR light. There are several obstacles a delivery vehicle must overcome

when being used for transgene delivery. The first such obstacle is cellular uptake(can der Aa et al., 2007). 1,4C-1,4Bis-GNRs that maintain strongly positive zeta potential following plasmid DNA loading will be able to bind to the negative cell membranes. It is hypothesized that if GNRs are irradiated while they are binding to cells it is likely that a weakening of the cell membrane may occur, allowing for easier uptake and transport. The second obstacle following uptake is for the delivery vehicle to escape the endosomes prior to being trafficked for degradation(Khalil, Kogure, Akita, & Harashima, 2006). It is hypothesized that if cells are exposed to NIR irradiation at an appropriate time following cellular uptake it can result in a "burst" of the endosomal compartment resulting in increased endosomal escape of the nanoplexes(Braun, et al.). Lastly, pulsed NIR irradiation has also been shown to induce shape change in gold nanorods from a rod to a spherical shape. This shape change has been used to trigger release of conjugated molecules(Wijaya, et al., 2009). This shape change can also be used in our case for triggered release of nucleic acids. In order to determine if NIR irradiation can increase transfection efficacies, cells treated with 1,4C-1,4Bis-GNRs loaded with plasmid DNA will be irradiated with pulsed NIR irradiation as different times after treatment and transfection efficacies will be compared to non-irradiated controls.

By determining whether or not laser irradiation can increase transfection efficacy will allow for further optimization of transfection systems. Additionally, by correlating the time at which the irradiation occurs with the cellular location of the nanoassemblies can allow for us to determine which step in the transfection process can be overcome. Additional methods can then be investigated to overcome other steps/barriers in cellular uptake through to transgene expression.

EXPERIMENTAL DESIGN

TEM to Determine Shape Change of 1,4C-1,4Bis-GNRs. Transmission Electron Microscopy (TEM) will be used in order to determine the shape change, if any, the gold nanorods assemblies undergo following exposure to NIR irradiation. 1,4C-1,4Bis-GNRs will be synthesized as previously described. Solutions will be exposed to near infrared (NIR) pulsed laser irradiation for 15 minutes (800 nm 20 W/cm^2). Non irradiated dispersions will be used as a control. Following, they will be characterized by Transmission Electron Microscopy (TEM) using a JEOL-JEM-2000FX microscope operating at 200 kV. JEOL-JEM2000FX TEM is equipped with a thin-window, light-element sensitive X-ray spectrometer for high spatial resolution microanalysis, and a low-drift-rate, double-tilt cryostage for microbeam experiments. Specimen samples for TEM will be prepared by casting a drop of the nanoassembly dispersions onto a carbon film on a 200 mesh copper mesh (Global Electron Microscopy Technology Co.) and air dried. Dried samples were examined by TEM at 200 kV and shape change if any will be determined.

Ethidium Bromide Assay for DNA Release. In order to determine if there NIR irradiation can facilitate transgene release from the 1,4C-1,4Bis-GNRs, an ethidium bromide assay will be used. 1,4C-1,4Bis-GNRs will be synthesized as previously described and will be incubated with different amounts (10-100 ng) of pGL3 and pEGFP expression vectors for 30 min in serum-free media, leading to the formation of vector-loaded nanoassemblies. Following nanoplex formation, samples will be irradiated with near infrared (NIR) pulsed laser irradiation for 15 minutes (800 nm 20 W/cm^2). Non-irradiated samples will be used as controls. Following irradiation, samples will be

immediately centrifuged to separate nanoparticles from any free DNA. The amount of plasmid expression vector remaining in the supernatant after centrifugation was determined using ethidium bromide, a DNA intercalating dye. Ethidium Bromide (1 µg of 0.5 mg/ml; Sigma-Aldrich, St. Louis, MO) will added to each sample. Solutions will be transferred to a black 96 well plate, and fluorescence will be measured using excitation at 320 nm and emission at 600 nm with a plate reader (Synergy 2 Multi-Mode Microplate Reader, BioTek, Winooski, VT), similar to methods previously described(K. Rege, et al., 2004; Rege, et al., 2005a). Known plasmid DNA amounts in solution will be used as standards for calibration of the assay. The amount of plasmid loaded on the nanoassemblies will be determined using mass balance by subtracting the amount of plasmid in the supernatant from the initial amount used for loading.

1,4C-1,4Bis-GNR Pulsed NIR Laser Transfection. 1,4C-1,4Bis-GNRs will be synthesized as previously described and the optimum transfection condition (to be identified based on previous proposed results) will be used to further investigate pulsed NIR laser transfection efficacies. 22Rv1 and MB49 cells will be treated with the nanoplexes loaded with pGL3 DNA as previously described. Cells will be irradiated with pulsed NIR laser (800 nm 20 W/cm^2) for 15 minutes immediately after treatment, 3, 6, and 24 hours after treatment. No laser irradiation will be used as a control. Luciferase expression will be determined 48 hours after initial treatment as previously described. Due to possible cell death from thermal ablation, luciferase expression will be normalized to the amount of viable cells determined by MTT assay (previously described).

By determining whether or not laser irradiation can increase transfection efficacy will allow for further optimization of transfection systems. Additionally, by correlating the time at which the irradiation occurs with the cellular location of the nanoassemblies can allow for us to determine which step in the transfection process can be overcome. Additional methods can then be investigated to overcome other steps/barriers in cellular uptake through to transgene expression.

REFERENCES

Agasti, S., Chompoosor, A., You, C., Ghosh, P., Kim, C., & Rotello, V. (2009). Photoregulated Release of Caged Anticancer Drugs From Gold Nanoparticles. *J Am Chem Soc, 131*(29), 5728-5729.

Akinc, A., Thomas, M., Klibanov, A. M., & Langer, R. (2005). Exploring polyethylenimine-mediated DNA transfection and the proton sponge hypothesis. *Journal of Gene Medicine, 7*(5), 657-663.

Al-Thabaiti, S. A., Al-Nowaiser, F. M., Obaid, A. Y., Al-Youbi, A. O., & Khan, Z. (2008). Formation and characterization of surfactant stabilized silver nanoparticles: A kinetic Study. *Colloids and Surfaces B: Biointerfaces, 67*, 230-237.

Arvizo, R. R., Bhattacharyya, S., Kudgus, R. A., Giri, K., Bhattacharya, R., & Mukherjee, P. (2012). Intrinsic therapeutic applications of noble metal nanoparticles: past present and future. *Chem Soc Rev, 41*, 2943-2970.

Averitt, R. D., Westcott, S. L., & Halas, N. J. (1999). Linear optical properties of gold nanoshells. *Journal of the Optical Society of America B-Optical Physics, 16*(10), 1824-1832.

Bardhan, R., Lal, S., Joshi, A., & Halas, N. J. (2011). Theranostic Nanoshells: From Probe Design to Imaging and Treatment of Cancer. *Accounts of Chemical Research, 44*(10), 936-946.

Bartlett, D. W., Su, H., Hildebrandt, I. J., Weber, W. A., & Davis, M. E. (2007). Impact of tumor-specific targeting on the biodistribution and efficacy of siRNA nanoparticles measured by multimodality in vivo imaging. *Proc Acad Sci USA, 104*(39), 15546-15554.

Barua, S., Joshi, A., Banerjee, A., Matthews, D., Sharfstein, S. T., Cramer, S. M., et al. (2009a). Parallel Synthesis and Screening of Polymers for Nonviral Gene Delivery. *Molecular Pharmaceutics, 6*(1), 86-97.

Barua, S., Ramos, J., Potta, T., Taylor, D., Huang, H. C., Montanez, G., et al. (2011a). Discovery of cationic polymers for non-viral gene delivery using combinatorial approaches. *Comb Chem High Throughput Screen, 14*(10), 908-924.

Barua, S., & Rege, K. (2010). The influence of mediators of intracellular trafficking on transgene expression efficacy of polymer-plasmid DNA complexes. *Biomaterials, 31*(22), 5894-5902.

Barua, S., Yoo, J.-W., Kolhar, P., Wakankar, A., Gokam, Y. R., & Mitragotri, S. (2013). Particle shape enhances specificity of antibody-displaying nanoparticles. *PNAS, 110*(9), 3270-3275.

Berthold, P. R., Shiraishi, T., & Nielsen, P. E. (2010). Cellular Delivery and Antisense Effects of Peptide Nucleic Acid Conjugated to Polyethyleneimine via Disulfide Linkers. *Bioconjugate Chemistry, 21*(10), 1933-1938.

Bhargava, S., Booth, J., Agrawal, S., Coloe, P., & Kar, G. (2005). Gold nanoparticle formation during bromoaurate reducion by amino acids. *Langmuir, 21*(13), 5949-5956.

Boger, D. L., Fink, B. E., Brunette, S. R., Tse, W. C., & Hedtick, M. R. (2001). A Simple, High-Resolution Method for Establishing DNA Binding Affinity and Sequence Selectivity. *Journal of the American Chemical Society, 123*(5878-5891).

Bonoiu, A., Bergey, E., Ding, H., Hu, R., Kumar, R., Prasad, P., et al. (2011). Gold nanorod-siRNA induces efficient in vivo gene silencing in the rat hippocampus. *Nanomedicine, 6*(4), 617-630.

Bonoiu, A. C., Mahajan, S. D., Ding, H., Roy, I., Yong, K.-T., Kumar, R., et al. (2009). Nanotechnology approach for drug addiction therapy: Gene silencing using delivery of gold nanorod-siRNA nanoplex in dopaminergic neurons. *Proc Natl Acad Sci USA, 106*(14), 5546-5550.

Boonstra, J., & Post, J. A. (2004). Molecular events associated with reactive oxygen species and cell cycle progression in mammalian cells. *Gene, 337*, 1-13.

Boussif, O., Lezoualch, F., Zanta, M. A., Mergny, M. D., Scherman, D., Demeneix, B., et al. (1995). A versatile vector for gene and oligonucleotide transfer into cells in culture and in-vivo – polyethylenimine. *Proceedings of the National Academy of Sciences of the United States of America, 92*(16), 7297-7301.

Braun, G. B., Pallaoro, A., Wu, G., Missirlis, D., Zasadzinski, J. A., Tirrell, M., et al. Laser-Activated Gene Silencing via Gold Nanoshell-siRNA Conjugates. *3*(7), 2007-2015.

Burdick, J., Alonas, E., Huang, H. C., Rege, K., & Wang, J. (2009). High-throughput templated multisegment synthesis of gold nanowires and nanorods. *Nanotechnology, 20*(6).

Butorac, R. R., Al-Deyab, S. S., & Cowley, A. H. (2011). Antimicrobial properties of some bis(iminoacenaphthene) (BIAN)-supported N-heterocyclic carbene complexes of silver and gold. *Molecules, 16*, 2285-2292.

can der Aa, M. A. E. M., Huth, U. S., Hafele, S. Y., Schubert, R., Oosting, R. S., Mastrobattista, E., et al. (2007). Cellular Uptake of Cationic Polymer-DNA Complexes Via Caveolae Plays a Pivotal Role in Gene Transfection in COS-7 Cells. *Pharm Res, 24*(8), 1590-1598.

Cao, G. (2004). *Nanostructures & nanomaterials: Synthesis, properties & applications* (1st ed.): Imperial College Press.

Castellana, E., Gamez, R., & Russell, D. (2011). Label-free biosensing with lipid funcionalized gold nanorods. *J Am Chem Soc, 133*(12), 4182-4185.

Champion, J. A., Ktare, Y. K., & Mitragotri, S. (2007). Particle Shape: A New Design Parameter for Micro- and Nanoscale Drug Delivery Carriers. *J. Control Release, 121*, 3-9.

Chang, S. S., Shih, C. W., Chen, C. D., Lai, W. C., & Wang, C. R. C. (1999). The shape transition of gold nanorods. *Langmuir, 15*(3), 701-709.

Chatterjee, D. K., Diagaradjane, P., & Krishnan, S. (2011). Nanoparticle-mediated hyperthermia in cancer therapy. *Ther Deliv, 2*(8), 1001-1014.

Chen, C., Lin, Y., Wang, C., Tzeng, H., Wu, C., Chen, Y., et al. (2006). DNA-Gold Nanorod Conjugates for Remote Control of Localized Gene Expression by near Infrared Irradiation. *J Am Chem Soc, 128*(11), 3709-3715.

Chen, J., Tian, B., Yin, X., Zhang, Y., Hu, D., Liu, M., et al. (2007). Preparation, characterization and transfection efficiency of cationic PEGylated PLA nanoparticles as gene delivery systems. *J Biotechnology, 130*(2), 107-113.

Chen, J. Y., McLellan, J. M., Siekkinen, A., Xiong, Y. J., Li, Z. Y., & Xia, Y. N. (2006). Facile synthesis of gold-silver nanocages with controllable pores on the surface. *Journal of the American Chemical Society, 128*(46), 14776-14777.

Chen, L., Mccrate, J. M., Lee, J. C.-M., & Li, H. (2011). The role of surface charge on the uptake and biocompatibility of hydroxyapatite nanoparticles with osteoblast cells. *Nanotechnology, 22*(10), 105708.

Cheng, Y., Samia, A. C., Li, J., Kenney, M. E., Resnick, A., & Burda, C. (2010). Delivery and Efficacy of a Cancer Drug as a Function of the Bond to the Gold Nanoparticle Surface. *Langmuir, 26*(4), 2248-2255.

Cherng, J. Y., Hung, W. C., & Kao, H. C. (2011). Blending of Polyethylenimine with a Cationic Polyurethane Greatly Enhances Both DNA Delivery Efficacy and Reduces the Overall Cytotoxicity. *Current Pharmaceutical Biotechnology, 12*(5), 839-846.

Chertok, B., David, A. E., & Yang, V. C. (2010). Polyethyleneimine-modified iron oxide nanoparticles for brain tumor drugdelivery using magnetic tar geting and intra-carotid administration. *Biomaterials, 31*(24), 6317-6324.

Cherukuri, P., Glazer, E. S., & Curley, S. A. (2010). Targeted Hyperthermia Using Metal Nanoparticles. *Adv Drug Deliv Rev, 62*(3), 339-345.

Chinnaiyan, P., Varambally, S., Tomlins, S. A., Ray, S., Huang, S. M., Chinnaiyan, A. M., et al. (2006). Enhancing the antitumor activity of ErbB blockade with histone deacetylase (HDAC) inhibition. *International Journal of Cancer, 118*(4), 1041-1050.

Chithrani, B. D., Ghazani, A. A., & Chan, W. C. W. (2006). Determining the Size and Shape Dependence of Gold Nanoparticle Uptake in Mammalian Cells. *Nano Letters, 6*(4), 662-668.

Cho, K., Wang, X., Nie, S., Chen, Z., & Shin, D. (2008). Therapeutic nanoparticles for drug delivery in cancer. *Clin Cancer Res, 14*(5), 1310-1316.

Choi, W. I., Kim, J.-Y., Kang, C., Byeon, C. C., Kim, Y. H., & Tae, G. (2011). Tumor Regression *In Vivo* by Photothermal Therapy Based on Gold-Nanorod-Loaded, Functional Nanocarriers. *ACS Nano, 5*(3), 1995-2003.

Chumakova, O. V., Liopo, A. V., Andreev, V. G., Cicenaite, I., Evers, B. M., Chakrabarty, S., et al. (2008). Composition of PLGA and PEI/DNA nanoparticles improves ultrasound-mediated gene delivery in solid tumors in vivo. *Cancer Letters, 261*(2), 215-225.

Coll, J. L., Chollet, P., Brambilla, E., Desplanques, D., Behr, J. P., & Favrot, M. (1999). In vivo delivery to tumors of DNA complexed with linear polyethylenimine. *Human Gene Therapy, 10*(10), 1659-1666.

Conde, J., Ambrosone, A., Sanz, V., Hernandez, Y., Marchesano, V., Tian, F., et al. (2012). Design of Multifunctional Gold Nanoparticles for *In Vitro* and *In Vivo* Gene Silencing. *ACS Nano, 6*(9), 8316-8324.

Cortie, M. B. (2004). The weird world of nanoscale gold. *Gold Bull, 37*, 12-19.

Cui, D., Huang, P., Zhang, C., Ozkan, C., Pan, B., & Xu, P. (2011). Dendrimer-modified gold nanorods as efficient controlled gene delivery systems under near-infrared light irradiation. *J Control Release, 152*(Suppl 1), e137-139.

Dallas, A., Ilves, H., Ge, Q., Kumar, P., Shorenstein, J., Kazakov, S., et al. (2012). Right- and left-loop short shRNAs have distinct and unusual mechanisms of gene silencing. *Nucleic Acids Res, 40*(18), 9255-9271.

Dayanc, B., Beachy, S., Ostberg, J., & Repasky, E. (2008). Dissecting the role of hyperthermia in natural killer cell mediated anti-tumor responses. *Int J Hyperthermia, 24*(1), 41-56.

Dickerson, E. B., Dreaden, E. C., Huang, X. H., El-Sayed, I. H., Chu, H. H., Pushpanketh, S., et al. (2008). Gold nanorod assisted near-infrared plasmonic photothermal therapy (PPTT) of squamous cell carcinoma in mice. *Cancer Letters, 269*(1), 57-66.

Ding, H., Yong, K.-T., Roy, I., Pudavar, H. E., Law, W. C., Bergey, E. J., et al. (2007). Gold Nanorods Coated with Multilayer Polyelectrolyte as Contrast Agents for Multimodal Imaging. *The Journal of Physical Chemistry C, 111*(34), 12552-12557.

Dorris, A., Rucareanu, S., Reven, L., Barrett, C., & Lennox, R. (2008). Preparation and characterization of polyelectrolyte-coated gold nanoparticles. *Langmuir, 18*(24), 2532-2538.

Dos Santos, D. j., Goulet, P., Pieczonka, N., Oliveira, O. J., & Aroca, R. (2004). Gold nanoparticle embedded, self-sustained chitosan films as substrates for surface-enhanced Raman scattering. *Langmuir, 20*(23), 10273-10277.

Durr, N. J., Larson, T., Smith, D. K., Korgel, B. A., Sokolov, K., & Ben-Yakar, A. (2007). Two-photon luminescence imaging of cancer cells using molecularly targeted gold nanorods. *Nano Letters, 7*(4), 941-945.

Duxbury, M. S., Ito, H., Zinner, M. J., Ashley, S. W., & Whang, E. E. (2004). Focal adhesion kinase gene silencing promotes anoikis and suppresses metastasis in human pancreatic adenocarcinoma cells. *Surgery, 135*, 555-562.

El-Sayed, I. H., Huang, X. H., & El-Sayed, M. A. (2005). Surface plasmon resonance scattering and absorption of anti-EGFR antibody conjugated gold nanoparticles in cancer diagnostics: Applications in oral cancer. *Nano Letters, 5*(5), 829-834.

El-Sayed, I. H., Huang, X. H., & El-Sayed, M. A. (2006). Selective laser photo-thermal therapy of epithelial carcinoma using anti-EGFR antibody conjugated gold nanoparticles. *Cancer Letters, 239*(1), 129-135.

Elsabahy, M., Nazarali, A., & Foldvari, M. (2011). Non-Viral Nucleic Acid Delivery: Key Challenges and Future Directions. *Current Drug Delivery, 8*(3), 235-244.

Emilitri, E., Ranucci, E., & Ferruti, P. (2005). New poly(amidoamine)s containing disulfide linkages in their main chain. *Journal of Polymer Science Part a-Polymer Chemistry, 43*(7), 1404-1416.

Esteban-Tejada, L., Malpartida, F., Esteban-Cubillo, A., Pecharroman, C., & Moya, J. S. (2009). The antibacterial and antifungal activity of a soda-lime glass containing silver nanoparticles. *Nanotechnology, 20*.

Eustis, S., & El-Sayed, M., A. (2006). Molecular Mechanism of the Photochemical Genereation of Gold Nanoparticles in Ethylene Glycol: Support for the Disproportionation Mechanism. *J Phys. Chem. B. Letters, 110*(29), 14014-14019.

Eustis, S., Hsu, H.-Y. H., & El-Sayed, M., A. (2005). Gold-Nanoparticle Formation from Photochemical Reduction of Au^{3+} by Continuous Excitation in Colloidal Solutions. A Proposed Molecular Mechanism. *J Phys. Chem. B. Letters, 109*(11), 4811-4815.

Faulds, K., Littleford, R., Graham, D., Dent, G., & Smith, W. (2004). Comparison of surface-enhanced resonance Raman scattering from unaggregated and aggregated nanoparticles. *Anal Chem, 76*(3), 592-598.

Fercher, A. F., Drexler, W., Hitzenberger, C. K., & Lasser, T. (2003). Optical coherence tomography - principles and applications. *Reports on Progress in Physics, 66*(2), 239-303.

Frohlich, E. (2012). The role of surface charge in cellular uptake and cytotoxicity of medical nanoparticles. *Int J Nanomedicine, 7*(5577-5591).

G., B., Cherukuri, P., Kingston, J., Cognet, L., Lemos, R., Leeuw, T. K., et al. (2009). In vivo therapeutic silencing of hypoxia-inducible factor 1 alpha (HIF-1 alpha) using single walled carbon nanotubes noncovalently coated with siRNA. *Nano Res, 2*(4), 279-291.

Gabrielson, N. P., & Pack, D. W. (2009). Efficient polyethylenimine-mediated gene delivery proceeds via a caveolar pathway in HeLa cells. *Journal of Controlled Release, 136*(1), 54-61.

Garnett, M. C. (1999). Gene-delivery systems using cationic polymers. *Crit Rev Ther Drug Carrier Syst, 16*(2), 147-207.

Geall, A., & Blagbrough, I. (2000). Rapid and sensitive ethidium bromide fluorescence quenching assay of polyamine conjugate-DNA interaction for the analysis of lipoplex formation in gene therapy. *Journal of Pharmaceutical and Biomedical Analysis, 22*(5), 849-859.

Ghosh, P., Han, G., De, M., Kyu Kim, C., & Rotello, V. M. (2008). Gold nanoparticles in delivery aplications. *Advanced Drug Delivery Reviews, 60*, 1307-1315.

Glazer, E. S., & Curley, S. A. (2010). Radiofrequency Field-Induced Thermal Cytotoxicity in Cancer Cells Treated with Fluorescent Nanoparticles. *Cancer, 116*(13), 3285-3293.

Glazer, E. S., Zhu, C. H., Massey, K. L., Thompson, C. S., Kaluarachchi, W. D., Hamir, A. N., et al. (2010). Noninvasive Radiofrequency Field Destruction of Pancreatic Adenocarcinoma Xenografts Treated with Targeted Gold Nanoparticles. *Clinical Cancer Research, 16*(23), 5712-5721.

Glover, D. J., Lipps, H. J., & Jans, D. A. (2005). Towards safe, non-viral therapeutic gene expression in humans. *Nature Reviews Genetics, 6*(4), 299-U229.

Gobin, A. M., Lee, M. H., Halas, N. J., James, W. D., Drezek, R. A., & West, J. L. (2007). Near-infrared resonant nanoshells for combined optical imaging and photothermal cancer therapy. *Nano Letters, 7*(7), 1929-1934.

Golub, G., Zilbermann, I., Cohen, H., & Meyerstein, D. (1996). Tertiary-poly-amine ligands as stabilisers of transition metal complexes with uncommon oxidation states. *Supramolecular Chemistry, 6*, 275-279.

Gong, M. C., Latouche, J. B., Krause, A., Heston, W. D., Bander, N. H., & Sadelain, M. (1999). Cancer Patient T Cells Genetically Targeted to Prostate-Specific Membrane Antigen Specifically Lyse Prostate Cancer Cells and Release Cytokines in Response to Prostate-Specific Membrane Antigen *Neoplasia, 1*, 123-127.

Goodrich, G. P., Bao, L. L., Gill-Sharp, K., Sang, K. L., Wang, J., & Payne, J. D. Photothermal therapy in a murine colon cancer model using near-infrared absorbing gold nanorods. *Journal of Biomedical Optics, 15*(1).

Gosnell, H., Kasman, L., Potta, T., Vu, L., Garrett-Mayer, E., Rege, K., et al. (2014). Polymer-enhanced delivery increases adenoviral gene expression in an orthotopic model of bladder cancer. *J Control Release, 176*, 35-43.

Gough-Palmer, A. L., & Gedroyc, W. M. W. (2008). Laser Ablation of hepatocellular carcinoma-A review. *World J Gastroenterol, 14*(47), 7170-7174.

Grace, A. N., & Pandian, K. (2006). One Pot Synthesis of Polymer Protected Gold Nanoaprticles and Nanoprisms in Glycerol. *Colloids Surf., A, 290*, 138-142.

Gratton, S. E. A., Ropp, P., A., Pohlhaus, P., D., Luft, J. C., Madden, V. J., Napier, M. E., et al. (2008). The Effect of Particle Design on Cellular Internalization Pathways. *Proc Natl Acad Sci USA, 105*(33), 11613-11618.

Grimm, D., Streetz, K., Jopling, C. L., Storm, T. A., Pandey, K., Davis, C. R., et al. (2006). Fatality in mice due to oversaturation of cellular microRNA/short hairpin RNA pathways. *Nature, 441*(25), 537-541.

Gross, G., Nelson, D., Grate, J., & Synovec, R. (2003). Monolayer-protected gold nanoparticles as a stationary phase for open tubular gas chromatography. *Anal Chem, 75*(17), 4558-4564.

Gu, Y., Chen, W., Xia, M., Jeong, S., & Liu, H. (2005). Effect of photothermal therapy on breast tumor vascular contents: noninvasive monitoring by near-infrared spectroscopy. *Photochem Photobiol, 81*(4), 1002-1009.

Guo, L., Zhou, X., & Kim, D. (2011). Facile fabrication of distance-tunable Au-nanorod chips for single nanoparticle plasmonic biosensors. *Biosens Bioelectron, 26*(5), 2246-2251.

Guo, S. T., Huang, Y. Y., Wei, T., Zhang, W. D., Wang, W. W., Lin, D., et al. (2011). Amphiphilic and biodegradable methoxy polyethylene glycol-block-(polycaprolactone-graft-poly(2-(dimethylamino)ethyl methacrylate)) as an effective gene carrier. *Biomaterials, 32*(3), 879-889.

Ha, S., Carson, A., Agarwai, A., Kotov, N., & Kim, K. (2011). Detection and monitoring of the multiple inflammatory responses by photoacoustic molecular imaging using selectively targeted gold nanorods. *Biomed Opt Express, 2*(3), 645-657.

Hahn, M. A., Singh, A. K., Sharma, P., Brown, S. C., & Moudgil, B. M. (2011). Nanoparticles as contrast agents for in-vivo bioimaging: current status and future perspectives. *Anal Bioanal Chem, 399*, 3-27.

Hamada, M., Ohtsuka, T., Kawaida, R., Koizumi, M., Morita, K., Furukawa, H., et al. (2002). Effects of RNA Interference in Gene Expression (RNAi) in the Cultured Mammalian Cells of Mismatches and the Introduction of Chemical Modifications at teh 3'-Ends of siRNA. *Antisense and Nucleic Acid Drug Development, 12*, 301-309.

Han, G., You, C.-C., Kim, B.-j., Turingan, R. S., Forbes, N. S., Martin, C. T., et al. (2006). Light-Regulated Release of DNA and Its Delivery to Nuclei by Means of Photolabile Gold Nanoparticles. *Angew Chem Int Ed Engl, 45*(19), 3165-3169.

Harada, M., Inada, Y., & Nomura, M. (2009). In situ time-resolved XAFS analysis of silver particle formation by photoreduction in polymer solutions. *J Colloid Interface Sci, 337*(2), 427-438.

Hayon, T., Dvilansky, A., Shpilberg, O., & Nathan, I. (2003). Appraisal of the MTT-based assay as a useful tool for predicting drug chemosensitivity in leukemia *Leuk. Lymphoma, 44*, 1957–1962.

He, C., Hu, Y., Yin, L., Tang, C., & Yin, C. (2010). Effects of particle size and surface charge on cellular uptake and biodistribution of polymeric nanoparticles. *Biomaterials, 31*(13), 3657-3666.

Heath, J., & Davis, M. (2008). Nanotechnology and cancer. *Annu Rev Med, 59*, 251-265.

Herbst, R. S., Kim, E. S., & Harari, P. M. (2001). IMC-C225, an anti-epidermal growth factor receptor monoclonal antibody, for treatment of head and neck cancer. *Expert Opin. Biol. Ther., 1*, 719-732.

Hildebrandt, B., Wust, P., Ahlers, O., Dieing, A., Sreenivasa, G., Kerner, T., et al. (2002). The cellular and molecular basis of hyperthermia. *Critical Reviews in Oncology/Hematology, 43*, 33-56.

Hirsch, L. R., Stafford, R. J., Bankson, J. A., Sershen, S. R., Rivera, B., Price, R. E., et al. (2003). Nanoshell-mediated near-infrared thermal therapy of tumors under magnetic resonance guidance. *Proceedings of the National Academy of Sciences of the United States of America, 100*(23), 13549-13554.

Hoppe, C. E., Lazzari, M., Pardinas-Blanco, I., & Lopez-Quintela, M. A. (2006). One-Step Synthesis of Gold and Silver Hydrosols Using Poly(V-vinyl-2-pyrrolidone) as a Reducing Agent. *Langmuir, 22*, 7027-7034.

Hsin, Y. H., Chen, C. F., Huang, S., Shih, T. S., Lai, P. S., & Chueh, P. J. (2008). The apoptotic effect of nanosilver is mediated by a ROS- and JNK-dependent mechanism involving the mitochondrial pathway in NIH3T3 cells. *Toxicol Lett*(179), 130-139.

Hu, C., Huang, Y., & Tsiang, R. (2009). Thermal and spectroscopic properties of polystyrene/gold nanocomposite containing well dispersed nanoparticles. *J Nanosci Nanotechnol, 9*(5), 3084-3091.

Hu, C., Peng, Q., Chen, F., Zhong, Z., & Zhuo, R. (2010). Low Molecular Weight Polyethylenimine Conjugated Gold Nanoparticles as Efficient Gene Vectors. *Bioconjug Chem, 20*(5), 836-844.

Huang, H.-C., Barua, S., Kay, D. B., & Rege, K. (2009). Simultaneous Enhancement of Photothermal Stability and Gene Delivery Efficacy of Gold Nanorods using Polyelectrolytes. *ACS Nano, 3*(10), 2941-2952.

Huang, H.-C., Barua, S., Sharma, G., Dey, S. K., & Rege, K. (2011). Inorganic nanoparticles for cancer imaging and therapy. *Journal of Controlled Release, 155*, 344-357.

Huang, H.-C., Ramos, J., Grandhi, T. S. P., Potta, T., & Rege, K. (2010). Gold Nanoparticles in Cancer Imaging and Therapeutics. *Nano LIFE (NL), 01*(03n04), 289-307.

Huang, H.-C., Yang, Y., Nanda, A., Koria, P., & Rege, K. (2011). Synergistic administration of photothermal therapy and chemotherapy to cancer cells using polypeptide-based degradable plasmonic matrices. *Nanomedicine (Lond), 6*(3), 459-473.

Huang, H. C., Koria, P., Parker, S. M., Selby, L., Megeed, Z., & Rege, K. (2008). Optically responsive gold nanorod-polypeptide assemblies. *Langmuir, 24*(24), 14139-14144.

Huang, H. C., Rege, K., & Heys, J. J. (2010). Spatiotemporal temperature distribution and cancer cell death in response to extracellular hyperthermia induced by gold nanorods. *ACS Nano, 4*(5), 2892-2900.

Huang, K., Ma, H., Liu, J., Huo, S., Kumar, A., Wei, T., et al. (2012). Size-Dependent Localization and Penetratino of Ultrasmall Gold Nanoparticles in Cancer Cells, Multicellular Spheriods, and Tumors *in Vivo*. *ACS Nano, 6*(5), 4483-4493.

Huang, X., Neretina, S., & El-Sayed, M. (2009). Gold Nanorods: From Synthesis and Properties to Biological and Biomedical Applications. *Advanced Biomaterials, 27*, 1-31.

Huang, X., Teng, X., Chen, F., Tang, F., & He, J. (2010). The Effect of the Shape of Mesoporous Silica Nanoparticles on Cellular Uptake and Cell Function. *Biomaterials, 3*, 438-448.

Huang, X. H., El-Sayed, I. H., Qian, W., & El-Sayed, M. A. (2006). Cancer cell imaging and photothermal therapy in the near-infrared region by using gold nanorods. *Journal of the American Chemical Society, 128*(6), 2115-2120.

Hynes, N. E., & Lane, H. A. (2005). ERBB receptors and cancer: the complexity of target inhibitors. *Nat. Rev. Cancer, 5*(341-354).

Jabr-Milane, L., van-Vlerken, L., Devalapally, H., Shenoy, D., Komareddy, S., Bhavsar, M., et al. (2008). Multi-functional nanocarriers for targeted delivery of drugs and genes. *J Control Release, 130*(2), 121-128.

Jain, P., Haung, X., El-Sayed, I. H., & El Sayed, M. A. (2007). Review of Some Interesting Surface Plasmon Resonance-ENhanced Properties of Noble Metal Nanoparticles and Their Applications to Biosystems. *Plasmonics, 2*, 107-118.

Jana, N. R., Gearheart, L., & Murphy, C. J. (2001a). Seed-mediated growth approach for shape-controlled synthesis of spheroidal and rod-like gold nanoparticles using a surfactant template. *Advanced Materials, 13*(18), 1389-1393.

Jana, N. R., Gearheart, L., & Murphy, C. J. (2001b). Wet chemical synthesis of high aspect ratio cylindrical gold nanorods. *Journal of Physical Chemistry B, 105*(19), 4065-4067.

Jana, N. R., Gearheart, L., Obare, S. O., & Murphy, C. J. (2002). Anisotropic chemical reactivity of gold spheroids and nanorods. *Langmuir, 18*(3), 922-927.

Jean, M., Alameh, M., Buschmann, M. D., & Merzouki, A. (2011). Effective and safe gene-based delivery of GLP-1 using chitosan/plasmid-DNA therapeutic nanocomplexes in an animal model of type 2 diabetes. *Gene Therapy, 18*(8), 807-816.

Jia, H., Zeng, J., Song, W., An, J., & Zhao, B. (2006). Preparation of silver nanoparticles by photo-reduction for surface-enhanced Ramoan scattering. *Thin Solid Films, 496*(2), 281-287.

Johnson, C., Dujardin, E., Davis, S., Murphy, C., & Mann, S. (2002). Growth and form of gold nanorod prepared by seed-mediated, surfactant-directed synthesis. *J. Mater. Chem., 12*, 1765-1770.

Jounaidi, Y., Chen, C. S., Veal, G. J., & Waxman, D. J. (2006). Enhanced antitumor activity of P450 prodrug-based gene therapy using the low K-m cyclophosphamide 4-hydroxylase P4502B11. *Molecular Cancer Therapeutics, 5*(3), 541-555.

Jounaidi, Y., & Waxman, D. J. (2004). Use of replication-conditional adenovirus as a helper system to enhance delivery of P450 prodrug-activation genes for cancer therapy. *Cancer Research, 64*(1), 292-303.

Kah, J. C. Y., Olivo, M., Chow, T. H., Song, K. S., Koh, K. Z. Y., Mhaisalkar, S., et al. (2009). Control of optical contrast using gold nanoshells for optical coherence tomography imaging of mouse xenograft tumor model in vivo. *Journal of Biomedical Optics, 14*(5).

Kampinga, H. (2006). Cell biological effects of hyperthermia alone or combined with radiation or drugs: a short introductionto newcomers in the field. *Int J Hyperthermia, 22*(3), 191-196.

Kang, H. C., Kang, H. J., & Bae, Y. H. (2011). A reducible polycationic gene vector derived from thiolated low molecular weight branched polyethyleneimine linked by 2-iminothiolane. *Biomaterials, 32*(4), 1193-1203.

Kasman, L. M., Barua, S., Lu, P., Rege, K., & Voelkel-Johnson, C. (2009a). Polymer-Enhanced Adenoviral Transduction of CAR-Negative Bladder Cancer Cells. *Mol Pharm, 6*(5), 1612-1619.

Kennedy, L. C., Bickford, L. R., Lewinski, N. A., Coughlin, A. J., Hu, Y., Day, E. S., et al. (2011). A New Era for Cancer Treatment: Gold-Nanoparticle-Mediated Thermal Therapies. *Small, 7*(2), 169-183.

Kesharwani, P., Gajbhiye, V., & Jain, N. K. (2012). A review of nanocarriers for the delivery of small interfering RNA. *Biomaterials, 33*(29), 7138-7150.

Khalil, I. A., Kogure, K., Akita, H., & Harashima, H. (2006). Uptake pathways and subsequent intracellular trafficking in nonviral gene delivery. *Pharmacological Reviews, 58*(1), 32-45.

Kim, C., Cho, E. C., Chen, J., Song, K. H., Au, L., Favazza, C., et al. (2010). *In Vivo* Molecular Photoacoustic Tomography of Melanomas Targeted by Bioconjugated Gold Nanocages. *ACS Nano, 4*(8), 4559-4564.

Kim, D., Behlke, M., Rose, S., Chang, M., Choi, S., & Rossi, J. (2005). Synthetic dsRNA Dicer substrates enhance RNAi potency and efficacy. *Nat Biotechnol, 23*(2), 222-226.

Kim, D., & Rossi, J. (2009). Overview of Gene Silencing by RNA Interference *Curr Protoc Nucleic Acid Chem*.

Kim, S. H., Jeong, J. H., Cho, C., Kyung, Kim, S. W., & Park, T. G. (2005). Target-specific gene silencing by siRNA plasmid DNA complexed with folate-modified poly(ethylenimine). *Journal of Controlled Release, 104*, 223-232.

Kim, S. T., Chompoosor, A., Yeh, Y.-C., Agasti, S. S., Solfiell, D. J., & Rotello, V. M. (2012a). Dendronized Gold Nanoparticles for siRNA Delivery. *Small, 8*(21), 3253-3256.

Kolhar, P., Anselmo, A., Gupta, V., Pant, K., Prabhakarpandian, B., Ruoslahti, E., et al. (2013). Using Shape Effects to target Antibody-Coated Nanoparticles to Lung and Brian Endothelium. *PNAS, 110*(26), 10753-10758.

Kulkarni, R. P., Mishra, S., Fraser, S. E., & Davis, M. E. (2005). Single Cell Kinetics of Intracellular, Nonviral, Nucleic Acid Delivery Vehicle Acidification and Trafficking. *Bioconjugate Chemistry, 16*, 986-994.

Kumagai, M., Sarma, T. K., Cabral, H., Kaida, S., Sekino, M., Herlambang, N., et al. (2010). Enhanced in vivo magnetic resonance imaging of tumors by PEGylated ironoxide-gold core-shell nanoparticles with prolonged blood circulation properties *Macromol. Rapid Commun., 31*, 1521-1528.

Kumar, S., Kumar, C., Mathiyarasu, J., & Phani, K. (2007). Stabilized gold nanoparticles by reductino using 3,4-ethylenedioxythiophene-polystyrenesulfonate in aqueous solutions: nanocomposite formation, stability, and application in catalysis. *Langmuir, 23*(6), 3401-3408.

Kurihara, K., Kizling, J., Stenius, P., & Fendler, J. (1983). Laser and pulse radiolytically induced colloidal gold formation in water and in water-in-oil microemulsions. *J. Am. Chem. Soc., 105*(9), 2574-2579.

Lai, T. C., Bae, Y., Yoshida, T., Kataoka, K., & Kwon, G. S. (2010). pH-Sensitive Multi-PEGylated Block Copolymer as a Bioresponsive pDNA Delivery Vector. *Pharmaceutical Research, 27*(11), 2260-2273.

Lambeth, L. S., Van Hateren, N. J., Wilson, S. A., & Nair, V. (2010). A direct comparison of strategies for combinatorial RNA interference. *BMC Molecular Biology, 11*(77), 10.1186/1471-2199-1111-1177.

Lee, H., Lee, S., Oh, E., Chung, H., Han, S., Kim, E., et al. (2001). Antimicrobial polyethyleneimine-silver nanoparticle in a stable colloidal dispersion. *Colloids Surf B Biointerfaces, 88*(1), 505-511.

Lee, J.-M., Yoon, T.-J., & Cho, Y.-S. (2013). Recent Developments in Nanoparticle-Based siRNA Delivery for Cancer Therapy. *BioMed Res Int, 2013*, doi: 10.1155/2013/782041.

Lee, M. (2007). Apoptosis induced by polyethylenimine/DNA complex in polymer mediated gene delivery. *Bulletin of the Korean Chemical Society, 28*(1), 95-98.

Lee, S.-M., Park, H., Choi, J.-W., Park, Y. N., Yun, C.-O., & Yoo, K.-H. (2011). Multifunctional Nanoparticles for Targeted Chemophotothermal Treatment of Cancer Cells. *Angew. Chem. Int. Ed., 50*, 7581-7586.

Lewis, F., & Crompton, E. (2004). SET Addition of Amines to Alkenes. In W. Horspool & F. Lenci (Eds.), *Organic Photochemistry and Photobiology* (pp. 7-1): CRC Press.

Li, C., Li, D., Wan, G., Xu, J., & Hou, W. (2011). Facile Synthesis of Concentrated Gold Nanoparticles with Low Size-Distribution in Water: Temperature and pH Controls. *Nanoscale Res. Lett., 6*(1), 440.

Li, J.-L., & Gu, M. (2010). Surface plasmonic gold nanorods for enhanced two-photon microscopic imaging and apoptosis induction of cancer cells. *Biomaterials, 31*, 9492-9498.

Libutti, S. K., Paciotti, G. F., Byrnes, A. A., Alexander, H. R., Gannon, S. A., Walker, M., et al. (2010). Phase I and Pharmacokinetic Studies of CYT-6091, a Novel PEGylated Colloidal Gold-rhTNF Nanomedicine. *Clinical Cancer Research, 16*(24), 6139-6149.

Link, S., & El-Sayed, M. A. (1999). Spectral properties and relaxation dynamics of surface plasmon electronic oscillations in gold and silver nanodots and nanorods. *Journal of Physical Chemistry B, 103*(40), 8410-8426.

Liu, H., Chen, D., Li, L., Liu, T., Tan, L., Wu, X., et al. (2011). Multifunctional Gold Nanoshells on Silica Nanorattles: A Platform for Combination of Photothermal Therapy and Chemotherapy with Low Systemis Toxicity. *Angew. Chem. Int. Ed., 50*, 891-895.

Liu, J., Bauer, H., Callahan, J., Kopeckovaa, P., Pan, H., & Kopecek, J. (2010). Endocytic uptake of a large array of HPMA copolymers: Elucidation into the dependence on the physicochemical characteristics. *J Control Release, 143*(1), 71-79.

Liu, Y., Tan, J., Thomas, A., Ou-Yang, D., & Muzkantov, V. R. (2012). The Shape of Things to Come: Importance of Design in Nanotechnology for Drug Delivery. *Ther Deliv, 3*(2), 181-194.

Liu, Y. P., von Eije, K. J., Schopman, N. C., Westerink, J.-T., ter Brake, O., Haasnoot, J., et al. (2009). Combinatorial RNAi Against HIV-1 Using Extended Short Hairpins RNAs. *Mol Ther, 17*(10), 1712-1723.

Lou, Y.-L., Peng, Y.-S., Chen, B.-H., Wang, L.-F., & W., L. K. (2009). Poly(ethylene imine)-g-chitosan using EX-810 as a spacer for nonviral gene delivery vectors. *Journal of Biomedical Materials Research. Part A., 88*(4), 1058-1068.

Lu, W., Zhang, G. D., Zhang, R., Flores, L. G., Huang, Q., Gelovani, J. G., et al. (2010). Tumor Site-Specific Silencing of NF-kappa B p65 by Targeted Hollow Gold Nanosphere-Mediated Photothermal Transfection. *Cancer Research, 70*(8), 3177-3188.

Ma, L. L., Feldman, M. D., Tam, J. M., Paranjape, A. S., Cheruku, K. K., Larson, T. A., et al. (2009). Small Multifunctional Nanoclusters (Nanoroses) for Targeted Cellular Imaging and Therapy. *Acs Nano, 3*(9), 2686-2696.

Maeda, H., Wu, J., Sawa, T., Matsumura, Y., & Hori, K. (2000). *Tumor vascular permeability and the EPR effect in macromolecular therapeutics: a review*.

Mahajan, S., R, A., Reynolds, J., Nair, B., Sykes, D., Bonoiu, A., et al. (2012). Suppression of MMP-9 expression in brain microvascular endothelial cell (BMVEC) using gold nanorod (GNR)-siRNA nanoplex. *Immunol Invest, 41*(4), 337-355.

Mallidi, S., Larson, T., Tam, J., Joshi, P. P., Karpiouk, A., Sokolov, K., et al. (2009). Multiwavelength Photoacoustic Imaging and Plasmon Resonance Coupling of Gold Nanoparticles for Selective Detection of Cancer. *Nano Letters, 9*(8), 2825-2831.

Martin, C. R. (1994). Nanomaterials - a membrane-based synthetic approach. *Science, 266*(5193), 1961-1966.

Martirosyan, K. S. (2012). Thermosensitive Magnetic Nanoparticles for Self-Controlled Hyperthermia Cancer Treatment. *J Nanomed Nanotechnol, 3*, 6.

Masood, R., Roy, I., Zu, S., Hochstim, C., Yong, K., Law, W., et al. (2012). Gold nanorod-sphingosine kinase siRNA nanocomplexes:a novel therapeutic tool for potent radiosensitization of head and neck cancer. *Integr Biol (Camb), 4*(2), 132-141.

McIntyre, G. J., & Fanning, G. C. (2006). Design and cloning strategies for constructing shRNA expression vectors. *BMC Biotechnology, 6*(1), 10.1186/1472-6750-1186-1181.

Merdan, T., Kopecek, J., & Kissel, T. (2002). Prospects for cationic polymers in gene and oligonucleotide therapy against cancer. *Advanced Drug Delivery Reviews, 54*(5), 715-758.

Mishra, D., Kang, H. C., & Bae, Y. H. (2011). Reconstitutable charged polymeric (PLGA)(2)-b-PEI micelles for gene therapeutics delivery. *Biomaterials, 32*(15), 3845-3854.

Miyagishi, M., Sumimoto, H., Miyoshi, H., Kawakami, Y., & Taira, K. (2004). Optimization of an siRNA-expression system with an improved hairpin and its significanct suppressive effects in mammalian cells. *J Gene Med, 6*, 715-723.

Motegi, Y., Katayama, K., Sakurai, F., Kato, T., Yamaguchi, T., Matsui, H., et al. (2011). An effective gene-knockdown using multiple shRNA-expression adenovirus vectors. *Journal of Controlled Release, 153*, 149-153.

Mualidharan, G., Subramanian, L., Nallamuthu, S. K., Santhanam, V., & Kumar, S. (2011). Effect of Reagent Addition Rate and Temperature on Synthesis of Gold Nanoparticles in Microemulsion Route. *Ind. Eng. Chem. Res., 50*(14), 8786-8791.

Munier, S., Messai, I., Delair, T., Verrier, B., & Atamon-Onal, Y. (2005). Cationic PLA nanoparticles for DNA delivery: Comparison of three surface polycations for DNA binding, protection and transfection properties. *Cooloids Surf B Biointerfaces, 43*(3-4), 163-173.

Nagao, A., Zhao, X., Takegami, T., Nakagawa, H., Matsui, S., Matsunaga, T., et al. (2008). Multiple shRNA expression in a single plasmid vector improve RNAi against the XPA gene. *Biochemical and Biophysical Research Communications, 370*, 301-305.

Nath, S., Ghosh, S. k., Kundu, S., Praharaj, S., Panigrahi, S., & Pal, T. (2006). Is Gold Really Softer than Silver? HSAB Principle Revisited. *J. Nanopart. Res., 8*, 111-116.

Navarro, G., Sawant, R. R., Essez, S., Tros de Ilarduya, C., & Torchillin, V. P. (2011). Phospholipid-polyethylenimine conjugate-based micelle-like nanoaprticles for siRNA delivery. *Drug Deliv. and Transl. Res., 1*, 25-33.

Newman, J. D. S., & Blanchard, G. J. (2006). Formation of Gold Nanoparticles Using Amine Reducing Agents. *Langmuir, 22*, 5882-5887.

Newman, J. D. S., & Blanchard, G. J. (2007). Formation and encapsulation of gold nanoaprticles using a polymeric amine reducing agent. *J. Nanopart. Res., 9*, 861-868.

Nguyen, D. T., Kim, D.-J., So, M. G., & Kim, K.-S. (2010). Experimental measurements of gold nanoparticle nucleation and growth by citrate reduction of $HAuCl_4$. *Advanced Powder Technology, 21*, 111-118.

Niidome, T., Akiyama, Y., Yamagata, M., Kawano, T., Mori, T., Niidome, Y., et al. (2009). Poly(ethylene glycol)-Modified Gold Nanorods as a Photothermal Nanodevice for Hyperthermia. *Journal of Biomaterials Science-Polymer Edition, 20*(9), 1203-1215.

Nikoobakht, B., & El-Sayed, M. A. (2003). Preparation and growth mechanism of gold nanorods (NRs) using seed-mediated growth method. *Chemistry of Materials, 15*(10), 1957-1962.

O'Neal, D. P., Hirsch, L. R., Halas, N. J., Payne, J. D., & West, J. L. (2004). Photo-thermal tumor ablation in mice using near infrared-absorbing nanoparticles. *Cancer Letters, 209*(2), 171-176.

Oldenburg, S. J., Averitt, R. D., Westcott, S. L., & Halas, N. J. (1998). Nanoengineering of optical resonances. *Chemical Physics Letters, 288*(2-4), 243-247.

Oldenburg, S. J., Jackson, J. B., Westcott, S. L., & Halas, N. J. (1999). Infrared extinction properties of gold nanoshells. *Applied Physics Letters, 75*(19), 2897-2899.

Oldenburg, S. J., Westcott, S. L., Averitt, R. D., & Halas, N. J. (1999). Surface enhanced Raman scattering in the near infrared using metal nanoshell substrates. *Journal of Chemical Physics, 111*(10), 4729-4735.

Osaka, T., Nakanishi, T., Shanmugam, S., & Zhang, H. (2009). Effect of surface charge of magnetite nanoparticles on their internalization into breast cancer and umbilical vein endothelial cells. *Colloids Surf B Biointerfaces, 71*(2), 325-330.

Ow Sullivan, M. M., Green, J. J., & Przybycien, T. M. (2003). Development of a novel gene delivery scaffold utilizing colloidal gold-polyethylenimine conjugates for DNA condensation. *Gene Ther, 10*(22), 1882-1890.

Paciotti, G. F., Myer, L., Weinreich, D., Goia, D., Pavel, N., McLaughlin, R. E., et al. (2004). Colloidal gold: A novel nanoparticle vector for tumor directed drug delivery. *Drug Delivery, 11*(3), 169-183.

Paddison, P., Caudy, A., Bernstein, E., Hannon, G., & Conklin, D. (2002). Short hairpin RNAs (shRNAs) induce sequuence-specific silencing in mammalian cells. *Genes Dev, 16*(8), 948-958.

Pan, D., Pramanik, M., Senpan, A., Wickline, S., Wang, L., & Lanza, G. (2010). A facile synthesis of novel self-assembled gold nanorods designed for near-infrared imaging. *J Nanosci Nanotechnol, 10*(12), 8118-8123.

Panacek, A., Kolar, M., Vacerova, R., Prucek, R., Soukupova, J., Krystof, V., et al. (2009). Antifungal activity of silver nanoparticles against *Candida*. *Biomaterials, 30*, 6333-6340.

Park, H., Yang, J., Lee, J., Haam, S., Choi, I.-H., & Yoo, K.-H. (2009). Multifunctional Nanoparticles for Combined Doxorubicin and Photothermal Treatments. *ACS Nano, 3*(10), 2919-2926.

Park, J. H., von Maltzahn, G., Ong, L. L., Centrone, A., Hatton, T. A., Ruoslahti, E., et al. (2010). Cooperative Nanoparticles for Tumor Detection and Photothermally Triggered Drug Delivery. *Advanced Materials, 22*(8), 880-+.

Park, Y., Kang, E., Kwon, O. J., Hwang, T., Park, H., Lee, J. M., et al. (2010). Ionically crosslinked Ad/chitosan nanocomplexes processed by electrospinning for targeted cancer gene therapy. *Journal of Controlled Release, 148*(1), 75-82.

Patra, C. R., Bhattacharya, R., D., M., & Mukherjee, P. (2008). Applications of gold nanoparticles for targeted therapy in cancer. *J Biomed Nanotechnol, 4*, 99-132.

Patra, C. R., R., B., Wang, E., Katarya, A., Lau, J. S., & Dutta, S. (2008). Targeted delivery of gemcitabine to pancreatic adenocarcinoma using cetuximab as a targeting agent. *Cancer Res., 68*, 1970-1978.

Pecot, C. V., Calin, G. A., Coleman, R. L., Lopez-Berestein, G., & Sood, A. K. (2011). RNA interference in the clinic: challenges and future directions. *Nat Rev Cancer, 11*(1), 59-67.

Perry, S. W., Burke, R. M., & Brown, E. B. (2012). Two-Photon and Second Harmonic Microscopy in Clinical and Translational Cancer Research. *Annals of Biomedical Engineering, 40*(2), 277-291.

Pilot Study of AuroLase(tm) Therapy in Refractory and/or Recurrent Tumors of the Head and Neck. October 2012

Plank, C., Zelphati, O., & Mykhaylyk, O. (2011). Magnetically enhanced nucleic acid delivery. Ten years of magnetofection-Progress and prospects. *Advanced Drug Delivery Reviews, 63*, 1300-1331.

Ramos, J., & Rege, K. (2012a). Transgene Delivery using Poly(amino ether)-Gold Nanorod Assemblies *Biotechnol Bioeng, 109*(5), 1336-1436.

Ramos, J., & Rege, K. (2013b). Poly(aminoether)-Gold Nanorod Assemblies for shRNA Plasmid-Induced Gene Silencing. *Molecular Pharmaceutics, 10*(11), 4107-4119.

Ramos, J., Taylor, D., & Rege, K. (2012). Gold Nanoparticle Mediated Photo-Chemotherapy. *J. Nanomed Nanotechnol, 3*(8), 1000e1125.

Rao, D. D., Vorhies, J. S., Senzer, N., & Nemunaitis, J. (2009). siRNA vs. shRNA: Similarities and differences. *Advanced Drig Delivery Reviews, 61*, 746-759.

Rege, K., Hu, S., Moore, J. A., Dordick, J. S., & Cramer, S. M. (2004). Chemoenzymatic Synthesis and High-Throughput Screening of an Aminoglycoside-Polyamine

Library: Identification of High-Affinity Displacers and DNA-Binding Ligands. *Journal of the American Chemical Society, 126*, 12306-12315.

Rege, K., Ladiwala, A., Hu, S. H., Breneman, C. M., Dordick, J. S., & Cramer, S. M. (2005b). Investigation of DNA-binding properties of an aminoglycoside-polyamine library using quantitative structure-activity relationship (QSAR) models. *Journal of Chemical Information and Modeling, 45*(6), 1854-1863.

Rose, S., Kim, D., Amarzguioui, M., Heidel, J., Collingwood, M., Davis, M., et al. (2005). Functional polarity is introduced by Dicer processing of short substrate RNAs. *Nucleic Acids Res, 33*(13), 4140-4156.

Rosenberg, C., Puls, R., Hegenscheid, K., Kuehn, J., Bollman, T., Westerholt, A., et al. (2009). Laser ablation of metastatic lesions of the lung: long-term outcome. *AJR Am J Roentgenol, 192*(3), 785-792.

Ryou, S., Kim, S., Jang, H., Kim, J., Yeom, J., Eom, M., et al. (2010). Delivery of shRNA using gold nanoparticle-DNA oligonucleotide conjugated as a universal carrier. *Biochem Biophys Res Commun, 398*(3), 542-546.

Ryou, S., Park, M., Kim, J., Jeon, C., CH, Y., Han, S., et al. (2011). Inhibition of xenograft tumor growth in mice by goldnanoparticle-assisted delivery of short hairpin RNAs against Mcl-1L. *156, 2*(89-94).

Sakai, T., & Alexandridis, P. (2005). Mechanism of Gold Metal Ion Reduction, Nanoparticle Growth ans Size Control in Aqueous Amphiphilic Block Copolymer Solutions at Ambient Conditions. *J Phys. Chem. B, 109*, 7766-7777.

Salem, A. K., Searson, P. C., & Leong, K. W. (2003). Multifunctional nanorods for gene delivery. *Nat Mater, 2*(10), 668-671.

Sandhu, K. K., McIntosh, C. M., Simard, J. M., Smith, S. W., & Rotello, V. M. (2002). Gold nanoparticle-mediated Transfection of mammalian cells. *Bioconjugate Chemistry, 13*(1), 3-6.

Sarkar, K., Srivastava, R., Chatterji, U., & Kundu, P. P. (2011). Evaluation of Chitosan and Their Self-Assembled Nanoparticles with pDNA for the Application in Gene Therapy. *Journal of Applied Polymer Science, 121*(4), 2239-2249.

Scherr, M., Battmer, K., Ganser, A., & Eder, M. (2003). Modulation of Gene Expression by Lentiviral-Mediated Delivery of Small Interfering RNA. *Cell Cycle, 2*(3), A65-A71.

Scherr, M., Battmer, T., Winkler, O., Heindenreich, A., Ganser, A., & Eder, M. (2003). Specific inhibition of bcr-abl gene expression by small interfering RNA. *Blood, 101*, 1566-1569.

Selvakannan, P., Mandal, S., Phadtare, S., Gole, A., Pasricha, R., Adyanthaya, S., et al. (2004). Water-dispersible tryptophan-protected gold nanoaprticles prepared by the spontaneous reduction of aqueous chloroaurate ions by the amino acid. *J Colloid Interface Sci, 269*(1), 97-102.

Sershen, S. R., Westcott, S. L., Halas, N. J., & West, J. L. (2000). Temperature-sensitive polymer-nanoshell composites for photothermally modulated drug delivery. *Journal of Biomedical Materials Research, 51*(3), 293-298.

Shi, J., Choi, J., Chou, B., Johnson, R., Schellinger, J., & Pun, S. (2013). Effect of Polyplex Morphology on Cellular Uptake, Intracellular Trafficking, and Transgene Expression. *ACS Nano, 7*(12), 10612-10620.

Shimmin, R. G., Schoch, A. B., & Braun, P. V. (2004). Polymer Size and Concentration Effects on the Size of Gold Nanoparticles Capped by Polymeric Thiols. *Langmuir, 20*, 5613-5620.

Shin, K. S., & Kim, J. H. (2011). One-Step Fabrication of Poly(ethylenimine)-Stabilized Silver Nanoparticles from Insoluble Silver Chloride Salt. *Bull. Korean Chem. Soc., 32*(7), 2469-2472.

Shirazi, A. N., Mandal, D., Tiwari, R. k., Guo, L., Lu, W., & Parang, K. (2012). Cyclic Peptide-Capped Gold Nanoaprticles as Drug Delivery Systems. *Mol. Pharm., 10*, 500-511.

Silver, S., Phung, L. T., & Silver, G. (2006). Silver as biocides in burn and wound dressing and bacterial resistance to silver compounds. *J. Ind. Microbiol. Biotechnol., 33*, 627-634.

Simeone, D. M., Cascarelli, A., & Logsdon, C. D. (1997). Adenoviral-mediated gene transfer of a constitutively active retinoblastoma gene inhibits human pancreatic tumor cell proliferation. *Surgery, 122*(2), 428-433.

Singh, A., Boldin-Adamsky, S., Thimmulappa, R. K., Rath, S. K., Ashush, H., Coulter, J., et al. (2008). RNAi-mediated silencing of nuclear factor erythroid-2-related factor 2 gene expression in nin-small cell lung cancer inhibits tumor growth and increases efficacy of chemotherapy. *Cancer Research, 68*, 7975-7984.

Singh, S., D'Britto, V., Prabhune, A. A., Ramana, C. V., Dhawan, A., & Prasad, B. L. V. (2010). Cytotoxic and genotoxic assessment of glycolipid-reduced and -capped gold and silver nanoparticles. *New J. Chem., 34*, 294-301.

Siolas, D., Lerner, C., Burchard, J., De, W., Linsley, P., Paddison, P., et al. (2005). Synthetic shRNAs as potent RNAi triggers. *Nat Biotechnol, 23*(2), 227-231.

Skrabalak, S. E., Au, L., Li, X. D., & Xia, Y. (2007). Facile synthesis of Ag nanocubes and Au nanocages. *Nature Protocols, 2*(9), 2182-2190.

Smith, A., Duan, H., Mohs, A., & Nie, S. (2008). Bioconjugated quantum dots for in vivo molecular and cellular imaging. *Adv Drug Deliv Rev, 60*(11), 1226-1240.

Sokolov, K., Follen, M., Aaron, J., Pavlova, I., Malpica, A., Lotan, R., et al. (2003). Real-Time Vital Optical Imaging of Precancer Using Anti-Epidermal Growth Factor Receptor Antibodies Conjugated to Gold Nanoparticles. *Cancer Research, 63*(9), 1999-2004.

Song, W. J., Du, J. Z., Sun, T. M., Zhang, P. Z., & Wang, J. (2010). Gold Nanoparticles Capped with Polyethyleneimine for Enhanced siRNA Delivery. *Small, 6*(2), 239-246.

Sotiriou, G. A., Hirt, A. M., Lozach, P. Y., Teleki, A., Krumeich, F., & Pratsinis, S. E. (2011). Hybrid, silica-coated, Janus-like plasmonic-magnetic nanoparticles. *Chem. Mater., 23*, 1985-1992.

Sotiriou, G. A., & Pratsinis, S. E. (2011). Engineering nanosilver as an antibacterial, biosensor and bioimaging material. *Opin CHem Eng, 1*, 3-10.

Sotiriou, G. A., Sannomiya, T., Teleki, A., Krumeich, F., Voros, J., & Pratsinis, S. E. (2010). Non-toxic dry-coated nanosilver for plasmonic biosensors. *Adv. Funct. Mater., 20*, 4250-4257.

Sramkoski, R., Pretlow, T., Giaconia, J., Pretlow, T., Schwartz, S., Sy, M., et al. (1999). A new human prostate carcinoma cell line, 22Rv1. *In Vitro Cell Dev Biol Anim, 35*(7), 403-409.

Sun, X., Dong, S., & Wang, E. (2005). One-step preperation of highly concentrated well-stable gold colloids by direct mix of polyelectrolyte and HAuCl4 aqueous solutions at room temperature. *Journal of Colloid and Interface Science, 288*, 301-303.

Sun, Y. G., Mayers, B. T., & Xia, Y. N. (2002). Template-engaged replacement reaction: A one-step approach to the large-scale synthesis of metal nanostructures with hollow interiors. *Nano Letters, 2*(5), 481-485.

Takei, Y., Kadomatsu, K., Yuzawa, Y., Matsuo, S., & Muramatsu, T. (2004). A small interfering RNA targeting vascular endothelial growth factor as cancer therapeutics. *Cnacer Research, 64*, 3365-3370.

Tam, S., Erol, M., Attygelle, A., Du, H., & Sukhishvili, S. (2007). Synthesis of Positively Charged Silver Nanoparticles via Photoreduction of $AgNO_3$ in Branched Polyethyleneimine/HEPES Solutions. *Langmuir, 23*, 9836-9843.

Tan, Y. N., Lee, J. Y., & Wang, D. I. C. (2010). Uncovering the Design Rules for Peptide Synthesis of Metal Nanoparticles. *J. Am. Chem. Soc., 132*, 5677-5686.

Polyethylenimine's Transfer of Plasmid DNA into Mammalian Cells. *Proc. Natl. Acad. Sci., 100*(16), 9138-9143.

Uchida, H., Tanaka, T., Sasaki, K., Kato, K., Dehari, H., Ito, Y., et al. (2004). Adneovirus-mediated transfer of siRNA against survivin induced apoptosis and attenuated tumor cell growth in vitro and in vivo. *Molecular Therapeutics, 10*, 162-171.

Vanwinkle, B. A., Bently, K. L. D., Malecki, J. M., Gunter, K. K., Evans, I. M., Elder, A., et al. (2009). Nanoparticle (NP) uptake by type I alveolar epithelial cells and their oxidant stress response. *Nanotoxicology, 3*, 307-318.

Varga, C. M., Tedford, N. C., Thomas, M., Klibanov, A. M., Griffith, L. G., & Lauffenburger, D. A. (2005). Quantitative comparison of polyethylenimine formulations and adenoviral vectors in terms of intracellular gene delivery processes. *Gene Therapy, 12*(13), 1023-1032.

Vasile, E., Serafim, A., Petre, D., Giol, D., Dubruel, P., Iovu, H., et al. (2014). Direct Synthesis and Morphological Characterization of Gold-Dendrimer Nanocomposites Prepared Using PAMAM Succinamic Acid Dendrimers: Preliminary Study of the Calcification Potential. *Sci. World J.*, 103462.

Vicennati, P., Giuliano, A., Ortaggi, G., & Masotti, A. (2008). Polyethylenimine In Medicinal Chemistry. *Current Medicinal Chemistry, 15*, 2826-2839.

Vogl, T., Straub, R., Eichler, K., Sollner, O., & Mack, M. (2004). Colorectal carcinoma metastases in liver: laser-induced interstitial thermotherapy—local tumor control rate and survival data. *Radiology, 230*(2), 450-458.

Vogl, T., Straub, R., Zangos, S., Mack, M., & Eichler, K. (2004). MR-guided laser-induced thermotherapy (LITT) of liver tumours: experimental and clinical data. *Int J Hyperthermia, 20*(7), 713-724.

von Maltzahn, G., Park, J. H., Agrawal, A., Bandaru, N. K., Das, S. K., Sailor, M. J., et al. (2009). Computationally guided photothermal tumor therapy using long-circulating gold nanorod antennas. *Cancer Res, 69*(9), 3892-3900.

Vu, L., Ramos, J., Potta, T., & Rege, K. (2012). Generation of a Focused Poly(amino ether) Library: Polymer-mediated Transgene Delivery and Gold-Nanorod based Theranostic Systems. *Theranostics, 2*(12), 1160-1173.

Waite, C., & Roth, C. (2009). PAMAM-RGD Conjugates Enhance siRNA Delivery Through a Multicellular Spheriod Model of Malignant Glioma. *Bioconj Chem, 20*(10), 1908-1916.

Walker, C. R., Pushpavanam, K., Nair, D. G., Potta, T., Sutiyoso, C., Kodibagkar, V. D., et al. (2013). Generation of Polypeptide-Templated Gold Nanoparticles using Ionizing Radiation. *Langmuir, 29*(32), 10166-10173.

Wang, H. F., Huff, T. B., Zweifel, D. A., He, W., Low, P. S., Wei, A., et al. (2005). In vitro and in vivo two-photon luminescence imaging of single gold nanorods. *Proceedings of the National Academy of Sciences of the United States of America, 102*(44), 15752-15756.

Wang, T., Mancuso, J., Kazmi, S., Dwelle, J., Sapozhnikova, V., Willsey, B., et al. (2012). Combined two-photon luminescence microscopy and OCT for macrophage detection in the hypercholesterolemic rabbit aorta using plasmonic gold nanorose. *Laser Surg Med, 1*, 49-45.

Wang, T., Mancuso, J., Sapozhnikova, V., Dwelle, J., Ma, L., Willsey, B., et al. (2012). Dual-wavelength multifrequency photothermal wave imaging combined with optical coherence tomography for macrophage and lipid detection in atherosclerotic plaques using gold nanoparticles. *J Biomed Opt, 17*(3), 036009.

Wang, Y. H., Zheng, M., Meng, F. H., Zhang, J., Peng, R., & Zhong, Z. Y. (2011). Branched Polyethylenimine Derivatives with Reductively Cleavable Periphery for Safe and Efficient In Vitro Gene Transfer. *Biomacromolecules, 12*(4), 1032-1040.

Wang, Y. W., Xie, X. Y., Wang, X. D., Ku, G., Gill, K. L., O'Neal, D. P., et al. (2004). Photoacoustic tomography of a nanoshell contrast agent in the in vivo rat brain. *Nano Letters, 4*(9), 1689-1692.

Wei, L., J., T., Zhang, Z., Chen, Y., Zhou, G., & Xi, T. (2010). Investigation of the cytotoxicity mechanism of silver nanoparticles in vitro. *Biomed Mater, 5*, 044103.

Wei, Q., Ji, J., & Shen, J. (2008). Synthesis of Near-Infrared Responsive Gold Nanorod/PNIPAAm Core/Shell Nanohybrids via Surface Initiated ATRP for Smart Drug Delivery. *Macromol Rapid Commun, 29*, 645-650.

Wijaya, A., Schaffer, S., Pallares, I., & Hamad-Schifferli, K. (2009). Selective Release of Multiple DNA Oligionucleotides from Gold Nanorods. *ACS Nano, 3*(1), 80-86.

Wu, C., Yu, C., & Chu, M. (2011). A gold nanoshell with a silica inner chell synthesized using liposome templates for doxorubicin loading and near-infrared photothermal therapy. *International Journal of Nanomedicine, 6*, 807-813.

Wu, H., Ma, H., Ye, C., Ramirez, D., Chen, S., Montoya, J., et al. (2011). Improved siRNA/shRNA funtionality by mismatched duplex. *PLos One, 6*(12), e28580.

Wu, W. T., Zhou, T., Berliner, A., Banerjee, P., & Zhou, S. Q. (2010). Smart Core-Shell Hybrid Nanogels with Ag Nanoparticle Core for Cancer Cell Imaging and Gel Shell for pH-Regulated Drug Delivery. *Chemistry of Materials, 22*(6), 1966-1976.

Yan, X., Blacklock, J., Li, J., & Mohwald, H. (2012). One-Pot Synthesis of Polypeptide-Gold Nanoconjugates for *in Vitro* Gene Transfection. *ACS Nano, 6*(1), 111-117.

Yang, G., Cai, K. Q., Thompson-Lanza, J. A., Bast Jr, R. C., & Liu, J. (2004). Inhibition of breast and ovarian tumor growth through multiple signaling pathways using retrovirus-mediated small interfering RNA against HER-2/Neu gene expression. *J. Biol. Chem., 279*, 4339-4345.

Yang, X., Stein, E. W., Ashkenazi, S., & Wang, L. V. (2009). Nanoparticles for photoacoustic imaging. *Wiley interdisciplinary reviews. Nanomedicine and nanobiotechnology, 1*, 360-368.

Yang, X. M., Skrabalak, S. E., Li, Z. Y., Xia, Y. N., & Wang, L. H. V. (2007). Photoacoustic tomography of a rat cerebral cortex in vivo with au nanocages as an optical contrast agent. *Nano Letters, 7*(12), 3798-3802.

Yezhelyev, M. V., Qi, L., O'Regan, R. M., Nie, S., & Gao, X. (2008). Proton-Sponge Coated Quantum Dots for siRNA Delivery and Intracellular Imaging. *J. Am. Chem. Soc., 130*(28), 9006-9012.

Yi, Y., Hahm, S. H., & Lee, K. H. (2005). Retroviral gene therapy: Safety issues and possible solutions. *Current Gene Therapy, 5*(1), 25-35.

You, C., Han, C., Wang, Z., Zheng, Y., Li, Q., Hu, X., et al. (2012). The progress of silver nanoparticles in the antibacterial mechanism, clinical application and cytotoxicity. *Mol Biol Rep, 39*, 9193-9201.

You, J., Zhang, G. D., & Li, C. (2010). Exceptionally High Payload of Doxorubicin in Hollow Gold Nanospheres for Near-Infrared Light-Triggered Drug Release. *ACS Nano, 4*(2), 1033-1041.

You, J., Zhang, R., Xong, C., Zhong, M., Melancon, M., Gupta, S., et al. (2012). Effective Photothermal Chemotherapy Using Doxorubicin-Loaded Gold Nanospheres That Target EphB4 Receptors in Tumors. *Cancer Research, 72*(18), 4777-4786.

You, J., Zhang, R., Zhang, G., Zhong, M., Liu, Y., Van Pelt, C. S., et al. (2012). Photothermal-Chemotherapy with doxorubicin -loaded hollow gold nanospheres: A platform for near-infrared light-triggered drug release. *Journal of Controlled Release, 158*, 319-328.

Young, J. K., Figueroa, E. R., & Drezek, R. A. (2012). Tunable Nanostructures as Photothermal Theranostic Agents. *Annals of Biomedical Engineering, 40*(2), 438-459.

Yu, J., Taylor, J., DeRuiter, S., Vojtek, A., & Turner, D. (2003). Simultaneou inhibition of GSK3alpha and GSK3beta using hairpin shRNA expression vectors. *Mol Ther, 7*(2), 228-236.

Yu, Y. Y., Chang, S. S., Lee, C. L., & Wang, C. R. C. (1997). Gold nanorods: Electrochemical synthesis and optical properties. *Journal of Physical Chemistry B, 101*(34), 6661-6664.

Yue, Z., Wei, W., Lv, P., Yue, H., Wang, L., Su, Z., et al. (2011). Surface charge affects cellular uptake and intracellular trafficking of chitosan-based nanoparticles. *Biomacromolecules, 12*(7), 2440-2446.

Zhang, H., Huang, X., Li, L., Hussain, I., Li, Z., & Tan, B. (2012). Photoreductive syntehsis of water-soluble fluorescent metal nanoclusters. *Chem Commun (Camb), 48*(4), 567-569.

Zhang, W., Meng, J., Ji, Y., Li, X., Kong, H., Wu, X., et al. (2011). Inhibiting metastasis of breast cancer cells in vitro using gold nanorod-siRNA delivery system. *Nanoscale, 3*(9), 3923-3932.

Zhao, E., Zhao, Z., Wang, J., Yang, C., Chen, C., Gao, L., et al. (2012). Surface engineering of gold nanoparticles for in vitro siRNA delivery. *Nanoscale, 4*(16), 5102-5109.

BIOGRAPHICAL SKETCH

James Ramos earned his Bachelor of Science degree in Bioengineering from Rice University in Spring 2009. After which he joined the doctoral program of biomedical engineering at Arizona State University in the Fall of 2009. James has been the recipient of numerous awards including the Ford graduate Engineering Fellowship, the Achievement Reward for College Scientists, the Science Foundation of Arizona graduate Research fellowship, and was recognized as an outstanding mentor by the graduate and professional student's association for his outreach work with high school students. While pursuing his degree James worked as a Graduate Research Assistant in the Molecular and Nanoscale Bioengineering lab under advisement by Dr. Kaushal Rege. His research focused on the engineering and modification of gold nanoparticles for delivery of plasmid DNA for potential therapeutics in cancer treatment. His research has been published in peer reviewed journals and he has presented his work at several national conferences.